

## Contents

<b>Editorial Preface to the Special Issue Dedicated to the Manufacturing_2021 Conference</b> ISTVÁN GYURIKA	1–1
<b>3D Scanning and Model Error Distribution-Based Characterisation of Welding Defects</b> JÁNOS HEGEDŰS-KUTI, JÓZSEF SZOLOSÍ, DÁNIEL VARGA, GÁBOR FARKAS, TAMÁS RUPPERT, JÁNOS ABONYI, AND MÁTYÁS ANDÓ	3–7
<b>The Effect of the Cutting Speed on the Surface Roughness When Ball-End Milling</b> ABDULWAHAB M. GHERONY AND BALÁZS MIKÓ	9–13
<b>Study on the Photo-Based 3d Scanning Process</b> ÁLMOSS KRISTÁLY AND PÉTER FICZERE	15–18
<b>Weight Reduction of a Drone Using Generative Design</b> BÁLINT LEON SEREGI AND PÉTER FICZERE	19–22
<b>Challenges of Industry 4.0 in the Visegrád Group</b> ANDREA ÉLTETŐ	23–27
<b>Design and Quality Assured Manufacturing of Free Form Metal Prostheses by Selective Laser Melting Technology</b> ARTÚR BENJÁMIN ACÉL, GYÖRGY FALK, FERENC DÖMÖTÖR, AND JÁNOS TAKÁCS	29–34
<b>Investigation of the Resistance a Sailboat is Subjected to in the Case of Draft Changes Caused by Modifying the Powertrain</b> EMESE LÉVAI AND PÉTER FICZERE	35–38
<b>Mechanical Deburring of Drilling-Induced Exit Burrs in Carbon Fibre Reinforced Polymer Composites</b> ANDRÁS GÖDRI, ANNA NIKOLETTA HELLE, AND NORBERT GEIER	39–45
<b>Comparative Analysis of Burrs in UD-CFRP Composites Using Advanced Hole Machining Technologies</b> ANNA NIKOLETTA HELLE, CSONGOR PERESZLAI, ANDRÁS GÖDRI, AND NORBERT GEIER	47–52
<b>Experimental Implementation of a Resource-Constrained Multi-Project Scheduling Problem Solver</b> KRISZTIÁN MIHÁLY, MÓNIKA KULCSÁRNÉ FORRAI, AND GYULA KULCSÁR	53–58
<b>Research on and Practice of Additive Manufacturing Technologies</b> PÉTER FICZERE	59–64
<b>Using Finite Element Analysis in the 3D Printing of Metals</b> HUSSEIN ALZYOD AND PÉTER FICZERE	65–70

<b>Analysis of Formed Chips in the Case of Turning Different Polymer Materials</b> ÁDÁM SARANKÓ, GÁBOR KALÁCSKA, AND RÓBERT ZSOLT KERESZTES	<b>71–75</b>
<b>Analysis of Roughness Parameters Determining Tribological Properties in Hard Turned Surfaces</b> VIKTOR MOLNÁR AND ISTVÁN SZTANKOVICS	<b>77–84</b>
<b>Complementary Manipulator Tool Development for Safe Cobot-Assisted Hydroponics</b> IMRE PANITI, JÁNOS NACSA, DÁVID SZUR, SÁNDOR RÁ CZ, AND JÓZSEF TÓTH	<b>85–89</b>
<b>Gripper Finger Design for Special Purpose Applications</b> MIKLÓS BOLERACZKI, ISTVÁN GÁBOR GYURIKA, AND DÉNES FODOR	<b>91–95</b>
<b>Building a Reusable Data Model to Support Systematic Layout Planning with Discrete Event Simulation of Flexible Manufacturing Systems</b> ZSOLT MOLNÁR, PÉTER TAMÁS, AND BÉLA ILLÉS	<b>97–100</b>

## EDITORIAL PREFACE TO THE SPECIAL ISSUE DEDICATED TO THE MANUFACTURING\_2021 CONFERENCE

ISTVÁN GYURIKA<sup>1</sup>

<sup>1</sup>Research Centre for Engineering Sciences, University of Pannonia, Egyetem u. 10, Veszprém, 8200, HUNGARY

The Association of Mechanical Engineers in Hungary, “GTE”, has a long tradition in organizing a nation-wide, scientific-technical conference devoted to MANUFACTURING. During the 29-30th October 2021, the University of Pannonia offered to host the 24th GTE MANUFACTURING Conference, where almost 50 presentations were delivered by engineering students with PhD or Post-Doc level. Participants from industry had also a good opportunity to present their new products and services, thus a fruitful collaboration platform had taken place at the premises of the University of Pannonia.

The highly appreciated Hungarian Journal of Industry and Chemistry is an excellent medium to convey the novelties and new scientific-technical achievements demonstrated during the conference. The PhD students are also grateful to HJIC for the chances to generate high-level publications at international level.

The presentations were mainly offered in English language, giving additional opportunities for PhD students to practice oral presentations of their scientific work and achieved results. All of the topics address one or more of the offered areas of manufacturing, including prod-

ucts, production, logistics, sensor-, monitoring-, robotics-thematic areas, as well as economic and human aspects, e.g., operator cooperation with robots. The review committee generated detailed feedback to the authors to show higher level of articulation of their ideas and results, and to maintain the scientific high level of the HJIC journal. The selected papers are included in this special issue of HJIC.

The GTE Association will continue to offer its members opportunities to share up-to-date technical and scientific information and build a reliable social-technical network in the new ecosystem needed for the transition from Industry 4.0 to Industry 5.0. We are looking ahead and inviting for the quad-centenarian, 25th jubilee MANUFACTURING Conference.

István Gyurika

Chairman of GTE’s Division of Manufacturing Systems

On behalf of the MANUFACTURING: 2021 Organising Committee.

Correspondence: [gyurika@almos.uni-pannon.hu](mailto:gyurika@almos.uni-pannon.hu)



## 3D SCANNING AND MODEL ERROR DISTRIBUTION-BASED CHARACTERISATION OF WELDING DEFECTS

JÁNOS HEGEDŰS-KUTI<sup>\*1,2</sup>, JÓZSEF SZŐLŐSI<sup>1</sup>, DÁNIEL VARGA<sup>1</sup>, GÁBOR FARKAS<sup>1</sup>, TAMÁS RUPPERT<sup>2</sup>, JÁNOS ABONYI<sup>2</sup>, AND MÁTYÁS ANDÓ<sup>1</sup>

<sup>1</sup>Savaria Institute of Technology, Eötvös Loránd University, Károlyi Gáspár tér 4, Szombathely, 9700, HUNGARY

<sup>2</sup>Complex Systems Monitoring Research Group, Research Centre for Biochemical, Environmental and Chemical Engineering, University of Pannonia, Egyetem u. 10, Veszprém, 8200, HUNGARY

The inspection of welded structures requires particular attention due to many aspects that define the quality of the product. Deciding on the suitability of welds is a complex process. This work aims to propose a method that can support this qualification. This paper presents a state-of-the-art data-driven evaluation method and its application in the quality assessment of welds. Image processing and CAD modelling software was applied to generate a reference using the Iterative Closest Point algorithm that can be used to generate datasets which represent the model errors. The results demonstrate that the distribution of these variables characterises the typical welding defects. Based on the automated analysis of these distributions, it is possible to reduce the turnaround time of testing, thereby improving the productivity of welding processes.

**Keywords:** Industry 4.0, Welding technology, 3D scanner, Iterative Closest Point, defect analysis

### 1. Introduction

During the Fourth Industrial Revolution, more modern industrial processes and tools, e.g., various testing instruments, are present in many technological fields. Advanced industrial tools are used in these technological environments [1, 2]. In addition to this new economic approach, the implementation of welding with a higher degree of automation has been a technological facilitation [3], while the complexity of the system has required the involvement of new disciplines such as applied informatics. The need to achieve autonomous production also means that quality control of the welding task carried out is also a significant concern [4]. In the meantime, human workers are also utilized [5]. The issues of compliance and standards of quality have become more prominent following adoption of the quality management principle [6].

The standard includes three distinct quality categories as well as indicates acceptability by the terms “*not permitted*” and “*permitted*”. The acceptability of a welded joint is based on the visible absence of defects in the weld and the adequacy of all the types of tests described in the relevant standard test procedure [4]. The basic physical principle of the various non-contact inspection tools,

which are successfully used in many industrial applications to detect quality non-conformities, relies on image recognition and image processing research. The future-oriented results of this research have also appeared in new fields such as face recognition by comparing three-dimensional objects or even in the development of image processing systems for self-driving cars [7, 8].

These applications have opened up new dimensions in the context of digitalisation, making industrial processes faster as well as easier and, therefore, more efficient [9]. Advanced image processing technologies are available in materials testing laboratories, helping researchers to study changes in material structures [10]. These methodological developments support the basic idea of digitisation, as they provide alternatives to the manual analysis of the past.

Structured light scanners work in a similar manner to laser scanners, but the light source is a high-resolution projector that projects a raster mesh onto the surface of the object. The optics measure both the reticle distortion and intensity of the reflected light, providing a much more accurate result than variants based on lasers - with a resolution of up to 10 microns. One possible solution for processing images from structured light scanners is to use the Iterative Closest Point (ICP) algorithm, which is used to create pairwise correspondences between two

\*Correspondence: [hj@inf.elte.hu](mailto:hj@inf.elte.hu)

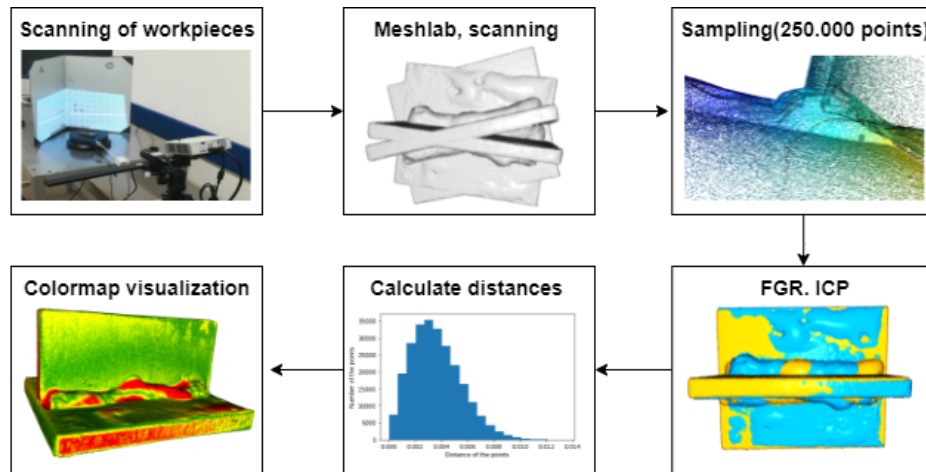


Figure 1: The steps of the proposed weld defect analysis method

cloud points. The method was developed in studies from the early 1990s by Besl and McKay [11] as well as Yang and Medioni [12]. This iterative algorithm is known in the field of matching three-dimensional shapes, a process in which the points of the source point cloud are matched to the points of the target point cloud (also known as the reference cloud). The matching is based on the root mean square error method, where originally a point-point metric was to be used, while other techniques use a point-plane metric [7].

In the following, the method is presented in Section 2, where sampling, point cloud generation, the use of the Fast Global Registration and ICP algorithm as well as the Root Mean Square Error is described. Finally, Section 3 presents the results of the developed framework.

## 2. The proposed CAD model-based method of the generation and analysis of error distributions

The proposed framework starts by scanning with a 3D scanner before reducing the number of points in the resulting point clouds. This is followed by a coarse and then a fine fitting, which uses a histogram containing a general comparison of the points and a colour map visualization. Its applicability in a specific technological field has been demonstrated. The objective is to investigate the weld geometry of selected welded samples using the available imaging tool to detect discrepancies. A point cloud is generated on the CAD models and the welded seams prepared using a camera system. The technique of matching point clouds by fast global registration is presented. An iterative closest point algorithm and a histogram of point features are used to perform the refined transformation. The comparison is carried out within a Python framework to solve the problem of matching the evaluation method to a neural network in topic processing. Finally, the deviations resulting from the comparison are evaluated in the light of the relevant standard.

The test method is illustrated in detail in Fig. 1. The

test starts by generating a reference point cloud, that is, a scanned point cloud of a welded workpiece (or a point cloud of a part created by CAD software), which is considered to be flawless. For the purpose of defect detection, the principle is to fit the original point cloud to the point cloud to be inspected, the geometry of which is nearly identical. As a second step, CAD models were created for which a single defect was modelled [13]. These defect modes were compared to the flawless CAD model. The analysis aims to obtain the deviations from the point cloud comparison in terms of the specific deviations and explore their correlations. The scanning process is as follows:

- When calibrating the tray, the grid is projected by the projector;
- Background scanning, after inserting a turntable;
- Positioning of the workpiece at the centre of the turntable;
- Start the scanning process;
- Create the three-dimensional model from the images;
- Fusion process from the image fragments can be exported in other (.stl/.obj) formats.

For optimal point matching, distance-based density distribution (sampling) is required. This is important because of the selected order of magnitude (250,000 points). The differences between the point clouds can be detected. An approximate - feature-based - registration, FGR (Fast Global Registration), is first performed based on the paired points to compare the two point clouds. This corresponds to an approximate estimate, which looks for similar corners, points and parts before pairing them. Although the approach used is faster than ICP, it still requires a local refinement algorithm. Since the performance is only flawless on a heavily sampled point cloud, a more accurate fitting procedure is also used to further refine the fitting. The ICP algorithm is a refined transformation that more closely aligns the two point clouds,

which usually iterates over two steps. First, a match is searched for from the target point cloud and then the transformation is updated by minimizing the objective function defined by the correspondence set.

The normal vector of a plane is the unit vector perpendicular to its plane and the normal vector is the vector perpendicular to the surface at a point on the surface. Calculating the normal vector of the point of detection involves a solution method based on the surface grid and a solution method based on the distribution of points in the surrounding neighbourhood. The axis, on which the normal vector is located, is the most dispersed direction of the neighbourhood distribution.

A final geometric feature is computed using the Point Feature Histogram (PFH), which is obtained by calculating the variation ratio between all pairs of points in the neighbourhood of the points. This high-dimensional space provides useful feature representations as well as can cope with different sampling densities and noise levels of neighbours. The PFH stores these variables together with the Euclidean distance between points and generates a histogram after computing all the pairs. The final descriptor is the sum of the histograms of each variable. Then, after selecting a percentage value (in this case 97%), a colour scale-based (green-near; red-distant) notation is applied according to the location of the pairs of points within a pixel distance of each other.

The deviation from the reference area is detected using the mean square deviation formula. The recommended setup parameters observed during the study and the results are detailed in the next section.

### 3. Results

A *Telwin Inverpulse 320* welding machine was used to create welded samples. 8 – 8 specimens, 50 mm long with  $a5$  welds (dimension of the height dimension of the triangle enclosing the corner weld), were T-welded. One side of the test specimens had a good weld configuration, while the other side had an unsatisfactory weld configuration. The welded samples were scanned using a *HP 3D Structured Light Scanner 5 Pro Edition* (software version 5.2.0.790) and the resulting point clouds compared to the point cloud of the reference part. It is important to note a few details about the 3D scanning process:

- Environmental preparation (from the projector light, from the harsh light in the room);
- System preparation (position the camera 6-8 cm to the left of the projector, adjust the camera angle to 10-12° from the guide rail perpendicular to the projector);
- Tripod adjustment up to 30° top view of the object.

In the second step of the test series, CAD models using the *Solid Edge Academic Edition* (version 221.00.00.114) were created for which a single defect was generated and compared to the flawless CAD model.

An algorithm running in Python (version 3.7.7) and using the Open3D (version 21.1.3) visualization interface was used to create a framework for the comparison. The study aims to determine the deviations from the point cloud comparison and to write correlations between them. The analysis method is similar to the first process step, but here no scanning process is required. The PFH in Fig. 2 indicates whether the points can be grouped according to their distribution or identified by their location.

The histogram shows the distances of the deviations. The typical distance values from the histogram data are expected to be close to the calculated deviation limits. A significant achievement in welding quality management is the application of the standard ISO 5817 : 2014, which lists surface and volume deviations with the display of defect categories and codes. The standard includes limits in three quality categories or indicates acceptability by the terms *not permitted* and *permitted*. The acceptability of a welded joint is based on the visible absence of defects in the weld and the adequacy of all the types of tests described in the relevant test procedure standard. The quality assessment of a welded joint is, therefore, a complex task.

As shown in Fig. 2, the evaluation is defined with different marginal deviations in each of the three quality categories (*B*, *C*, *D*). By progressing down to *BCD*, the standard becomes more permissive; for example, the height of the excessive convexity can be up to 3 mm for category *B*, up to 4 mm for category *C* and up to 5 mm for category *D*. The summary results for each of the three root sizes are as follows:

- 1. Crack: no borderline deviation is allowed in any category. However, for the test, a "brick body cavity" of 0.5 mm × 0.2 mm × 0.1 mm was created in the CAD model. The deviation could not be detected by the algorithm used;
- 2. Cavities: modelled as a 2 mm deep cone-shaped material void in category *D* and a 1 mm deep cone-shaped material void in category *C*. No deviation is allowed in category *B*. The deviation cannot be detected even by the most sensitive adjustments;
- 3. Solid inclusion: 1 mm in category *D*, 0.5 mm in categories *C* and *B*. The algorithm detects special distributions.

### 4. Summary

An image and data analyses-based method for the qualification of welding defects was developed. The corner welded joints were studied and the quality deviations of such welded joints observed, these deviations being defects that can be detected by visual inspection. For the detection of volumetric defects, the industry has practically and consistently used X-ray and ultrasonic testing. A results-oriented approach to the CAD visualisation of

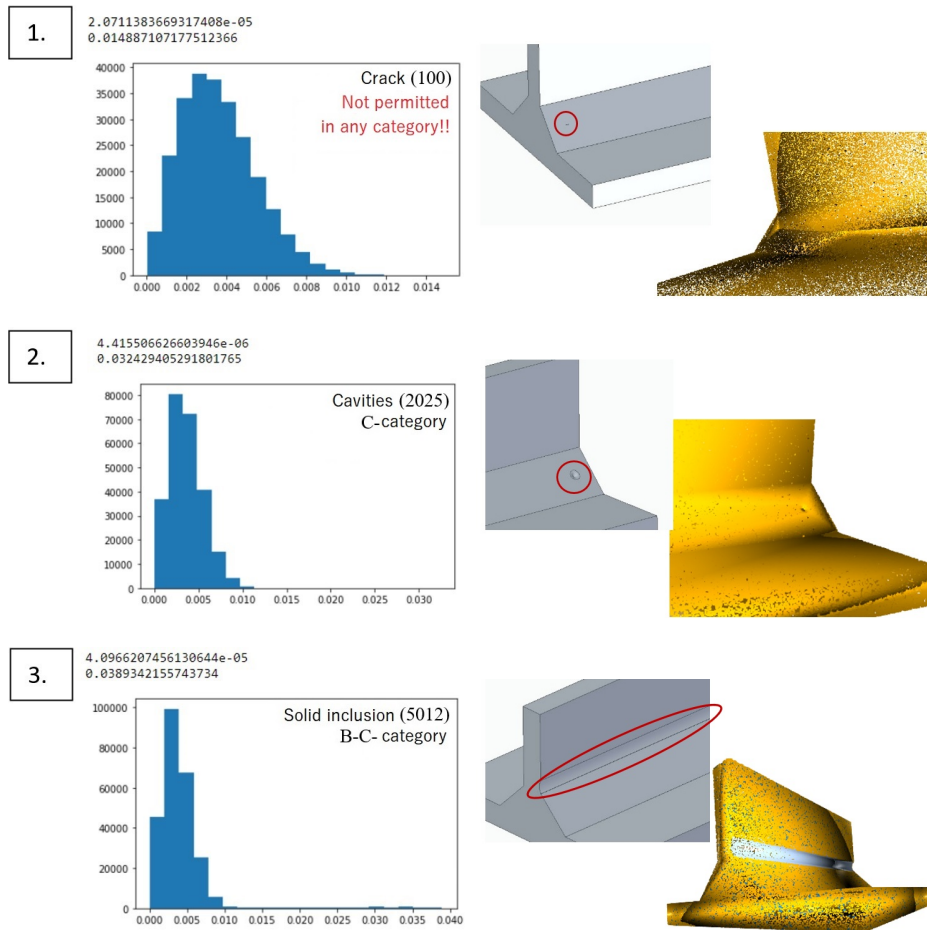


Figure 2: Exemplary distributions, CAD models of welding deviations .

defects has been adopted. Since several defects can occur on a real welded part, it can be said that by including CAD models of each deviation in the analysis, the deviations could be kept under control. Even though this tool alone cannot be used to perform a comprehensive analysis of a weld, when complemented with other procedures, the steps of the welding process analysis can be accelerated. Our investigations have led to the conclusion that, apart from defective joints, all the other categories of defects listed can be detected with certain limitations. The results, treated as differences between components of point clouds, can be subsequently identified and grouped.

## REFERENCES

- [1] Mishra, D.; Pal, S.K.; Chakravarty, D.: Industry 4.0 in Welding. *Welding Technology*, 2021, 253–298 DOI: [10.1007/978-3-030-63986-0](https://doi.org/10.1007/978-3-030-63986-0)
- [2] Farkas, A.: Impact of Industry 4.0 on robotic welding, XXIII International Conference on Manufacturing (Manufacturing 2018), *IOP Conf. Ser.: Mater. Sci. Eng.*, 2018, **448**, 012034 DOI: [10.1088/1757-899X/448/1/012034](https://doi.org/10.1088/1757-899X/448/1/012034)
- [3] Frolov, A.: Automation the Welding Trajectory Control. 2020 International Multi-Conference on Industrial Engineering and Modern Technologies (FarEastCon) (IEEE), 1–5 DOI: [10.1109/FarEastCon50210.2020.9271607](https://doi.org/10.1109/FarEastCon50210.2020.9271607)
- [4] Stavridis, J.; Papacharalampopoulos, A.; Stavropoulos, P.: Quality assessment in laser welding: a critical review. *Int. J. Adv. Manuf. Tech.*, 2018, **94**(5), 1825–1847 DOI: [10.1007/s00170-017-0461-4](https://doi.org/10.1007/s00170-017-0461-4)
- [5] Ruppert, T.; Abonyi, J.: Worker movement diagram based stochastic model of open paced conveyors. *Hung. J. Ind. Chem.*, 2018, **46**(2), 55–62 DOI: [10.1515/hjic-2018-0019](https://doi.org/10.1515/hjic-2018-0019)
- [6] László, S.: Hegesztés és rokon technológiák. *Gépipari Tudományos Egyesület, Budapest*, 2007, 191–204
- [7] Zhang, Z.: Iterative point matching for registration of free-form curves and surfaces. *Int. J. Comput. Vis.*, 1994, **13**(2), 119–152 DOI: [10.1007/BF01427149](https://doi.org/10.1007/BF01427149)
- [8] Lee, M.: An analysis of the effects of artificial intelligence on electric vehicle technology innovation using patent data. *World Pat. Inf.*, 2020, **63**, 102002 DOI: [10.1016/j.wpi.2020.102002](https://doi.org/10.1016/j.wpi.2020.102002)
- [9] Urminsky, J.; Marônek, M.; Jána, M.; Morovič, L.: Analysis of weld joint deformations by optical 3D scanning. *Acta Polytech.* 2016, **56**(1), 76–80 DOI: [10.14311/APP.2016.56.0076](https://doi.org/10.14311/APP.2016.56.0076)

- [10] Dastres, R.; Soori, M.: Advanced Image Processing Systems. *Int. J. Imaging Robot.*, 2021, **21**(1), 27–44 <https://hal.archives-ouvertes.fr/hal-03168963>
- [11] Wold, S.; Esbensen, K.; Geladi, P.: Principal component analysis, *Chemometr. Intell. Lab. Syst.*, 1987, **2**(1-3), 37–52 DOI: [10.1016/0169-7439\(87\)80084-9](https://doi.org/10.1016/0169-7439(87)80084-9)
- [12] Chen, Y.; Medioni, G.: Object modelling by registration of multiple range images. *Image Vis. Comput.*, 1992, **10**(3), 145–155 DOI: [10.1016/0262-8856\(92\)90066-C](https://doi.org/10.1016/0262-8856(92)90066-C)
- [13] Bęczkowski, R.; Gucwa, M.: Defects appearing in the surfacing layers of abrasion resistant. *Arch. Foundry Eng.*, 2016, **16**(4), 23–28 DOI: [10.1515/afe-2016-0077](https://doi.org/10.1515/afe-2016-0077)



## THE EFFECT OF THE CUTTING SPEED ON THE SURFACE ROUGHNESS WHEN BALL-END MILLING

ABDULWAHAB MGHERONY\*<sup>1</sup> AND BALÁZS MIKÓ<sup>1</sup>

<sup>1</sup>Institute of Materials and Manufacturing Sciences, Óbuda University, Népszínház u. 8, Budapest, 1081, HUNGARY

Using freeform surfaces in advanced industries is becoming ubiquitous and widely applied in many fields such as the aerospace, automobile, consumer products as well as the die and mold industries. The ball-end mill is mainly used in machining such surfaces. However, the manufacture of this type of surface is still somewhat difficult when machining using a 3D ball-end milling machine. Due to changes in the surface inclination, the working diameter of the tool also changes. Variations in the working diameter leads to an unstable cutting speed, affecting the roughness homogeneity of the smoothed surface. This article discusses the effect of changing the cutting speed on the surface roughness in the case of concave and convex surfaces.

**Keywords:** surface roughness, cutting speed, concave surface, convex surface, milling

### 1. Introduction

The implementation of ball-end mills has become widespread in manufacturing, especially in high-speed machining processes. The extended product life, high-precision machining, low cost of the manufacturing process, its ability to feed axially and the unique shape of the cutting edge (Helix-type, S-type, etc.) of this tool mean it plays a vital role in machining freeform surfaces [1]. However, when freeform surfaces are machined using a ball-end mill, the working diameter of the tool continuously varies as the surface inclination changes, despite the constant toolpath. Using a five-dimensional milling machine can solve this problem. However, due to its high cost and difficulties associated with installing this machine at many workstations, 3D milling machines are still common.

Radhwan et al. [2] studied the effect of various cutting parameters, including cutting speed, feed rate and depth of cut on the surface roughness. Their findings show that the cutting speed and feed rate have significant effects on the surface roughness. Wojciechowski et al. [3] analyzed the forces and process efficiency whilst machining hardened 55NiCrMoV6 steel using ball-end milling. Their results indicate that the surface inclination has a significant effect on the cutting forces. Mersni et al. [4] used the Taguchi method to optimize the milling parameters to obtain a better surface finish using ball-end milling of a titanium alloy Ti-6Al-4V. They point out that the radial depth of cut ( $a_p$ ) is the most

important factor followed by the cutting speed ( $v_c$ ) and then the feed per tooth ( $f_z$ ). Yao et al. [5] studied the influence of the tool orientation on the surface of the TC17 titanium alloy. Their findings emphasize the importance of tool orientation on surface roughness during ball-end milling. Similarly, Gao et al. [6] investigated the effect of the tool inclination angle on the surface roughness while machining the titanium alloy Ti-6Al-4V using a ball-end mill. They point out that tilting the tool has a significant effect on the quality of the grooveS and using the appropriate inclination angle can reduce the roughness of the surface and improve its form. Vyboishchik [7] presented a geometric model of the surface topology in the case of flat, concave (CV) and convex (CX) surfaces. According to this model, the surface inclination has a significant effect. Matras and Zębala [8] optimized the cutting data and tool path pattern for machining the freeform surface of steel in a hardened state using a ball-end mill. The results show that the surface roughness and cutting-force components can be controlled by modifying the feed rate based on the locally machined cross-sectional area. Magalhães and Ferreira [9] used different tool path strategies to machine parts with complex geometries from hardened H13 steel. Their findings show that the tool path has a significant effect on the roughness of the complex surface. Daymi et al. [10] highlighted the importance of the inclination angle in ball-end milling when machining the titanium alloy Ti-6Al-4V.

This research investigates the effect of changing the surface inclination on the cutting speed and the

\*Correspondence: [mgherony.abdulwhab@uni-obuda.hu](mailto:mgherony.abdulwhab@uni-obuda.hu)

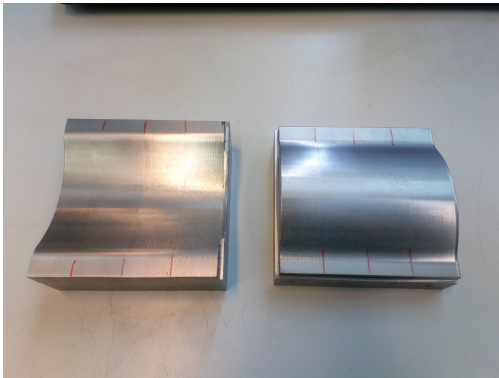


Figure 1: The CV and CX workpieces

consequences of a variable cutting speed on the surface roughness as well as provides an insight into the importance of the feed rate and width of cut on the machining process when using a 3D ball-end mill.

## 2. Materials and Methods

The machining tests were performed on CV and CX surfaces of the same material, namely the low-alloy steel 42CrMo4. 42CrMo4 is used to manufacture parts with high-TENSILE strengths of compressors, turbines and working elements of heavy equipment used aboveground and underground as well as components of agricultural machinery. The chemical composition of 42CrMo4 is given in Table 1.

The CV and CX parts consist of a cylindrical surface with a 45 mm radius connected to a horizontal plane with a 10 mm radius. Fig. 1 shows both workpieces and Table 2 shows the angles of the normal vector of the surface.

The machining was performed by a Mazak Vertical Center Nexus 410A-II CNC vertical machining centre. The surface roughness was measured by a Mahr's MarSurf GD120 instrument. The Ra and Rz parameters were measured in the  $x$ -direction perpendicular to the milling direction at 11 different positions. The milling was done using a Fraisa X7450.450 ball-end milling cutter with a diameter of 10 mm ( $D_c = 10$  mm) and 4 teeth ( $z = 4$ ).

Five test surfaces were created by ball-end milling with different feed rates and widths of cut. Table 3 shows the applied cutting parameters in machining these surfaces.

Since the surface inclination changes, the effective diameter also changes. A geometrical model is presented by Mikó and Zentay [11] to calculate the effective diameter. Fig. 2 shows the calculated effective diameter at each measured point in the case of the CV and CX workpieces.

The actual cutting speed can be calculated depending on the effective diameter at each measured point using the following formula:

$$v_c = \frac{D_{\text{eff}} n \pi}{1000} \quad (1)$$

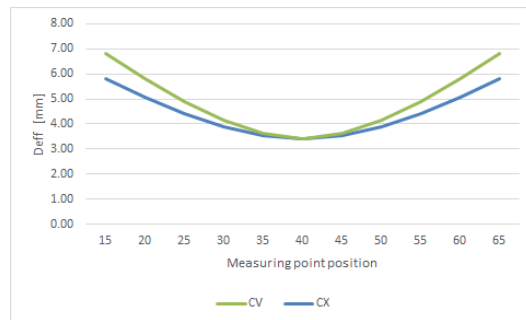


Figure 2: The Effective diameters at each measured point

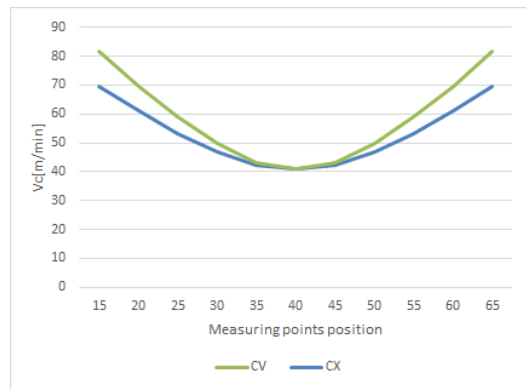


Figure 3: The actual cutting speed at each measured point

Figs. 2 and 3 show the effective diameter and actual cutting speed. Even though the diameter of the tool is 10 mm, the actual cutting diameter is smaller. In the case of the CV surfaces, it changes between (3.4 and 6.8 mm), while in the case of the CX surfaces, it changes between (3.4 and 5.8 mm). On the other hand, the effective diameter and, as a result, the cutting speed are the smallest in the middle of the workpieces, where the value of the normal vector is  $0^\circ$ . In addition, although it can be seen from Fig. 3 that the value of the cutting speed is higher in the case of the CV surfaces compared to the CX equivalents, the cutting speed curve is similar for both CV and CX test parts.

## 3. Results and Discussion

Fig. 4 shows the average surface roughness of the test pieces. The diagram shows that the surface of the CV test parts is better than that of the CX test parts under the same cutting parameters, as the actual cutting speed in the case of CV surfaces is higher than that of the CX equivalents.

On the other hand, when the feed rate is 0.08 mm and the width of cut is 0.35 mm, the surface roughness is the worst for both CV and CX surfaces.

The surface roughness of the workpieces was measured at several points. The results show that the surface inclination has a significant effect on the surface roughness, as can be seen in Figs. 5–9, since the quality of the surface is less at the middle of the test pieces where the cutting speed is at its minimum.

Table 1: Chemical composition of the low-alloy steel 42CrMo4: (analysis in %)

C	Si	Mn	P	S	Cr	Mo	Cu
0.38 – 0.45	0.1 – 0.4	0.6 – 0.9	≤ 0.025	≤ 0.035	0.9 – 1.2	0.15 – 0.3	≤ 0.4

Table 2: Angles of the normal vector of the surface

Measuring points (y)	25	20	15	10	5	0	5	10	15	20	25
CX angles (°)	30	23.58	17.46	11.54	5.74	0	-5.74	-11.54	-17.46	-23.58	-30°
CV angles (°)	-38.7	-30	-22	-14.5	-7.2	0	7.2	14.5	22	30	38.7

Table 3: Cutting parameters used in the test

Test part id.	CV-01	CV-02	CV-05	CV-03	CV-04
	CX-01	CX-02	CX-05	CX-03	CX-04
Cutting speed $v_c$ [m/min]	160				
Spindle speed $n$ [rpm]	5100				
Feed per tooth $f_z$ [mm]	0.08	0.08	0.08	0.12	0.16
Feed speed $v_f$ [mm/min]	1630	1630	1630	2450	3260
Depth of cut $a_p$ [mm]	0.3				
Width of cut $a_e$ [mm]	0.35	0.25	0.15	0.15	0.15

In the case of CX-01 and CX-02, the surface roughness is worse than on the other three pieces. On these two pieces, Rz is approximately 16  $\mu\text{m}$  at the middle compared to 10  $\mu\text{m}$  at the middle of the other pieces.

In the case of the CV pieces, CV-05 exhibits the best

surface roughness and the value of Rz is less than 6  $\mu\text{m}$  at the middle, while it is approximately 12  $\mu\text{m}$  on the other pieces.

This variation in the surface roughness from piece to piece is due to changes in the feed rate and width of cut. The feed rate is at its minimum when machining CX-01

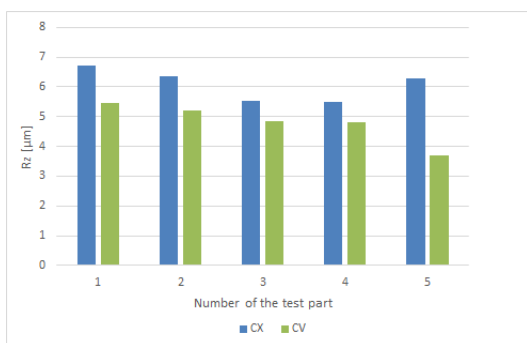


Figure 4: Average Rz of each test parts

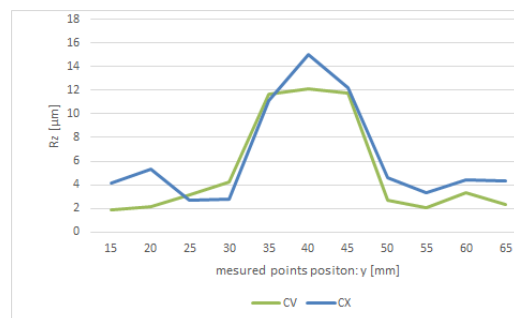


Figure 6: Rz surface roughness in the case of CX-02 and CV-02

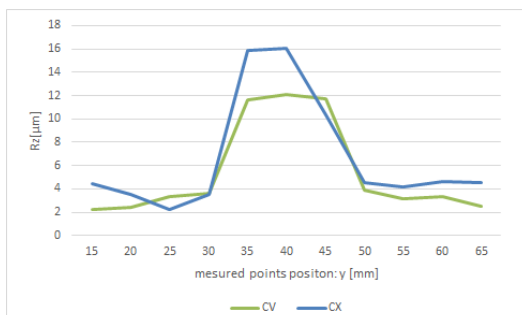


Figure 5: Rz surface roughness in the case of CX-01 and CV-01

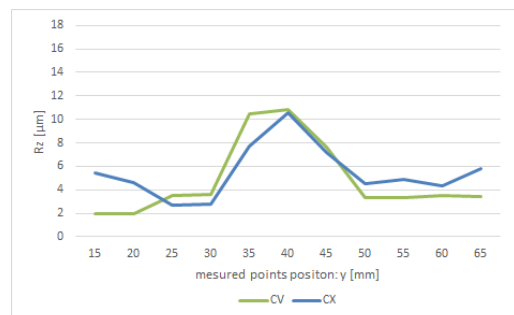


Figure 7: Rz surface roughness in the case of CX-03 and CV-03

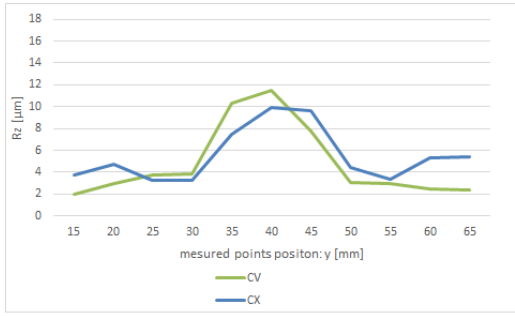


Figure 8: Rz surface roughness in the case of CX-04 and CV-04

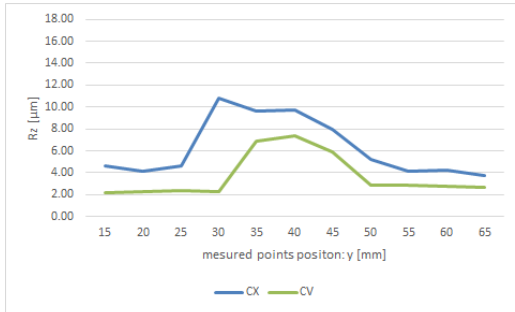


Figure 9: Rz surface roughness in the case of CX-05 and CV-05

and CV-01 but increases to its maximum when machining CX-04 and CV-04. However, the width of cut decreases gradually to its minimum when machining CX-04 and CV-04.

Figs. 10 and 11 show the main effect of changing the width of cut and feed rate on the surface roughness in the case of CV and CX surfaces. As is shown, the width of cut has a significant effect on the surface roughness. By increasing the width of cut, the Rz value of surface roughness increases. On the other hand, the feed rate has a minor effect on the surface roughness, especially in the case of CV surfaces.

The actual cutting speed and the effective diameter have exactly the same effect on the surface roughness, as can be seen in Figs. 12 and 13. The Rz value of surface roughness decreases by increasing the effective diameter and the cutting speed. However, in the case of CX surfaces, the roughness of the surface increases again by about 1 µm at a cutting speed of 70 m/min.

#### 4. Conclusion

In this article, the effect of the cutting speed on surface roughness has been studied. Based on the obtained data, under the same cutting parameters, the surface roughness of the CV test parts is better than that of the CX equivalents. However, changes in the surface inclination cause the actual cutting speed to vary, which affects the surface quality. The cutting speed reduces to a very low value when the normal axis of the ball-end mill is applied on the workpiece surface. Given that the

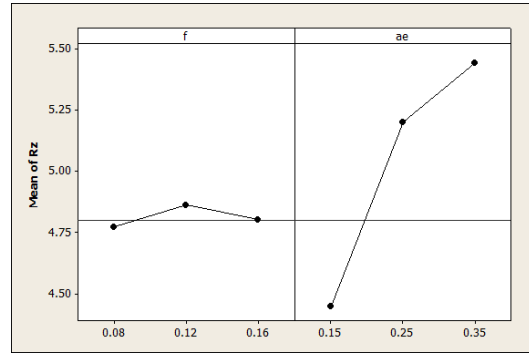


Figure 10: The effect of the width of cut and feed rate in the case of CV surfaces

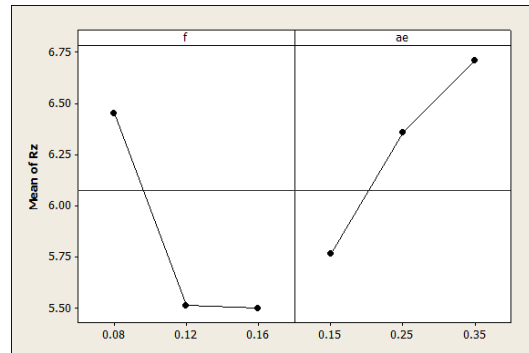


Figure 11: The effect of the width of cut and feed rate in the case of CX surfaces

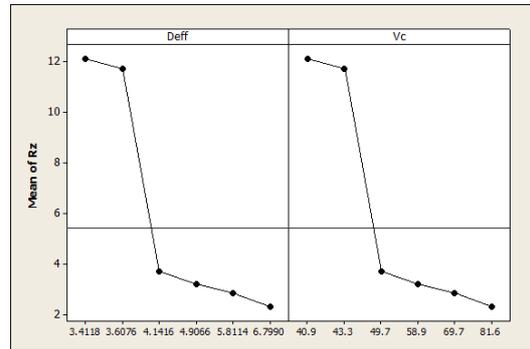


Figure 12: The effect of the effective diameter and actual cutting speed in the case of CV surfaces

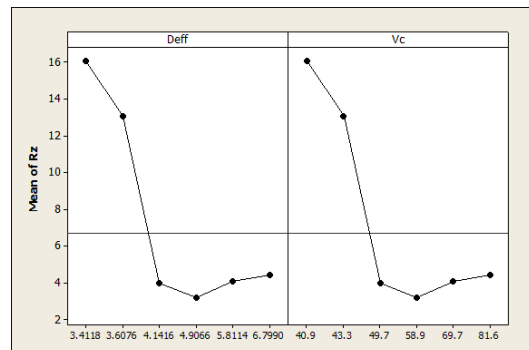


Figure 13: The effect of the effective diameter and actual cutting speed in the case of CX surfaces

variation in cutting speed is a major problem in the case of 3-axis milling machines, modifying the cutting speed during the milling process can solve this problem and ensure a higher surface quality.

On the other hand, the surface roughness depends on other cutting parameters as well such as feed rate and width of cut. It has been determined that by increasing the width of cut, the surface roughness is increased, while changing the feed rate only has a minor effect.

### Acknowledgment

This publication was financed by the National Research, Development and Innovation Fund under project 2018-1.3.1-VKE-2018-00041.

### REFERENCES

- [1] Chang, L.: A Parametric Design of Ball End Mill and Simulating Process (Concordia University), 2016
- [2] Radhwan, H.; Sharif, S.; Shayfull, Z.; Suhaimi, M.; Khushairi, M.M.; Najmi, M.: Optimization of cutting parameters for surface roughness in ball end milling of aluminium epoxy using Taguchi method. *AIP Conference Proceedings*, **2129**(1), 020156 DOI: [10.1063/1.5118164](https://doi.org/10.1063/1.5118164)
- [3] Wojciechowski, S.; Maruda, R.; Barrans, S.; Nieslony, P.; Krolczyk, G.: Optimisation of machining parameters during ball end milling of hardened steel with various surface inclinations. *Measurement*, 2017, **111**, 18–28 DOI: [10.1016/j.measurement.2017.07.020](https://doi.org/10.1016/j.measurement.2017.07.020)
- [4] Mersni, W.; Boujelbene, M.; Salem, S.B.; Alghamdi, A.S.: Optimization of the surface roughness in ball end milling of titanium alloy Ti-6Al-4V using the Taguchi Method. *Procedia Manuf.*, 2018, **20**, 271–276, 2nd International Conference on Materials, Manufacturing and Design Engineering (iCMMD2017), 11-12 December 2017, MIT Aurangabad, Maharashtra, India DOI: [10.1016/j.promfg.2018.02.040](https://doi.org/10.1016/j.promfg.2018.02.040)
- [5] Yao, C.; Tan, L.; Yang, P.; Zhang, D.: Effects of tool orientation and surface curvature on surface integrity in ball end milling of TC17. *Int. J. Adv. Manuf. Technol.*, 2018, **94**(5), 1699–1710 DOI: [10.1007/s00170-017-0523-7](https://doi.org/10.1007/s00170-017-0523-7)
- [6] Gao, P.; Wang, X.; Liang, Z.; Zhang, S.; Zhou, T.; Yan, P.; Jiao, L.: Effects of machining inclination angles on microgroove quality in micro ball end milling of Ti-6Al-4V. *Int. J. Adv. Manuf. Technol.*, 2017, **92**(5), 2725–2734 DOI: [10.1007/s00170-017-0305-2](https://doi.org/10.1007/s00170-017-0305-2)
- [7] Vyboishchik, A.: Modelling Topology of Freeform Surfaces with Ball-end Milling. *Procedia Eng.*, 2016, **150**, 761–767, 2nd International Conference on Industrial Engineering (ICIE-2016) DOI: [10.1016/j.proeng.2016.07.103](https://doi.org/10.1016/j.proeng.2016.07.103)
- [8] Matras, A.; Zębala, W.: Optimization of Cutting Data and Tool Inclination Angles During Hard Milling with CBN Tools, Based on Force Predictions and Surface Roughness Measurements. *Materials*, 2020, **13**(5), 1109 DOI: [10.3390/ma13051109](https://doi.org/10.3390/ma13051109)
- [9] Magalhães, L.C.; Ferreira, J.C.E.: Assessment of tool path strategies for milling complex surfaces in hardened H13 steel. *Proc. Inst. Mech. Eng. B*, 2019, **233**(3), 834–849 DOI: [10.1177/0954405418755824](https://doi.org/10.1177/0954405418755824)
- [10] Daymi, A.; Boujelbene, M.; Linares, J.; Bayraktar, E.; Amara, A.B.: Influence of workpiece inclination angle on the surface roughness in ball end milling of the titanium alloy Ti-6Al-4V. *J. Achiev. Mater. Manuf. Eng.*, 2009, **35**(1), 79–86 [http://jamm.acmsse.h2.pl/papers\\_vol35\\_1/35110.pdf](http://jamm.acmsse.h2.pl/papers_vol35_1/35110.pdf)
- [11] Mikó, B.; Zentay, P.: A geometric approach of working tool diameter in 3-axis ball-end milling. *Int. J. Adv. Manuf. Technol.*, 2019, **104**(1), 1497–1507 DOI: [10.1007/s00170-019-03968-9](https://doi.org/10.1007/s00170-019-03968-9)



## STUDY ON THE PHOTO-BASED 3D SCANNING PROCESS

ÁLMOS KRISTÁLY\*<sup>1</sup> AND PÉTER FICZERE<sup>1</sup>

<sup>1</sup>Department of Railway Vehicles and Vehicle System Analysis, Budapest University of Technology and Economics, Műegyetem rkp. 3, Budapest, 1111, HUNGARY

The experiment aims to determine the practical applicability of photo-based 3D scanning technologies. With the help of computer software, 3D printable, simulation-ready models are created from regular photographs. The accuracy and consistency of such models are evaluated regarding usability engineering.

**Keywords:** 3D modelling, 3D scanning, photo-based 3D models

### 1. Introduction

With the development of manufacturing and modelling technologies, more and more complex geometries can be created. At the beginning of the 20th century, point-perfect shop drawings were used for production. Nowadays, computer numerical control (CNC) is used exclusively for the control of machine tools worldwide. CNC codes can be generated directly from digital 3D geometries (CAD models, Fig. 1) and immediately sent to the machine tool via online connected systems.

CAD models are created based on planned or measured dimensions. Although this method is faster than handmade shop drawings, a complex CAD model can still take months to create from scratch.

A more straightforward method is reverse engineering, during which all data necessary for simulation or manufacturing is documented from an already existing part [1]. Planning is unnecessary; for the purpose of creating the CAD model, it is sufficient to measure the part. Difficulties can occur in the case of spherical, parabolic or other irregular surfaces that are hard to measure.

3D scanning technologies substantially simplify this process. Since the 1960s, numerous methods have been invented [2]. At first, contact probes were used to measure each point of a surface, which were then saved as coordinates with regard to the machine coordinate system. Later on, optical methods were developed. By photographing an object from two different positions, the respective focal lengths can be compared to determine the dimensions of the object. A more advanced method uses laser beams and sensors to calculate these lengths based on the speed of the beam and the duration of the reflection from the surface. The



Figure 1: CAD model of the shell of a handheld game console.

current position of the device is also required [2]. None of these methods requires physical contact with the object.

Today, 3D scanning devices fit in our pockets: numerous smartphones and pieces of computer software are available that can create 3D models based on photos. Entry-level, free software typically offers cloud-based processing that may take days to finish. In order to access higher-end, engineering-level software, a subscription must be taken out, however, instant results are provided.

At least 40 photos are required to model the geometry - the more photos, the better the result. Photos should be taken from roughly equiangular positions on a circle with a 30 – 300 cm radius around the object in a static environment. The software overlaps the photos based on the surroundings of the target object (like pieces of a jigsaw puzzle), ultimately creating a three-dimensional replica of the environment with the

\*Correspondence: [almos99@freemail.hu](mailto:almos99@freemail.hu)



Figure 2: Rubbish bin and garden chair.

object in the middle.

This technology is applied in practice to map nature reserves [3], to investigate crime and accident scenes [4], as well as in medical and production technologies [5].

## 2. Experiment

The piece of software “Autodesk ReCap Photo” was used with an educational license to generate models during the experiment. The accuracy of their size, shape and ratio was evaluated, along with their potential practical applications. However, this strongly depends on the type of usage and an accuracy within a range of 1 – 2 % is generally expected [6].

The photos were taken with a 16-megapixel smartphone camera. The software supports both landscape and portrait image orientations. Model generation is cloud-based, meaning powerful hardware is not required, however, a processing time of 20 – 70 hours should be expected.

Models are generated by the aforementioned overlaying principle. The more photos there are, the more accurate the layering and, therefore, the model itself will be [7]. A total of 4 objects of different sizes and complexities were modelled. The experiments and their results are presented below.

The first objects that were attempted to be modelled were a plastic rubbish bin and a garden chair (Fig. 2).

Photos were taken from both sides and above. The photographic parameters used are summarized in Table 1. Since the photos were taken outdoors, a heightened level of attention was needed to include any moving objects (tree branches, cats, birds, etc.) in the photos as well as achieve consistent lighting and minimal shading or glistening off the surfaces. These distractions had a negative effect on the generated model. The results (cut and positioned) can be seen in Fig. 3.

Table 1: Photographic parameters.

Object	Distance from camera	Number of photos
rubbish bin	120 – 150 cm	49
garden chair	120 – 150 cm	40



Figure 3: Models of the rubbish bin and garden chair.

The bottom parts of the models are visibly inaccurate and hollow since no information was present in the photos. The model of the rubbish bin is specifically inaccurate around the wheels and a minimal degree of waviness of the side panels can be observed. The model of the garden chair features one large and several smaller holes on the back, supposedly as a result of its thin structure, inappropriate lighting and shades.

Nevertheless, the fundamental shapes and details are present, significantly reducing the post-processing time to create a perfect model compared to manual measurements and modelling from scratch.

Although the models are highly detailed, a high level of accuracy and rational dimensions are also crucial for practical applications. A rectangular box was used to determine the accuracy of the software. The box along with its dimensions can be seen in Fig. 4.

Once the project has been processed, the model can



Figure 4: Rectangular box with dimensions used to validate the level of accuracy.

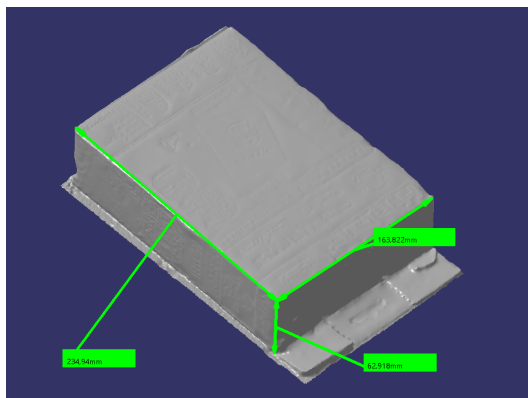


Figure 5: Generated dimensions.

be edited directly from ReCap Photo. It is possible to move, rotate or remove parts of the object. A dimension can be set manually between two arbitrary points, after which all the dimensions are calculated by the software proportionally. The model can then be exported in various polygon mesh formats and imported into various pieces of CAD software for post-processing. Dassault Systèmes’ CATIA software was used to measure the generated dimensions. The results can be seen in Fig. 5.

The comparison between the actual and generated dimensions is presented in Table 2.

As can be seen in Table 2, the most significant deviation is  $-4.863\%$ . However, this is the only dimension in connection with the deformed bottom surface, the geometry of which is inaccurate due to the photography. The deviation in the other two directions is under  $1\%$ ; this accuracy is acceptable in most branches of engineering. In the case of a significant practical application, a higher-quality camera should be used to achieve better photographs as well as a pedestal to prevent any surfaces from touching the ground, thereby achieving an exponentially higher-quality model.

As a final project, an attempt was made to model an automobile and a motorcycle. These objects include extensive, complex geometries and irregular, glistening, transparent surfaces, which pose a challenge for the software. Photos of both vehicles and the generated models can be seen in Figs. 6 and 7, respectively.

Several faults can be observed in the models. The roof of the car is inaccurate due to the lack of top view photos. The windows are not smooth and its surface is wavy in certain areas as if it was “molten”. This can also



Figure 6: Photographs of the automobile and the motorcycle.



Figure 7: Generated models of the automobile and the motorcycle.

Table 2: Comparison between the actual and generated dimensions.

Actual dimensions	Generated dimensions	Difference (mm)	Difference (%)
235 mm	234.94 mm	0.06 mm	0.0256 %
165 mm	163.822 mm	1.178 mm	0.714 %
60 mm	62.918 mm	2.918 mm	$-4.863\%$

be seen on the motorcycle, along with the inaccuracy of the tires, especially on areas close to the ground. Despite these faults, the main shapes and ratios are maintained. Modifying these models by post-processing is more straightforward and quicker than creating one from scratch.

### 3. Conclusion

With the development of 3D printing, an increased emphasis is being placed on reverse-engineering technologies to quickly and efficiently copy existing geometries either for the purpose of recreation or simulations. Photo-based 3D scanning software play a crucial role in simplifying and drastically shortening this process, offering an economical, quick and space-saving alternative to traditional 3D scanning devices. The method can be used outside of engineering applications, e.g., in medicine to create custom implants and prostheses or in accident scene investigation by running simulations on the modelled wreckage. The study shows that the accuracy of ReCap Photo is sufficient for these applications, offering expert solutions in various fields.

### REFERENCES

- [1] Rekoff, M.G.: On Reverse Engineering, *IEEE Trans. Syst. Man Cybern.*, 1985, **15**(2), 244–252 DOI: [10.1109/TSMC.1985.6313354](https://doi.org/10.1109/TSMC.1985.6313354)
- [2] Edl, H.; Mizerák, M.; Trojan, J.: 3D Laser Scanners: History and Applications. *Acta Simulatio*, 2018, **4**(4), 1–5 DOI: [10.22306/asim.v4i4.54](https://doi.org/10.22306/asim.v4i4.54)
- [3] Remondino, F.: Heritage Recording and 3D Modeling with Photogrammetry and 3D Scanning. *Remote Sensing*, 2011, **3**(6), 1104–1138 DOI: [10.3390/rs3061104](https://doi.org/10.3390/rs3061104)
- [4] Barazzetti, L.; Sala, R.; Scaioni, M.; Cattaneo, C.; Gibelli, D.; Giussani, A.; Poppa, P.; Roncoroni, F.; Vandone, A.: 3D scanning and imaging for quick documentation of crime and accident scenes. *Sensors, and Command, Control, Communications, and Intelligence (C3I) Technologies for Homeland Security and Homeland Defense XI*, Ed. Carapezza, E.M., 2012, **8359**, 208–221 DOI: [10.1117/12.920728](https://doi.org/10.1117/12.920728)
- [5] Ciobanu, O.; Xu, W.; Ciobanu, G.: The Use of 3D Scanning and Rapid Prototyping in Medical Engineering. *Fiability & Durability*, 2013, **1**, 241–247 ISSN: 1844-640X
- [6] Mankovits, T.; Szabó, T.; Kocsis, I.; Páczelt, I.: Optimization of the shape of axi-symmetric rubber bumpers. *Stroj. Vestn.-J. Mech. E.*, 2014, **60**(1), 61–71 DOI: [10.5545/sv-jme.2013.1315](https://doi.org/10.5545/sv-jme.2013.1315)
- [7] Fedorko, G.; Stanova, E.; Molnar, V.; Husakova, N.; Kmet, S.: Computer modelling and finite element analysis of spiral triangular strands. *Adv. Eng. Softw.*, 2014, **73**, 11–21 DOI: [10.1016/j.advengsoft.2014.02.004](https://doi.org/10.1016/j.advengsoft.2014.02.004)

## WEIGHT REDUCTION OF A DRONE USING GENERATIVE DESIGN

BÁLINT LEON SEREGI\*<sup>1</sup> AND PÉTER FICZERE<sup>1</sup>

<sup>1</sup>Department of Vehicle Elements and Vehicle-Structure Analysis, Budapest University of Technology and Economics, Műegyetem rkp. 3, Budapest, 1111, HUNGARY

Generative design has the potential to be optimized with different parameters using a design method based on artificial intelligence and by defining the design problem. The use of this method on a drone frame is presented with explanations of the various design phases. The goal of the optimisation was to be able to fit a battery with a larger capacity onto the Unmanned Aerial Vehicle and compensate for its increased weight by reducing the weight of the drone frame using a generative algorithm. As the production possibilities were limited, adaptation to the selected manufacturing technology was also taken into account during the optimization.

**Keywords:** generative design, additive manufacturing, weight reduction

### 1. Introduction

Mechanical design is a complex process. Engineers not only design a construction to meet functional and safety requirements, but also have to take into consideration the costs, functional expectations, safety, usage needs, lifespan and manufacturability. That is why the most optimal design, which appropriately fulfils every need, must be selected from several versions when designing a product. The spread of rapid prototyping facilitates the rapid creation and testing of these versions. In connection with this, the phenomenon of the design paradox can be observed, which concerns the relationship between product knowledge and design decisions over time as a function of the product from its design to production (Fig. 1). [1] This engineering influence has an outstanding effect on costs, mainly during the design phase and the production preparation process. If an error in the product concept is revealed during the testing phase immediately before production, its reworking increases costs significantly.

Rapid prototyping is suitable for eliminating this paradox. The main reasons for this are that it

- makes communication during the design phase with faster iterations more effective;
- reduces the development time;
- reduces the likelihood of costly errors (hidden design errors) and those following the release of the product from occurring;
- extends the product life cycle by adding required and eliminating unnecessary features early on in the design phase;

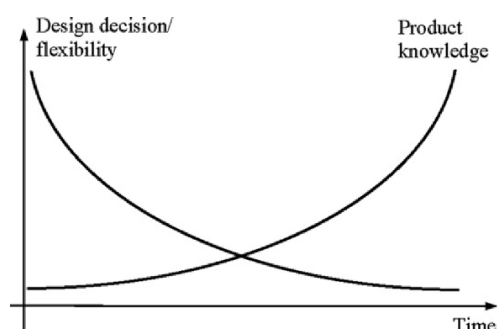


Figure 1: The design paradox[1]

- can avoid design flaws from occurring early on, even in the concept phase.

The generative design is a great solution to lower this influence by making many versions. These outcomes all meet the given requirements (if any one of them cannot be achieved, the algorithm stops as a result of a failure). Usually the generative design concerns automotive applications where one or more components are merged into one solid component, thereby also reducing the weight. This is obvious from a transportation point of view since it can reduce the environmental impact by reducing fuel consumption and using less raw materials. For instance, General Motors (GM) optimized their seat bracket, which is a standard component that fixes the seat and seat belt lock to the car's floor. While previously this bracket consisted of 8 components, generative software could come up with more than 150 organic-looking outcomes (Fig. 2). The chosen outcome by GM was 40% lighter and 20% stiffer than the original design. [2]

\*Correspondence: [seregibalint@edu.bme.hu](mailto:seregibalint@edu.bme.hu)



Figure 2: The original and the generative concept [2]

Additive manufacturing is very different from its predecessor, that is, subtractive manufacturing. Over the history of machining, as a result of Computer Numerical Control, technology has made great strides in terms of efficiency, productivity and accuracy. 5-axis machines as well as 6-axis robotic arms have also appeared, which in the case of the tool and material to be machined are the limiting factors. There are geometries which cannot be produced even by 6-axis robotic arms as the tool simply does not fit in some concave areas. For harder materials that are difficult to machine, a tool made of a stronger material is required, which must be specially designed with customised machining parameters. Furthermore, depending on the amount of material deposited, the chips as loss are displayed. [3]

To demonstrate the reduction in weight as a result of generative design, a small-scale drone frame was optimized. The goal was to create a small flying Unmanned Aerial Vehicle (UAV) with a generative designed frame that reduces the overall weight of the vehicle as the maximum speed and range of UAVs strongly depend on the performance of their motors and their overall weight. The weight of the battery cannot be reduced because decreasing its capacity would also shorten its available range. Therefore, the weight of the frame had to be reduced just as a larger battery with a greater capacity would have had to have been, thereby increasing its range. Concerning the size of the motors, the acquirement of high-performing and small ones on the commercial market is preferred. Its electronics and control consist of the Electronic Speed Controller, PXFmini autopilot card and a Raspberry Pi Zero. The PXFmini autopilot card contains the basic sensors, e.g., a compass, GPS and barometer, which are connected to the onboard computer, that is, the Raspberry Pi. This electronics stack can facilitate basic functions like stabilization and RC communication.

## 2. Methodology

As the combined performance of its four motors can lift 2800 grams in total, this equates to the critical weight of the UAV during the design phase. Its weight without the frame (the electronics, motors and battery) is 404 grams. This is 1/7 of the critical weight which means that the vehicle can achieve higher speeds and accelerations, moreover, the energy consumption can also be

Table 1: Mechanical parameters of ABS [4]

Young's modulus [GPa]	2.2
Tensile strength [MPa]	30
Density [g/cm <sup>3</sup> ]	1.1
Poisson's ratio	0.4

more favourable especially with the reduced weight of the frame. The frame is composed of the plastic Acrylonitrile Butadiene Styrene (ABS), the parameters of which can be seen in Table 1. These mechanical parameters were used during its generation.

First, the basic concept must be created. The electronics can be placed in stacks as a block thanks to their dimensions (Fig. 3).

The battery was placed under the electronics stack 38 millimetres from the plane of the motors to somewhat increase its in-flight stability. During the design phase, a basic model is required to determine the preserve and obstacle geometries, loads and constraints. The preserve geometry means the volume that cannot be modified by the algorithm (Fig. 4). The loads and constraints can be determined on the following areas; in this case the mounting discs of the motors and mounting rails of the electronics. The obstacle geometry is the volume within which the algorithm is not allowed to place material (Fig. 5), since it is a placeholder for other components like bolts, batteries and motors. The constraints and loads were defined in different load cases which simulate the lift, weight force of the battery and three crash-landings from different angles. Specifying design criteria is also mandatory.

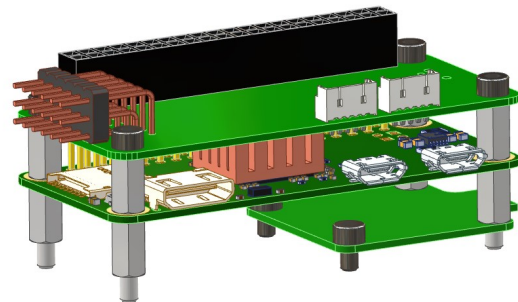


Figure 3: The electronics stack

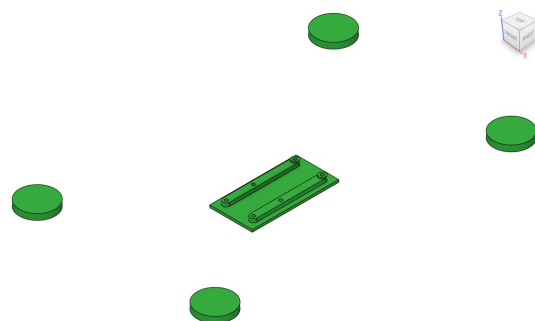


Figure 4: Preserve geometry

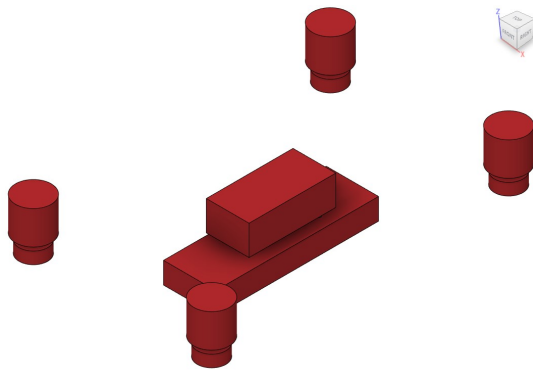


Figure 5: Obstacle geometry

Although by default the program is set to minimize the mass, it is possible to specify a specific target mass with a safety factor. In addition, the manufacturing technology can be specified to optimize the result and meet needs. The available options are 2.5 – 5 axis cutting, additive fabrication, casting and indefinite. The indefinite option differs in that it does not take into account the limiting factors of the technologies such as the smallest tool diameter or tool overhang for cutting, alternatively, in the case of additive manufacturing, the manufacturing direction, orientation and maximum overhang angle of the workpiece. During one run, several technologies can be selected according to needs. The weight reduction was set with a target mass of 84 grams and safety factor of 1.2.

### 3. Investigation

Using Fusion 360's generative design algorithm, 6 different results were generated, from which the most optimal frame was chosen (Table 2). The reason for the 6 results is the possibility of different build directions (a key parameter in additive manufacturing), which the program also takes into account and the given model is once more iterated based on this. The generative model generated by the preserve geometry can be seen where the algorithm did not remove any volume and the robotic arms were reduced to smaller robotic arm braces. The amount of weight reduction made it possible to use a battery with a larger capacity that lengthens the flight time. The basic concept was fitted with a 2200 mAh battery. From this product family, the next largest capacity of the battery is 2650 mAh. The smaller and larger batteries weigh 168 grams and 232 grams, respectively. Compared to the orig-

Table 2: Parameters of the outcomes

Mass [kg]	Max. displacement [mm]	Volume [mm <sup>3</sup> ]
0.079	3.15	74962.69
0.073	5.11	68565.46
0.136	2.98	128678.19
0.135	2.42	127491.83
0.23	1.76	217371.08
0.135	2.43	127823.45

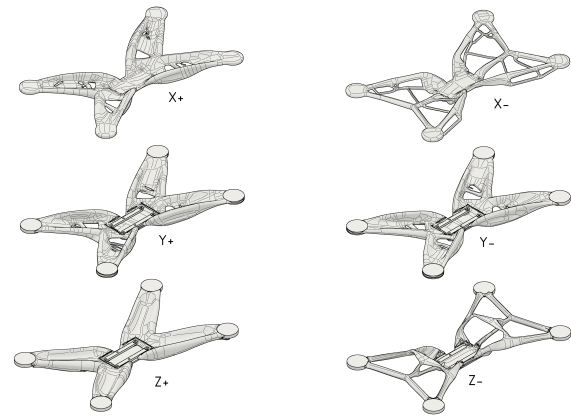


Figure 6: Outcomes of the different orientations

inal design, its overall weight was reduced by 25 grams, as the difference in weight between the two batteries is smaller than the weight reduction as a result of changing the frame, resulting in the flight time increasing by about 65 seconds (Fig. 7).

### 4. Summary

The reduction in the weight of a drone as a result of generative design was presented (the full assembly can be seen in Fig. 8). By following this method, a more efficient concept could be created. Proper use of generative design helps to develop a new or existing concept in many areas. Reducing the weight of vehicles has always been an important aspect of the industry, so further reductions in this field are expected. [5] E-mobility can also be greatly beneficial as the biggest problem is always the size and weight of batteries, which has a big impact on fuel consumption and range. Although the weight reduction of passenger cars is more complex, the example presented illustrates that this could be a revolutionary solution for the automotive industry in the future. From another point of view, it is also important to recognise that increased computational capacities make it possible to compare many more types of concepts, thereby providing the opportunity to choose the most optimal solution when designing.

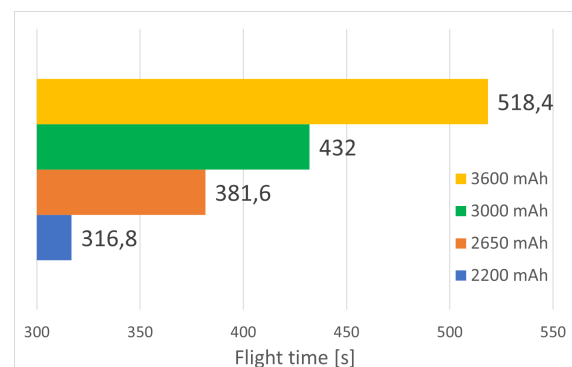


Figure 7: Flight times with different battery capacities



Figure 8: Assembly of the drone

## 5. Additional questions that arise

It can be seen that the results are free form surfaces of organic forms that are aesthetically pleasing which also make a positive contribution to the concept. Nevertheless, it is noticeable that although the given loads were symmetrical in all directions, the frame did not become completely symmetrical. This can be eliminated by post-mirroring the model, however, the question is will the mirrored construct be equally effective?

## 6. Acknowledgements

The authors would like to express their gratitude to Arkance Systems HU Kft. for supporting this work by providing pieces of software.

## REFERENCES

- [1] Chang, K.H.: *Product Performance Evaluation using CAD/CAE* (Academic Press), 2013. ISBN: 0123984696
- [2] Alderton, M.: Driving a lighter, more efficient future of automotive part design, 2021. <https://www.autodesk.com/customer-stories/general-motors-generative-design>
- [3] Siva Rama Krishna, L.; Srikanth, P.: Evaluation of environmental impact of additive and subtractive manufacturing processes for sustainable manufacturing. *Mater. Today: Proc.*, 2021, **45**(2), 3054–3060, international Conference on Advances in Materials Research - 2019. DOI: 10.1016/j.matpr.2020.12.060
- [4] Martinetti, A.; Margaryan, M.; van Dongen, L.: Simulating mechanical stress on a micro Unmanned Aerial Vehicle (UAV) body frame for selecting maintenance actions. *Procedia Manuf.*, 2018, **16**, 61–66, Proceedings of the 7th International Conference on Through-life Engineering Services. DOI: 10.1016/j.promfg.2018.10.160
- [5] Shahrubudin, N.; Lee, T.; Ramlan, R.: An Overview on 3D Printing Technology: Technological, Materials, and Applications. *Procedia Manuf.*, 2019, **35**, 1286–1296, The 2nd International Conference on Sustainable Materials Processing and Manufacturing, SMPM 2019, 8-10 March 2019, Sun City, South Africa. DOI: 10.1016/j.promfg.2019.06.089

## CHALLENGES OF INDUSTRY 4.0 IN THE VISEGRÁD GROUP

ANDREA ÉLTETŐ\*<sup>1</sup>

<sup>1</sup>Centre for Economic and Regional Studies, Institute of World Economics, Tóth Kálmán u. 4, Budapest, 1097, HUNGARY

This article provides a snapshot describing the position of the Visegrád Group in terms of adopting Industry 4.0 technologies. Despite being promoted and supported by the state, the introduction of these modern methods is still not as widespread as in other EU member states. The reason for this is the heterogeneity of firms: there are substantial differences between large and small as well as foreign and domestic firms. Statistics, surveys and interviews have proven that foreign-owned, larger companies are front-runners, while smaller domestic ones face considerable financial and technological challenges. However, it is concluded that the main problem is the continued lack of the necessary skilled labour force.

**Keywords:** Industry 4.0, Visegrád Group, Foreign Direct Investment

### 1. Introduction

The term “Industry 4.0” stems from Germany (opening speech of the Hannover Messe in 2011). Industry 4.0 is a complex concept, composed of nine main pillars: robotisation, simulation, the Internet of Things, additive manufacturing, cybersecurity, cloud computing, big data, augmented reality as well as horizontal and vertical system integration. Nowadays, it means a new kind of corporate and production organisation combining physical and digital production.

The concept and application of Industry 4.0 have also been promoted in the Visegrád Group. Industry associations and governmental organisations have launched strategies as well as programmes to inform and help companies; mainly small and medium-sized enterprises (SMEs). In spite of these efforts, statistics show that the Visegrád Group remains underdeveloped in the field of Industry 4.0. [1] This article tries to detect the reasons for this lag by summarising the available statistics and findings concerning this topic.

First, the Organisation for Economic Co-operation and Development (OECD) Information and Communications Technology (ICT) usage data and robotisation data are examined before the results of several surveys concerning the introduction of Industry 4.0 are analysed. Finally, the personal interviews conducted in the Visegrád Group are evaluated. Among the problems and challenges of small domestic companies, it was found that the most important is the human factor, namely the lack of necessary skills and the risk-avoiding managerial mindset.

\*Correspondence: [elteto.andrea@krtk.hu](mailto:elteto.andrea@krtk.hu)

### 2. Data on Industry 4.0 in the Visegrad Group

The OECD “ICT Access and Usage by Businesses” database contains several such elements that can be bound to a functioning Industry 4.0 system. These statistics show to what extent the companies in the given country use certain elements of digitalisation and automation. Compared to all the European Union (EU) member states, the Visegrád Group is situated relatively close to the bottom of the ranking. Naturally, differences according to the indicators and countries are present.

Table 1 shows the relevant figures with regard to the use of some basic digital tools (having a website or high-speed broadband) as well as the share of companies applying big data analytics, cloud computing, additive manufacturing, digital company resources and customer relationship management software. As a “reference country”, Germany was included in the table because the concept of Industry 4.0 stems from this country, moreover, business contacts and production chains between the Visegrád Group and Germany are highly significant. (It must be noted that although the performance of Germany is good, its indicators are not always the best among the EU member states.)

The table shows three phenomena. Firstly, in the selected areas, Slovakia and Hungary are the weak performers and the Czech Republic is the best in the Visegrád Group. Secondly, Germany performs much better than the Visegrád Group in all fields. Thirdly, although the use of 3D printing and Enterprise Resource Planning (ERP) software in every country is more widespread with regard

*Table 1:* Selected indicators of Industry 4.0 for manufacturing sectors compared to all sectors in 2020 as a % of all companies (Source: OECD ICT Access and Usage by Businesses database)

Sector	Poland		Czech Republic	
	All	Man.	All	Man.
Website	71.32	77.13	83.32	85.02
Broadband	42.77	38.47	34.44	28.99
ERP*	28.54	32.48	38	48.36
CRM*	30.92	20.91	20.86	20.19
Cloud Comp.	24.42	23.06	28.89	26.52
Big Data	8.47	6.51	9.12	7.98
3D printing	3.42	7.56	6.25	12.89
ICT training	17.75	16.14	24.74	27.6

Sector	Slovakia		Hungary	
	All	Man.	All	Man.
Website	75.82	75.22	63.23	72.96
Broadband	32.12	27.45	35.77	31.11
ERP*	31.12	38.11	14.33	20.41
CRM*	22.19	20.88	12.10	11.44
Cloud Comp.	25.57	24.2	25.21	23.17
Big Data	5.6	3.93	6.99	7.12
3D printing	3.89	7.99	3.4	6.78
ICT training	16.18	17.83	15.97	17.25

Sector	Germany	
	All	Man.
Website	88.35	92.52
Broadband	44.86	40.38
ERP*	29.26	50.33
CRM*	44.21	47.15
Cloud Comp.	33.32	30.71
Big Data	17.83	12.25
3D printing	7.35	18.02
ICT training	23.76	26.58

\*Data for Businesses using Enterprise Resource Planning (ERP) and Customer Relationship Management (CRM) software are from 2019

- Man.: Manufacturing
- Website: businesses with a website or home page
- Broadband: Businesses with a broadband download speed of at least 100 Mbps
- Cloud Computing: Businesses purchasing cloud computing services
- Big Data: Businesses implementing big data analytics
- 3D printing: Businesses using 3D printing technology
- ICT training: Businesses that have provided any type of training to develop the ICT-related skills of their employees within the last 12 months.

to manufacturing than the average, in other areas no significant sectoral difference is found. Around 16 – 25% of companies within the Visegrád Group provided some kind of ICT training to their employees in the previous year.

In the database, data are also classified according to

*Table 2:* Selected percentage indicators of Industry 4.0 for large and medium-sized enterprises in 2020 (Source: OECD ICT Access and Usage by Businesses database)

Company size	Poland		Czech Republic	
	Large	Medium	Large	Medium
Website	92.49	88.64	93.47	90.52
Broadband	69.4	52.17	55.44	38.5
ERP/2019	87.27	53.87	87.02	68.05
CRM/2019	79.66	52.47	46.33	35.19
Cloud comp.	59.55	37.68	55.63	36.88
Big data	28.37	12.76	24.75	13.5
3D printing	17.39	6.28	25.83	10.35
ICT training	71.02	32.67	77.22	43.96

Company size	Slovakia		Hungary	
	Large	Medium	Large	Medium
Website	88.84	79.66	86.24	78.05
Broadband	41.39	33.62	55.27	40.46
ERP/2019	72.24	47.95	62.03	31.97
CRM/2019	48.34	33.9	34.44	21.91
Cloud comp.	50.62	33.28	58.83	36.75
Big data	16.7	7.71	19.28	10.69
3D printing	17.79	5.43	14.67	4.65
ICT training	62.19	32.84	65.45	30.64

Company size	Germany	
	Large	Medium
Website	97.17	93.16
Broadband	73.41	54.16
ERP/2019	77.35	55.62
CRM/2019	68.15	58.28
Cloud comp.	62.05	41.18
Big data	35.81	22.23
3D printing	23.2	11.55
ICT training	73.07	43.22

the size of the company. As is presented in [Table 2](#), it is salient that large firms are by far the best, not only compared to small ones but also compared to medium-sized firms. This is true of Germany as well, although differences here are smaller than in the case of companies from the Visegrád Group. As for the countries from the Visegrád Group that have been integrated into the global supply chains and host affiliates of large multinational enterprises (MNEs) [2], these data, which is later underlined by surveys, show that the application of Industry 4.0 is most advanced at large foreign companies. Therefore, Industry 4.0 reinforces duality among local firms and the dependency on foreign capital (Foreign Direct Investment (FDI) led development model) in the Visegrád Group. [1]

With the reduction in the price of robots, automation has gained momentum worldwide. Even though the Visegrád Group has rapidly increased its stock of industrial robots, it is still overshadowed by the level of Germany. The robot densities of the given countries are

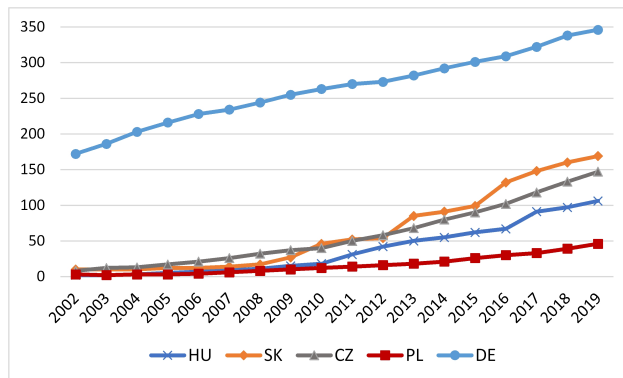


Figure 1: Robot density (No. of multipurpose industrial robots per 10,000 employees) in the manufacturing sector (Source: International Federation of Robotics)

shown in Fig. 1. It can be seen that this indicator is the lowest in Poland and the highest in Slovakia. According to the International Federation of Robotics, the automotive industry is the largest customer of robots, followed by the electrical/electronics sector, which is also true of the economies in the Visegrád Group. The automotive industry plays the biggest role in the Czech Republic, Slovakia and Hungary in the region, moreover, robotisation is more advanced in these economies.

### 3. Experiences according to surveys and interviews

With the spread of the Industry 4.0 concept, several surveys have been conducted among companies in the Visegrád Group concerning the introduction of these technologies as well as the opportunities, barriers and challenges they present. The main findings of these surveys were grouped according to certain areas of concern and the literature references are provided at the end.

**Introduction of Industry 4.0** The Visegrád Group is less prepared for Industry 4.0 than Western European economies. Generally, it is an important feature of this region that the main actors of Industry 4.0 are foreign companies, mostly multinationals. Based on international indices as well as rankings of governance, technology and entrepreneurial competences, the Czech Republic and Hungary performed better than the other two countries. [3, 4]

**The readiness of domestic firms** Given that domestic companies usually do not have strategies, a fear of taking risks is present. Managerial attitude and capability is often inadequate. The activity and knowledge of domestic firms with regard to Industry 4.0 are relatively weak, sometimes even perceiving it as a threat. However, as time passes, the domestic companies have become more confident and started to apply the new technologies of Industry 4.0. [5–14]

**Opportunities for domestic firms** It is beneficial that Industry 4.0 tools detect organisational weaknesses.

Opportunities stemming from Industry 4.0 are different for SMEs and MNEs. Companies are re-thinking their pricing strategies by making it more sophisticated and room for price setting is growing. [15–18]

**Challenges and problems** Automation in many cases was induced by labour shortages and the obsolete production technologies that were available. Data storage and security is a challenge as companies do not want to share their data with business partners. The shortage of skilled labour is acute. Production complexity and customer requirements have increased. The compatibility of new technologies is problematic and information on them is insufficient. There is a lack of financial resources for introducing Industry 4.0 technologies at SMEs. The corporate culture in domestic companies needs to change. [14, 19–22]

**Production control and organisation** In the Visegrád Group, since robotization relies on the localization decisions of MNEs and is mainly based on the automotive industry, it is “robotisation-dependent.” Competition as well as the lower cost and better quality of robots encourage automation. At some companies, functional upgrading is taking place but the structure of value creation remains, that is, no specialisation occurs in terms of advanced activities and higher value added per unit. [19, 23]

In a study from 2020 [24], interviews were completed with experts from the business and academic fields. In Poland, Hungary, the Czech Republic and Slovakia, 16, 13, 6, and 6 interviews were conducted in person, over the phone or online, respectively. Although this sample is relatively small, different institutions, companies and agencies were questioned so the opinions of various groups were gathered. Table 3 shows the essence of these opinions concerning the aforementioned topics.

### 4. Discussion

The described surveys and interviews show that the perception as well as maturity of Industry 4.0 vary among firms in the Visegrád Group. Some companies are just beginning to contemplate such technologies, while others already regard them as necessary. Over the past decade, “Industry 4.0 awareness” has clearly developed. A lot depends on the managerial mindset. Contrary to foreign firms, a constant development culture in domestic firms is often lacking, therefore, risks and novelties are avoided. However, a change in generation is occurring at many firms, the retirement of old owners is bringing about new possibilities. Once a plan or strategy to implement Industry 4.0 has been drawn up, preparation, piloting and testing are important. Adaptation can be time-consuming, moreover, the investment can take as long as two years

Table 3: Industry 4.0 in the Visegrád Group – issues raised during the interviews (Source: own compilation from the interviews conducted as part of the study [24])

Topic	Opinions from the interviews
Introduction of Industry 4.0	Primarily foreign firms apply for these technologies
Readiness of domestic firms	Poor and lagging. The degree of innovation is low, few enterprises have a plan or strategy.
Opportunities for domestic firms	Mental adjustment at the executive level is necessary. A change in generation may improve the situation.
Challenges and problems	Long-term and expensive investment with delayed benefits. Inadequate education system. Skills needed; managerial capabilities are mostly weak and brain drain.
Production control and organisation	MNE headquarters usually retain the know-how and R&D, Industry 4.0 gives more power to MNEs, decisions about its usage are made locally by the management of the subsidiaries.

to be implemented, leading to results only materialising later.

The results of surveys and interviews support the statistics, proving a duality among firms from the Visegrád Group: large, mostly foreign companies perform much better than smaller domestic firms. The interviews confirmed that business models as well as cooperation between foreign headquarters and local subsidiaries will be changed due to Industry 4.0 technologies. Although multinational enterprise (MNEs) develop R&D on their own, they partly share their results with local subsidiaries. Decisions about the usage of Industry 4.0-related technologies are mostly made by the management of local subsidiaries. For the successful functioning of a production chain, the absorptive capacity and collaboration of the subsidiaries are essential.

Several challenges of and barriers to Industry 4.0 for domestic SMEs were presented, which can be grouped into technological, financial and human factors. In my opinion, the problem of the human labour force is the most difficult to surmount. Data from Eurostat show that the number of graduates per thousand inhabitants in science, technology, engineering, mathematics and computing is only 60% of the EU average in Hungary and Slovakia, 80% in the Czech Republic and 96% in Poland.<sup>†</sup> A considerable proportion of these graduates later work abroad, diminishing the skilled workforce in the home countries.

Industry 4.0 is changing the characteristics of human capital, decreasing the labour intensity of certain produc-

tion phases. Those jobs that cannot or can hardly be automated require creativity, social intelligence and high cognitive abilities. The risk of unemployment is less with better education indicators (logic, mathematics, reading comprehension). [25] Suitable competencies in an Industry 4.0 world are the ability to learn, cooperation, flexibility, problem-solving, creativity and also non-cognitive skills. [26] These competencies – that should have already been developed at primary school – facilitate retraining, which has become critical in this rapidly changing technological environment, not to mention during a pandemic. At present, the education systems in the Visegrád Group do not strengthen these competencies and any reforms only bring about results in the long run.

## 5. Conclusion

Regarding several elements of the complex technologies of Industry 4.0, the statistics show the slowness of the Visegrád Group to adopt them compared not only to Germany but also to other semi-periphery EU member states. However, the statistics on automation (robot density in manufacturing) demonstrate that rapid development has taken place especially in Slovakia, the Czech Republic and Hungary. This contradiction can be explained by the fact that automation is driven mostly by the automotive industry, while in the other statistics the characteristics of all sectors are reflected. The statistics for an entire country also cover the differences between large and small as well as foreign and domestic companies. Large and foreign companies are much more advanced in terms of applying Industry 4.0 technologies in the Visegrád Group.

Despite government incentives and programmes, domestic firms are in general less willing to introduce new technologies, e.g., few of them have a strategy for implementing Industry 4.0, however, a learning process is present. Traditional corporate culture, obsolete technologies and the lack of financial resources are important challenges for a small or medium-sized firm. The major barrier, however, is that the bulk of the human labour force lacks the proper skills and competencies to meet the demands of Industry 4.0. Since the present education system is not ready to deal with this problem, huge and rapid changes in this regard cannot be expected.

## REFERENCES

- [1] Éltető, A.; Sass, M.: A kapitalizmus változatai és az ipar 4.0 a visegrádi országokban. *Közgazdasági Szemle*, 2021, **68**(5), 490–514 DOI: [10.18414/KSZ.2021.5.490](https://doi.org/10.18414/KSZ.2021.5.490)
- [2] Sass, M.: FDI-based models in the Visegrád countries and what the future may have in store for them, *wiiw Monthly Report 2021/02*, Vienna, wiiw, pp. 18–26
- [3] Naudé, W.; Surdej, A.; Cameron, M.: The Past and Future of Manufacturing in Central and Eastern Europe: Ready for Industry 4.0? *IZA Discussion Paper*, 2019, 12141 <http://hdl.handle.net/10419/196639>

<sup>†</sup>Eurostat (educ\_uoe\_grad04).

- [4] Szabó, S.: Transition to Industry 4.0 in the Visegrád Countries. *European Economy Economic Brief 052*, Brussels, European Commission, 2020.
- [5] Nagy, J.; Oláh, J.; Erdei, E.; Máté, D.; Popp, J.: The Role and Impact of Industry 4.0 and the Internet of Things on the Business Strategy of the Value Chain—The Case of Hungary. *Sustainability*, 2018, **10**, 3491 DOI: [10.3390/su10103491](https://doi.org/10.3390/su10103491)
- [6] Nick, G.: Az Ipar 4.0 hazai adaptációjának kihívásai a vállalati és területi összefüggések tükrében. *PhD Dissertation*, 2018.
- [7] Stasiak-Betlejewska, R.; Luminita, P.; Glin, W.: The Influence of Industry 4.0 on the Enterprise Competitiveness. *Multidisciplinary Aspects of Production Engineering*, 2018, **1**, 641–648 DOI: [10.2478/mape-2018-0081](https://doi.org/10.2478/mape-2018-0081)
- [8] Adamik, A.; Novicki, M.: Preparedness of Companies for Digital Transformation and Creating a Competitive Advantage in the Age of Industry 4.0. *Proceedings of the International Conference on Business Excellence*, 2018, **12**(1), 10–24 DOI: [10.2478/picbe-2018-0003](https://doi.org/10.2478/picbe-2018-0003)
- [9] Gryzb, K.: Industry 4.0 Market in Poland from the International Perspective. *Hradec Economic Discussion Papers*, 2019, **9**, 252–262 DOI: [10.36689/uhk/hed/2019-01-025](https://doi.org/10.36689/uhk/hed/2019-01-025)
- [10] Mohelska, H.; Sokolova, M.: Management Approaches for Industry 4.0 – the Organizational Culture Perspective. *Technological and Economic Development of Economy*, 2018, **24**(6), 2225–2240. DOI: [10.3846/tede.2018.6397](https://doi.org/10.3846/tede.2018.6397)
- [11] Vrchota, J.; Volek, T.; Novotná, M.: Factors Introducing Industry 4.0 to SMEs. *Soc. Sci.*, 2019, **8**(5), 130 DOI: [10.3390/socsci8050130](https://doi.org/10.3390/socsci8050130)
- [12] Greciková, A.; Kordos, M.; Sokol, J.: The Approach to Industry 4.0 within the Slovak Business Environment. *Soc. Sci.*, 2019, **8**(4), 104. DOI: [10.3390/SOCSCI8040104](https://doi.org/10.3390/SOCSCI8040104)
- [13] Soukupová, N.; Adamová, M.; Krninská, R.: Industry 4.0: An Employee Perception (Case of the Czech Republic). *Acta Universitatis Agriculturae et Silviculturae Mendelianae Brunensis*, 2020, **68**, 637–644 DOI: [10.11118/actaun202068030637](https://doi.org/10.11118/actaun202068030637)
- [14] Obermayer, N.; Csizmadia, T.; Hargitai, D. M.; Kígyós, T. A.: Az Ipar 4.0. implementációval kapcsolatos vezetői motivációk és akadályozó tényezők elemzése hazai vállalatvezetők véleménye alapján. *Vezetéstudomány/Budapest Management Review*, 2021, **52**(2), 60–72 DOI: [10.14267/VEZTUD.2021.02.06](https://doi.org/10.14267/VEZTUD.2021.02.06)
- [15] Halmosi, P.: A technológiaorientált start-up cégek lehetőségei és korlátai az ipar 4.0 korszakában – kérdőíves felmérés alapján / The possibilities and limits of technology-oriented start-ups under Industry 4.0 – a survey-based study. *Vezetéstudomány/Budapest Management Review*, 2019, **50**(9), 40–48 DOI: [10.14267/VEZTUD.2019.09.05](https://doi.org/10.14267/VEZTUD.2019.09.05)
- [16] Horváth, D.; Szabó, R. Z.: Driving forces and barriers of Industry 4.0: Do multinational and small and medium-sized companies have equal opportunities? *Technological Forecasting and Social Change*, 2019, **146**, 116–132 DOI: [10.1016/j.techfore.2019.05.021](https://doi.org/10.1016/j.techfore.2019.05.021)
- [17] Rekettye, G.: Az ipar 4.0 hatása az árakra és a vállalati árképzés gyakorlatára = The effects of industry 4.0 on prices and price settings. *Vezetéstudomány / Budapest Management Review*, 2020, **51**(4), 15–25 DOI: [10.14267/VEZTUD.2020.04.02](https://doi.org/10.14267/VEZTUD.2020.04.02)
- [18] Szabó, R. Z.; Horváth, D.; Hortoványi, L.: Hálózati tanulás az ipar 4.0 korában. *Közgazdasági Szemle*, 2019, **66**, 72–94 DOI: [10.18414/KSZ.2019.1.72](https://doi.org/10.18414/KSZ.2019.1.72)
- [19] Szalavetz, A.: Digital transformation and local manufacturing subsidiaries in central and eastern Europe: Changing prospects for upgrading? *The challenge of digital transformation in the automotive industry*, Brussels, ETUI, 47–64, 2020.
- [20] Nagy, J.: Az ipar 4.0 fogalma és kritikus kérdései – vállalati interjúk alapján. *Vezetéstudomány / Budapest Management Review*, 2019, **50**(1), 14–26 DOI: [10.14267/VEZTUD.2019.01.02](https://doi.org/10.14267/VEZTUD.2019.01.02)
- [21] Papula, J.; Kohnová, L.; Papulová, Z.; Suchoba, M.: Industry 4.0: Preparation of Slovak Companies, the Comparative Study. *Smart Technology Trends in Industrial and Business Management*, New York, Springer International Publishing, 101–114, 2019.
- [22] Slusarczyk, B.: Industry 4.0: are we ready? *Polish Journal of Management Studies*, 2018, **17**, 232–248 DOI: [10.17512/PJMS.2018.17.1.19](https://doi.org/10.17512/PJMS.2018.17.1.19)
- [23] Cséfalvay, Z.: Robotization in Central and Eastern Europe: catching up or dependence? *European Planning Studies*, 2020, **28**(8), 1534–1553 DOI: [10.1080/09654313.2019.1694647](https://doi.org/10.1080/09654313.2019.1694647)
- [24] Götz, M.; Éltető, A.; Sass, M.; Vlcková, J.; Zacharová, A.; Ferenciková, S.; Bic, J.; Kaczowska-Serafinska, M.: Effects of Industry 4.0 on FDI in the Visegrád countries. Final report. Vistula University, Supported by the International Visegrad Fund, 2020.
- [25] Nedelkoska, L.; Quintini, G.: *Automation, skills use and training*, OECD Social, Employment and Migration Working Papers, 2018, **202** DOI: [10.1787/1815199X](https://doi.org/10.1787/1815199X)
- [26] Pató, G.; Kovács, K.; Abonyi, J.: A negyedik ipari forradalom hatása a kompetenciacserélődésre. *Vezetéstudomány / Budapest Management Review*, 2021, **52**(1), 56–70 DOI: [10.14267/VEZTUD.2021.1.05](https://doi.org/10.14267/VEZTUD.2021.1.05)



## DESIGN AND QUALITY ASSURED MANUFACTURING OF FREE FORM METAL PROSTHESES BY SELECTIVE LASER MELTING TECHNOLOGY

ARTÚR BENJÁMIN ACÉL<sup>1</sup>, GYÖRGY FALK<sup>2</sup>, FERENC DÖMÖTÖR<sup>3</sup>, AND JÁNOS TAKÁCS<sup>\*3</sup>

<sup>1</sup>eCon Engineering Kft., Kondorosi út 3, Budapest, 1116, HUNGARY

<sup>2</sup>VARINEX Informatics Inc., Fehér út 10, Budapest, 1106, HUNGARY

<sup>3</sup>Department of Automotive Technologies, Budapest University of Technology and Economics, Stoczek u. 4, Budapest, 1111, HUNGARY

This paper concerns the key steps in the design, manufacturing and certification of customized acetabular cups. The process is based on the compilation of computed tomography scans to create a surface that is generated from the point cloud of the surface model. As a result, the surface model is obtained. The final step is the manufacturing itself. The features of Selective Laser Melting, also referred to as Direct Metal Laser Sintering in the literature, the placement of workpieces in the construction space and peculiarities of the support design are described. Important technological preparations of the EOS M 100 3D camera for the manufacturing of implants will be described. Implants were made of the 316L and Ti6Al4V metal powders. The finished test pieces were subjected to non-destructive as well as destructive mechanical and material structural testing to qualify implants by using the appropriate quality assurance system.

**Keywords:** 3D printing, computed tomography, metal prostheses

### 1. Introduction

Recently, the level of development of additive manufacturing has advanced. During the first level, the basics of the technology were elaborated on before the various fields of application were discovered during the following stage. Barriers have been removed and the application has become more and more effective. In the clinical and medical sciences, several companies have been trying to replace traditional implants with those produced by additive manufacturing. Although the imagination of designers in the field of engineering technology has no limits, limitations are imposed by medical doctors. Nowadays, individual implants can be applied in many individual cases without any complications [4]. Our paper describes the full sequence of preparing a real, customized acetabular cup.

### 2. Tailor-made human implant

#### 2.1 Accessing the necessary input data

Unfortunately, the scapula of a woman was attacked by bone cancer. Since important muscles join to its surface, it is vital that this bone be replaced. Using computed tomography (CT) and magnetic resonance imaging (MRI)



Figure 1: Tailor-made implant to replace the scapula [1]

images, engineers and medical doctors were able to reconstruct the bone to be replaced. The implant before and after implantation can be seen in Fig. 1. [1]

The left-hand side of Fig. 1 shows that the implant can be lightened or the solid (dense) material replaced by a barred structure. To properly attach the muscles at the edge of the implants, suitable connections can be created. Even in this case, the implant was fixed properly; it sat properly and the patient did not exhibit any symptoms after the operation. This case study can form the basis for proving that implants are useful and important. [1]

#### 2.2 DICOM to STL conversion

Tailor-made requirements were formulated during a meeting between a doctor and engineer. As a first step,

\*Correspondence: [janos.takacs@gjt.bme.hu](mailto:janos.takacs@gjt.bme.hu)

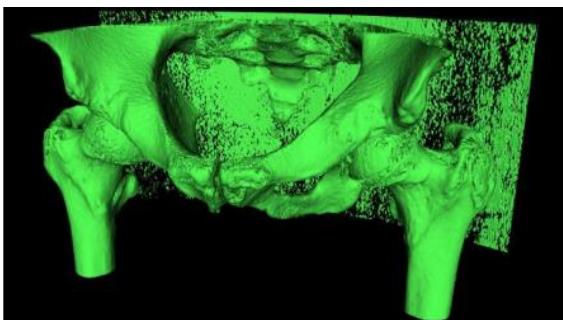


Figure 2: The object model compiled from CT scans

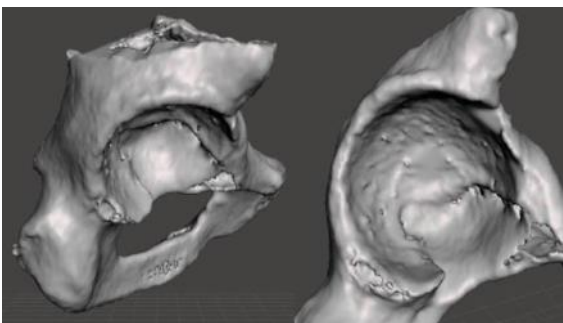


Figure 3: The “cleaned” surface model and the surface the socket must be adjusted to

the doctor has to submit proper records stored on CDs to the engineer. These records are usually stored on CDs or DVDs that can be read by any CD/DVD drive. The InVesalius software carries out the conversion, which is very user-friendly. The surface model for the socket to be manufactured, prepared by InVesalius software, can be seen in Fig. 2.

Given that the model generated by the InVesalius software can be imported and the surfaces that are unnecessary for designing implants removed from the surface model, the surface model is simpler and the storage of big files is not required. The Autodesk Meshmixer software can carry out this type of cleaning. In Fig. 3, the part of the surface where the implant has to be inserted can be seen. The background produced by the CT scanner on this surface model was removed from the femur and one half of the hip bone. During the next step, the file of the model had to be saved as an “STL” file to create the surface from triangles before proceeding with the design.

### 2.3 Creation of the socket model

If the corners of the triangles can be determined and substituted by points, a point cloud is produced. This point cloud has to be cleaned further, moreover, for the remaining points, a surface can be adjusted. By highlighting the adjusted surface, the shape and volume model of the socket is obtained. The Rhino 6 program can do this task. The point cloud generated from the saved surface model can be seen in Fig. 4.

It is also possible to simply delete any unnecessary points. During this step, how to fix the implant and what

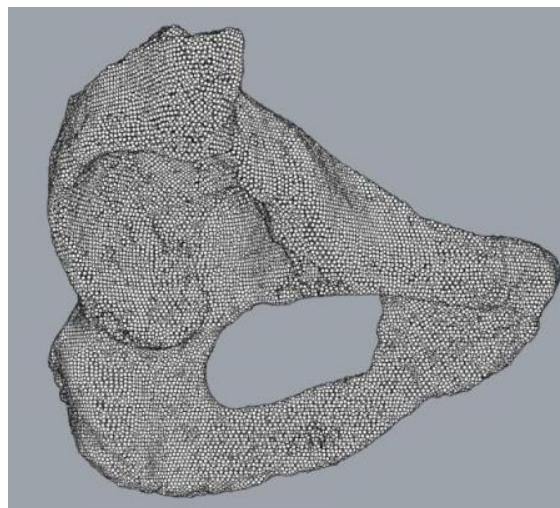


Figure 4: The point cloud generated from the “STL” file

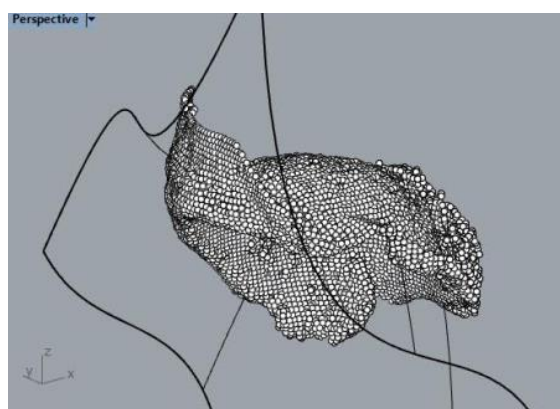


Figure 5: Generated surface with an insufficient number of control points

its role will be must be taken into account. It is important to mention that the fixed points cannot be determined from the CT images. The location of the screws in the bones is based on the experience of medical professionals.

The general purpose of the socket is to compensate for the missing bone that disintegrated on the surface of the femur. It is important that it can be fixed in several ways, e.g. the volume of the implant is cavernous so the bone can grow into the holes of the bones.

Bolts are used to fix traditional implants. This implant is designed to be fixed to the highly strong hip bone. At least three fastening points are required to safely fasten the socket while ensuring that a sufficient amount of space remains for the bolts.

By taking into account all of the aforementioned points, the point cloud can be approximated by a surface. The program must follow set conditions to determine how many control points the surface should be generated from. In this case,  $20 \times 20$  was determined as suitable. If the number of control points is any less, the point cloud cannot be simulated properly. This case is shown in Fig. 5.



Figure 6: The superfluous points of the point cloud are shown in detail on the generated surface



Figure 7: After determining the limitations of the socket, the directions of the normal vectors of the surface are designated by red circles.

As can be seen in Fig. 6, should too many control points be present, the program shows the undesirable defects of the surface that result. When the surface is ready, then the point cloud can be removed. The boundaries of the surface are not determined. The control points cannot be given in such a way that they reach the boundary of the point cloud.

The limitations of the implant have to be determined. In this piece of software, it is possible to reshape the surface that results. Predetermined sections can be projected onto the surface. Using these projected sections, the individual parts of the surface can be detached, as can be seen in Fig. 7.

After forming the required shape, it is possible to stretch the surface in the direction of its normal vector to create the required thickness of the wall. It should be noted that this surface will make contact with the bone, so must be stretched in the opposite direction. The stretched surfaces can be seen in Fig. 8. It is important that the surface model forms a closed surface to imitate the body. This closed surface model can be transferred into a body using the Rhino 6 program. This model of a body can be stored in an “STP” file format. Any traditional CAD program is capable of opening this format.

As the next step, the holes for fixing the bolts have to be created in the CAD system before the model of the body can be prepared for manufacturing and its verifica-

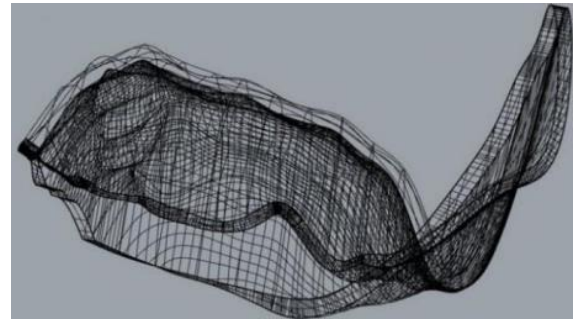


Figure 8: The final closed surface model after being stretched in the direction of the normal vector

tion.

#### 2.4 Powder bed fusion for the additive manufacturing of metal parts using laser beams

Selective Laser Melting, similarly to other additive manufacturing technologies like Direct Metal Laser Sintering, constructs the workpiece layers by layer. At the Department of Automotive Technologies at BME, a special method has been developed for the EOS M 100 3D camera with the following operating principles:

- The first step is to build a layer (on a heated base plate) that sinks proportionally to the thickness of the powder.
- The second step is to provide a dose of powder from the automated supply equipment.
- The third step is to spread the dose of powder over the work surface and push the superfluous amount into the container located on the other side of the work surface.
- The fourth step is to scan the laser beam over the work surface before melting and fastening the particles of powder. The melting will result in the thickness of the layer of powder decreasing.
- The fifth step is that the recoter returns to its original position (end position on the left-hand side) before being prepared for the portioning.

Four doses (denoted as 1-2-3-4) can be set on the working set and spread by the working blade to a thickness of 20  $\mu\text{m}$ .

#### Positioning of the workpiece in the building space

Should several workpieces be present, their positions are important. The working blade must spread the powder smoothly and any fluctuations of forces acting on the blade must be avoided since these might cause vibrations leading to variations in the thickness of the powder.

Another problem can occur if the workpieces are arranged in a row because the separated small workpieces

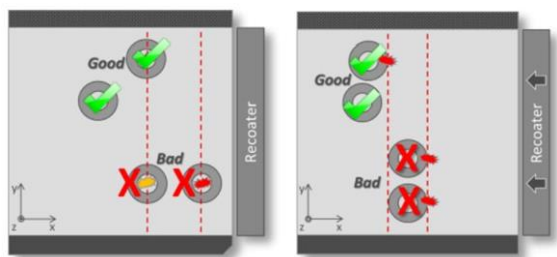


Figure 9: An optional advantageous arrangement of the workpieces [2]

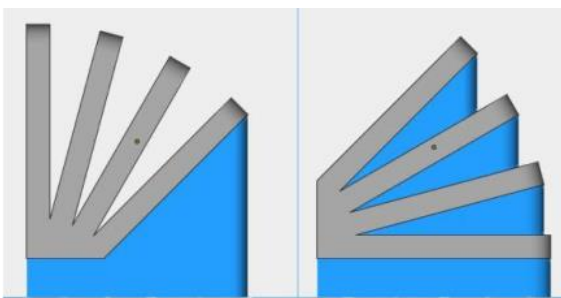


Figure 10: Generation of a support (denoted in blue) depending on the angle of incidence [3]

might jam the blade. An optional advantageous arrangement can be seen in Fig. 9.

According to our experience, small workpieces should not be placed on an edge because the temperature distribution here is not uniform which can cause problems.

### Design of a workpiece support on the heated base plate

Proper binding of the initial layer of the workpiece is essential, otherwise the support will be subjected to thermal stress due to differences in temperature. If the support is not fastened properly to the base plate, then the workpiece might be torn and, consequently, production might have to be stopped. Another important factor is heat transfer and cooling because the workpiece can burn due to a prolonged period at high temperatures resulting in failure of the surface and structural features. The Materialise Magics program can design a support for the workpieces. The following recommendations should be followed.

It is undesirable to leave the surface unsupported if the angle of incidence is more than 45 degrees (Fig. 10).

Bulging, overhanging parts also have to be supported. They might become superfluous as well because the workpiece can be placed in different orientations in the workspace.

### Preparation for the manufacturing of a tailor-made socket

As a first step, the workpiece has to be imported into the Materialise Magics program before being placed in the

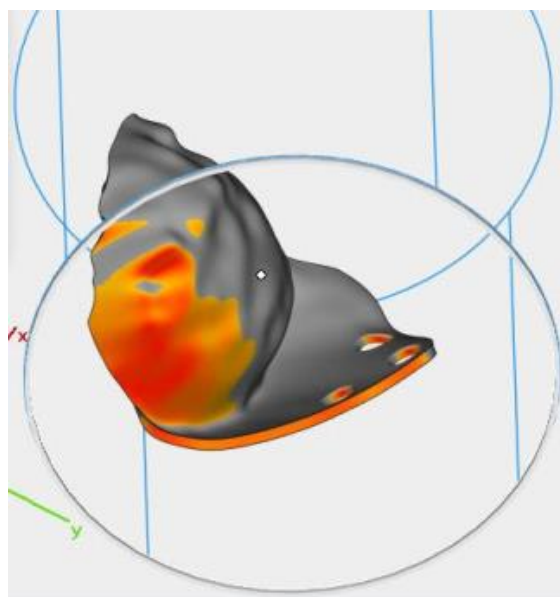


Figure 11: Bottom view of the surfaces with a maximum angle of declination of 45 degrees.

proper position. It is advisable to minimize the number of supports. Once the model has been placed in the building space, it can be adjusted into its final position. For this purpose, the module "Supported area preview" is an excellent tool providing coloured data about the steepness of the surfaces. The location of the socket can be seen in Fig. 11.

The next step is to partition common supports by following the command "fragmentation," resulting in a reduction in the total manufacturing time because no additional supports are required and consequently less powder is needed. Lightening of load-bearing walls means the holes should be diamond-shaped or rectangular. This enables powder which is not molten to be cleared from the load-bearing walls. After clearing, the superfluous material can easily be removed and the construction time reduced because the laser no longer needs to scan the vector section. "Fragmentation" and lightening of the diamond shape can be seen in Fig. 12.

The so-called "teeth" connect the workpiece to the supports. Since the program separates the workpiece and the supports, it is no longer necessary to scan the teeth supporting the workpiece. Ingrowing can be prevented by following the "Z Offset" command as shown in Fig. 13.

### 2.5 Checking the manufacturing of the prepared socket model

Due to thermal deformation during the manufacturing process, the blade may get jammed in the workpiece. Furthermore, it is possible that the workpiece will crack due to the tension. The production process will stop in both cases due to overloading of the blade. To avoid this, the manufacturing plan has to be checked. Naturally, the signals have to be verified and taken into account or manually neglected by the supervisor.



Figure 12: “Fragmentation” and lightening of the diamond shape highlighted by a red circle

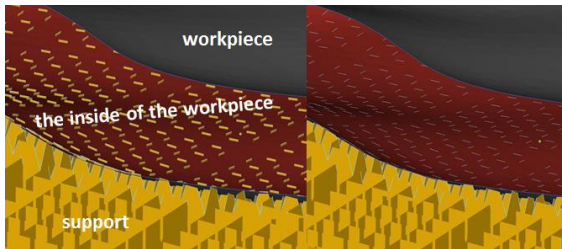


Figure 13: Prevention of the ingrowing of the teeth on the workpiece

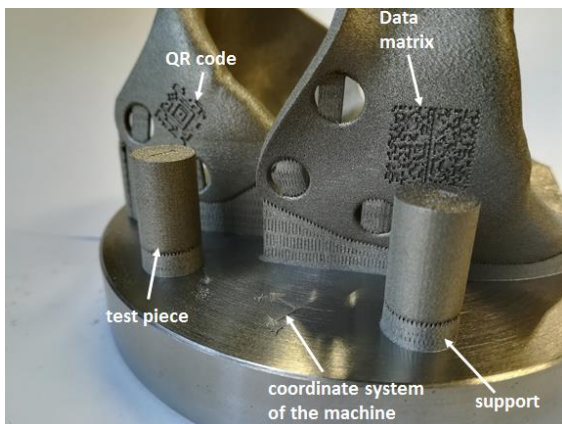


Figure 14: Sockets made of the alloy 316L

The building platform is fastened in place by a vacuum system. The zero positions in the vertical direction must be fixed and the whole building surface levelled to achieve the required degree of flatness. The powder container must be filled and pushed into place. The protective cover must be cleaned with alcoholic tissue paper before manufacturing. The next step is to cover the door of the workspace. The entire manufacturing process takes place in an atmosphere of inert argon gas.

Two sockets were designed. The workspace was filled with 99.99% argon gas, which is heavier than air so fills

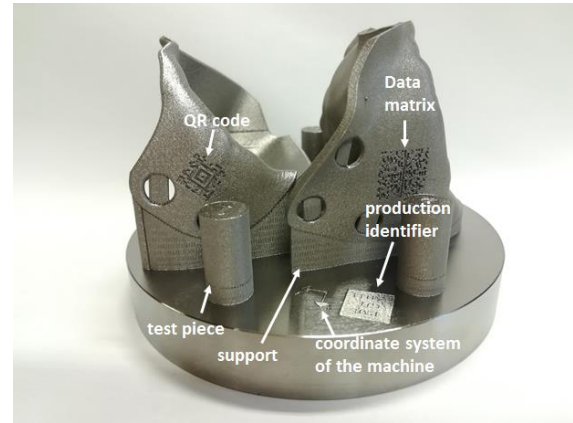


Figure 15: Sockets made of the alloy Ti6Al4V

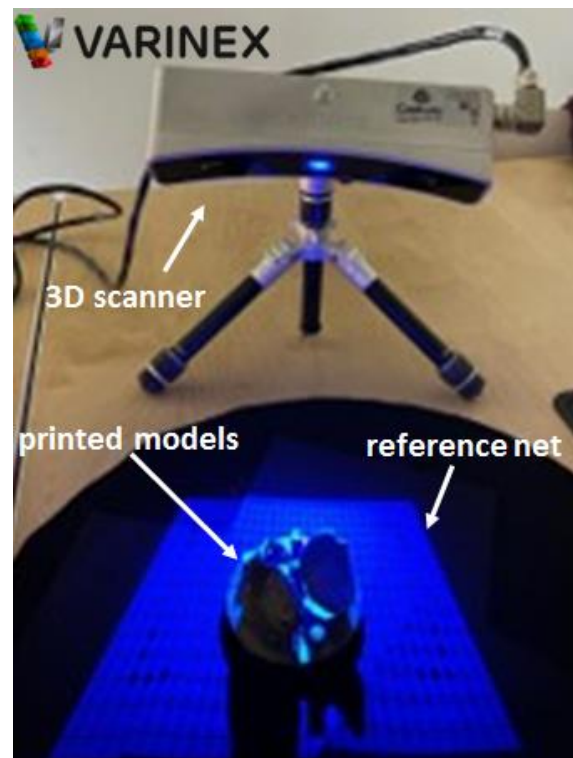


Figure 16: Measurement arrangement of the 3D Systems Capture scanner

the space from the bottom up. If less than 0.1% of oxygen is present, then the manufacturing process can commence. During the first manufacturing process, the designed sockets were made of the alloy 316L. One of the sockets was designed by using the Simufact program to facilitate geometrical measurements. In the manufacturing workspace, more trial workpieces were placed. The sockets were manufactured successfully, as can be seen in Fig. 14. During the second manufacturing process, the sockets were made of the alloy Ti6Al4V supplied by EOS and can be seen in Fig. 15.

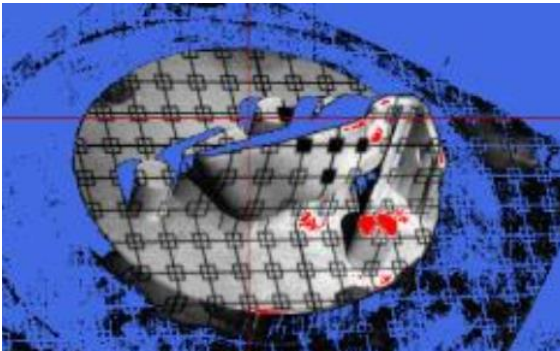


Figure 17: Surface with the reference net after being scanned by the 3D camera

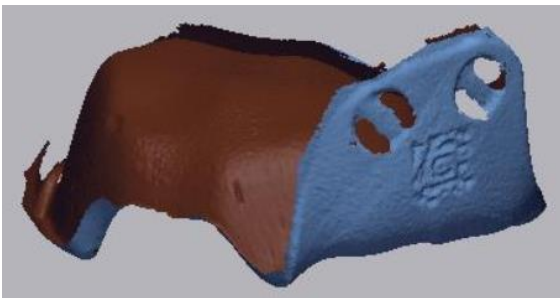


Figure 18: Surface model after smoothing

### 3. Evaluation and quality control by the geometrical measurements

VARINEX Informatics Inc. carried out the geometrical measurements using the scanner presented in Fig. 16.

Before the measurements were taken, the workpieces were sprayed in a “processing powder” to avoid glittering. The workpieces to be measured are placed at the centre of the reference net. The exposition time has to be adjusted according to the light conditions.

During the scanning, two images of the workpiece are made before the program generates a powder cloud of the surface as can be seen in Fig. 17.

Surfaces scanned from several directions have to be compiled manually because the forms are unusual and the program is unable to smoothen these surfaces, which can be seen in Fig. 18. Unfortunately, due to the support, one part of the surface could not be scanned.

This surface model can be compared with the original CAD model using the Geomagic Design X program. The socket models were scanned in raw, heat-treated and cut statuses. These surfaces were compared with the original CAD geometry and the results can be seen in Fig. 19. The limits of measurements during the comparison were between 1 mm and  $-1$  mm. Differences in size are denoted by colours. The maximum values and distributions are also presented in this image.

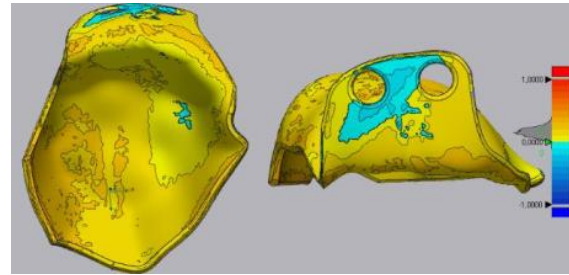


Figure 19: Results of the comparison of the scanned surface with the original CAD model

In conclusion, based on the results of the comparison, it can be seen that the calibration of the Simufact program was successful. The geometry of the preformed model approximates better to the original CAD model after being subjected to heat treatment and cut than to the model without preformation. The accuracy of the measured data always fall within the acceptable range of  $\pm 0.5$  mm.

### Acknowledgement

The authors are grateful that this project was carried out with the full support of the National Research, Development and Innovation Office. The title of the project was “The Design and Quality Assured Manufacturing of Free-Form Metal Prostheses by Selective Laser Melting.” The identification number of the project is NVKP\_16-1-2016-0022.

### REFERENCES

- [1] Willemsen, K.; Nizak, R.; Noordmans, H. J.; Castelein, R. M.; Weinans, H.; Kruij, M. C.: Challenges in the design and regulatory approval of 3D-printed surgical implants: a two-case series. *The Lancet Digital Health*, 2019, **1**(4): e163-e171; DOI: [10.1016/S2589-7500\(19\)30067-6](https://doi.org/10.1016/S2589-7500(19)30067-6)
- [2] Summary for the EOS M290 System Advanced User Training – Level 1 <https://www.eos.info>
- [3] D. Magyar: Testing features of models manufactured by laser additive manufacturing, Scientific Work of Students, 2018, Faculty of Transportation Engineering and Vehicle Engineering, BME Budapest University of Technology and Economics <https://tdk.bme.hu>
- [4] Hoang, D.; Perrault, D.; Stevanovic, M.; Ghiassi, A.: Surgical applications of three-dimensional printing: a review of the current literature & how to get started. *Ann. Transl. Med.*, 2016, **4**(23):456 DOI: [10.21037/atm.2016.12.18](https://doi.org/10.21037/atm.2016.12.18)

## INVESTIGATION OF THE RESISTANCE A SAILBOAT IS SUBJECTED TO IN THE CASE OF DRAFT CHANGES CAUSED BY MODIFYING THE POWERTRAIN

EMESE LÉVAI\*<sup>1</sup> AND PÉTER FICZERE<sup>1</sup>

<sup>1</sup>Department of Railway Vehicles and Vehicle System Analysis, Budapest University of Technology and Economics, Műgyetem rkp. 3, Budapest, 1111, HUNGARY

In our research, calculations were performed using the example of a specific ship when a modification was made to the powertrain of a vehicle. These results were used to observe whether the ship is expected to decelerate or the change in the draft is likely to cause stability problems. In recent years, the rules concerning the use of inland waterways by recreational crafts have been tightened for environmental reasons. In many cases, these restrictions affect the drive chain, making the workflow of the conversion involved frequent. In this case, it is extremely important for shipowners to know how the draft will change and at what speed the ship will operate after the conversion. This study on a numerical flow simulation provides an excellent opportunity to find out.

**Keywords:** sailing, computational fluid dynamics, simulation, modifying the powertrain

### 1. Introduction

With the boom in lake navigation, the technical equipment of small watercraft has also expanded to include important details. Since the number of sailing vessels, which were originally only wind-powered, has increased in ports, in order to prevent subsequent disruptions and facilitate emergency maneuvering, these vessels carry an engine as a secondary source of propulsion. In addition, small boats that are purely motor-powered have also entered the market for private individuals. Generally speaking, this size of engine has had a detrimental effect on life in shallow lakes, such as Lake Balaton, in several ways and emissions have noticeably increased. As a result, a regulation [1] came into force whereby recreational (i.e., not emergency, port maneuvering, etc.) trips can only be powered by electric motors on Lake Balaton. For this reason, shipowners have had to convert their propulsion systems from internal combustion engines to electric versions.

Although the effect of this on the draft and speed varies from boat to boat, this data is important for shipowners. Our article presents a method for calculating such data for a specific ship.

### 2. Methods

#### 2.1 Weight and dive calculation

The examined vessel is a 50 m<sup>2</sup> cruising, capital-weighted sailboat designed for tours that is 13.2 m long and weighs 6.8 t (Figs. 1 and 2). The differences between the results of the weight calculations on the blueprints and the actual ship, as well as the knowledge of the mass of the elements of the electric and diesel powertrain, were sufficient to determine the change in the draft [2]. The draft varies from 1.68 m to 1.7 m (Fig. 3). The calculation was performed using the MAXSURF Hydromax program.

#### 2.2 Fluid dynamics simulation

The purpose of the calculation in this case is twofold: to determine the drag (resistance) force acting on the hull while in motion ('*x*' component) and the buoyancy ('*z*' component). The practical goal of the tests is to calculate the resistance force acting on the boat during two different dives using the same engine power, as this has a major impact on the speed of travel (because if the boat moves in the '*x*' direction, the resistance force will always be in the '*x*' direction). The tests were performed using the FloEFD extension of the Siemens Solid Edge program. The initial values were the dive (1.68 m and 1.7 m according to the weight calculation) (Fig. 3), flow characteristics - test, free surface, and the boundary between

\*Correspondence: [levai.emese@edu.bme.hu](mailto:levai.emese@edu.bme.hu)

Figure 1: A piece of the original item and weight chart (1950)

different media, as well as their required properties (e.g., density, method, etc.). As an external force, the magnitude and direction of gravity had to be taken into account. The flow rate of the tested medium was also adjusted to the medium in the appropriate direction, that is, opposite to the direction of travel. The mesh was compressed locally by 3-stage compression around the surfaces delimiting the body (Figs. 4 and 5).

This is partly due to the fact that unnecessarily accurate calculations of values at points unrelated to the hull would lengthen the duration of the test and partly the result of the calculation being as accurate as possible at critical locations (where plating and water intersect). The load cases were chosen according to the dives and the selected speed points at a Froude number of up to 0.45 can be assigned to the characteristic operating conditions of the ship (while displacing water) [3]. The values at the selected speed points were recorded within this range.

### 3. Results

After running the analysis, the series of measurements was tested separately for each load case at each of the six speed points. Convergence was observed under all circumstances. The results, which are shown in Figs. 6 and 7, were plotted on graphs and presented in tables. It can be seen that in both the 'x' and 'z' direction, the higher the speed at which the vessel travels, the greater both the force acting on the hull and the greater the vertical distances measured between the points of the curve on the graphs are. As can be seen in Fig. 4, the resistance (vertical axis) resulting from lighter load cases (denoted by the orange line) was less than for heavier load cases when the electric drive chain was in use (denoted by the gray line). The expected results were also recorded in the evaluation of the buoyancy forces. Regarding the load case belonging to the original drive chain (denoted by the gray line), the buoyancy forces are lower than in terms of the load

Berevészet teljes tömegének számbája (általános elrendezésű rajzokról)				
Tétel	Száma	Tömeg [kg]	Darabszám [db]	Össztömeg [kg]
Hőköszűrő fal	1	4,60788		4,60788
Hőköszűrő ajtó	1	2,81136375		2,81136375
Polkok (előző)	2	3,89661		7,79322
Árnyéktartó	1	8,554		8,554
Pereméc	1	0,1203475		0,1203475
Padló betétkészlet	1	1,7954382		1,7954382
Támasztartó	1	0,684		0,684
Szekrény ajtó (kicsi)	1	1,1109		1,1109
WC betét tereveléskészítő	1	1,4283		1,4283
WC ajtó	1	46,229773		46,229773
Ágy tartó	4	13,09275		52,371
Ágy fal	4	7,6375		30,55
Szekrényajtó	8	10,575		84,6
Mennyezet borítása	1	1,587		1,587
Szekrényajtó felő	8	0,532		4,256
Szekrény ajtó (oldalt)	4	0,981824		3,927296
Szekrény oldalsó padlót	4	1,52		6,08
Szekrényajtó (oldalt)	4	7,6		30,4
Szekrényajtó (előző)	2	2,2876		4,5752
Szekrényoldalt (előző)	1	0,608		0,608
Szekrényoldalt (előző)	1	27,508		27,508
Polkok (előző)	2	0,73696		1,47392
Polkok (új)	4	1,0904		4,3616
Polkok oldalsó	8	0,36472		2,91776
Polkok elője	4	0,264422		1,057688
Hüllőajtó	1	15,47325		15,47325
Felépítési alváz	1	3,57075		3,57075
Felépítési alváz	1	2,0829375		2,0829375
Padló betétkészlet 1.	1	3,3605		3,3605
Padló betétkészlet 2.	1	3,3605		3,3605
Padló betétkészlet 3.	1	5,2734		5,2734
Padló betétkészlet 4.	1	6,8244		6,8244
Padló betétkészlet 5.	1	3,48975		3,48975
Kövérhöz padló	2	4,9632		9,9264
Fix padló 1.	2	4,9115		9,823
Fix padló 2.	1	6,0489		6,0489
Fix padló 3.	1	7,1346		7,1346
Padló tartó	17	0,752		12,784
Összekötő lécz	2	0,0110352		0,0220704
Felépítési fal	2	0,0715208		0,1430416
Fedélzet borítás	22	0,887		19,314
Közdícs	2	0,009522		0,019044
Szengélyléc	2	0,003174		0,006348
gerenda lécz	2	0,010158		0,020316
vezető lécz	2	0,256036		0,512072
keresztmerevítő	1	8,993		8,993
Fal rész	1	3,8088		3,8088
Sarok rész	2	7,401		14,812
Padló szegélyléc	2	0,00199961		0,00399922
Borítás	1	247		247
Mennyezet borítása	1	197,4		197,4
Változófal (11. borda)	1	16,0975		16,0975
Változófal (15. borda)	2	7,6375		15,275
Változófal (20. borda)	1	15,275		15,275
Fedélzet borítás	1	124,55		124,55
WC	1	0		0
Mozdó	1	0		0
Végcső	1	0		0
Szerelőnyílás keret	1	0		0
Indukciós főátlap	1	0		0
Hosszúcsús fények	1	0		0
HŐS	1	0		0
TV	1	0		0
Hűtőszelvény	1	0		0
Nézővilágítás	3	0		0
Ventilátor	1	0		0

Figure 2: A portion of the new batch and weight chart (2020, field survey)

case belonging to the new drive chain (denoted by the blue line). The parabolic nature of the curves was also in line with the preliminary expectations as the resistance and velocity are square proportional. On the curve depicting the resistance, the wavy nature (at a Froude number of approximately 0.5) is due to the effect of the wave resistance on the total resistance.

This also means that even as a result of small changes in dive, the increase in resistance becomes more significant as the vessel accelerates. Therefore, even on a larger ship, it might be beneficial to select lighter components for the powertrain.

Not only does dive cropping change the size of the wetted surface and thus the resistance force, the shape of the wetted surface and the waterline section is also modified. In the present case, it geometrically cuts a wider shape out of the water surface as a result of the hull, so

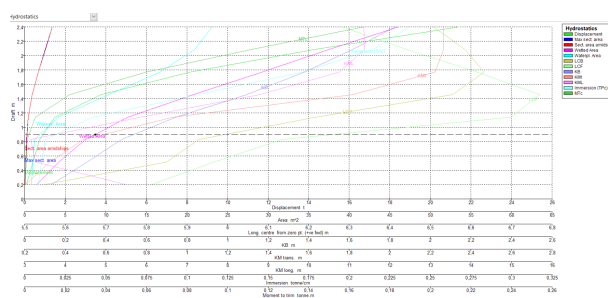


Figure 3: Characteristic curves calculated from vessel data

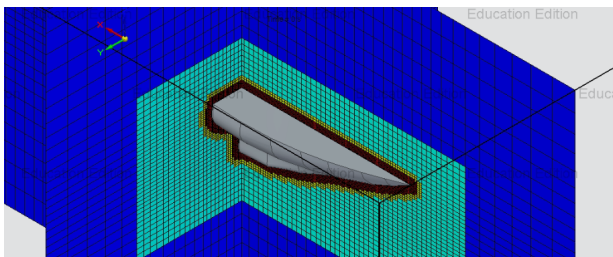


Figure 4: Locally compressed mesh around the stern of the hull

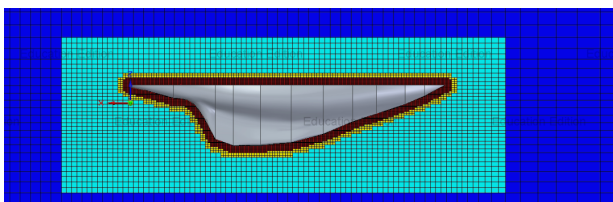


Figure 5: Locally compressed mesh around the stern of the hull (side view)

the current image must also be examined (Fig. 7). If the immersion shape changes leading to the flow rate generating early-breaking vortices around the hull or accelerating too quickly around the maximum width, a drastic reduction in speed results.

#### 4. Analysis

By examining the results, several findings are made. At higher speeds, as was expected, the resistance force on the ship differs greatly between the two dives, increasing the draft from 1.68 m to 1.7 m by 4606 N. Therefore, the effect of changing the draft in the order of a few centimeters is also significant. By plotting the velocity distribution around the vessel from the current image, it was found that behind the point where the width of the vessel is greatest (towards the stern) next to the side plate, the flow rate accelerates locally and then decelerates again back to the velocity observed around the front of the vessel. Around the ship, in addition to the surface that is in the shadow of the overflow (i.e., the accelerated flowlines next to the ship do not—or only partially—affect), the velocity of the medium decreases significantly. The velocity of the medium at and around the intersection of the waterline area and the axis of the steering bearing is close to 0 m/s. It can be seen that neither the magnitude (13.7 m/s) nor the location of the maximum flow velocity (the narrowing arc behind the main rib) causes a large decrease in velocity (Fig. 8).

#### 5. Conclusion

It can be said that by replacing the internal combustion engine and its associated drive chain, this ship will be subjected to an excessive resistance force which will reduce its forward speed. The test vessel is mass-produced

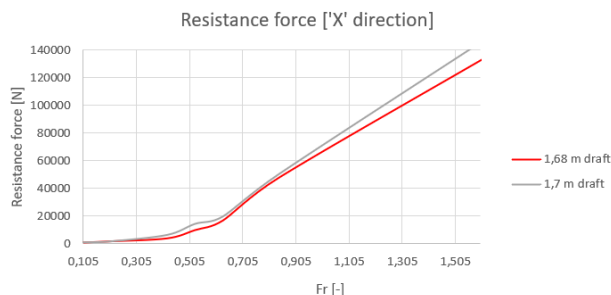


Figure 6: Comparison of the magnitude of the resistance a ship is subjected to under two load cases



Figure 7: Comparison of the magnitude of the buoyancy acting on a ship under two load cases

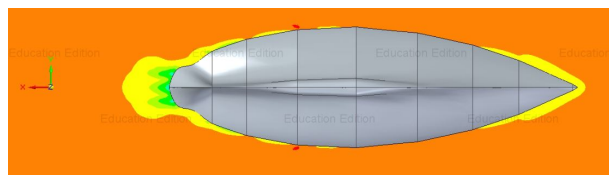


Figure 8: Flow velocity around the ship (higher: red, lower: orange)

and, in the case of vessels operating with possible minor modifications to its class, the calculation is expected to yield the same result with similar engines. For other types of vessels, by following the testing methodology, accurate answers to the questions raised in Section 2.2 are provided, which are vital, for example, before a sailing race (in which case, the engine is merely excess ballast). Since the calculations were performed on a horizontally floating sailboat, the subject of a further study could be the examination of a tilted vessel or of a hull protruding whilst accelerating using the same methodology. Questions may also be raised about an excessive number of additional batteries that may be inserted to increase the range of the electric motor and their possible placement in the light of swimmers as this presupposes additional dive options.

#### REFERENCES

[1] XLII/2000, Water Transport Act  
 [2] Lévai, E.: Elektromos segédhajtás beépítése egy acél építési anyagú, 50 m<sup>2</sup>-es tengeri cirkáló típusú,

kedvtelési célú vitorlás kishajóba, 2021, 2–21, 30–35

[3] Simongáti, Gy.; Hargitai, L.: Kishajók. Budapest,

2012, 14–15 ISBN: [978-963-279-643-7](#)

## MECHANICAL DEBURRING OF DRILLING-INDUCED EXIT BURRS IN CARBON FIBRE REINFORCED POLYMER COMPOSITES

ANDRÁS GÖDRI<sup>1</sup>, ANNA NIKOLETTA HELLE<sup>1</sup>, AND NORBERT GEIER\*<sup>1</sup>

<sup>1</sup>Department of Manufacturing Science and Engineering, Budapest University of Technology and Economics, Műegyetem rkp. 3, Budapest, 1111, HUNGARY

Carbon fibre reinforced polymer (CFRP) composites have excellent specific mechanical properties, which have contributed to the replacement of metallic structural components in high-tech sectors. However, the anisotropic and inhomogeneous properties of CFRPs render them difficult to cut. Burr is one of the main machining-induced macro-geometrical defects in CFRPs. Even though burr does not weaken the resultant strength of the composites (unlike delamination), its removal is time-consuming and costly. The main aim of the present paper is to investigate the efficiency of the mechanical deburring method. Deburring experiments were carried out on unidirectional CFRP, based on a full factorial experimental design using a special solid carbide cutting tool. The effects of feed and cutting speed were analysed using digital image processing and visual evaluation of high-resolution images. The experimental results show that the examined factors seem to have no significant effect on the results over the applied parameter range, because the exit burrs were successfully removed at each parameter setting. Furthermore, during the deburring process, the formation of a significant amount of chamfers was observed. Since the size of the chamfers depends on the size of delamination-induced material deformation and process control, it should be either compensated for or monitored in the future to develop a more reliable deburring process.

**Keywords:** deburring, carbon fibre reinforced polymer, exit burr, drilling, digital image processing

### 1. Introduction

Nowadays, carbon fibre reinforced polymer (CFRP) composites make up a significant proportion of materials used in the automotive, defence, aerospace, marine and space technology industries where it is almost indispensable [?]. The reason for their popularity is due to the fact that they have excellent mechanical properties, however, their anisotropic and inhomogeneous properties cause major problems like delamination, microcracks and burrs which have to be solved in machining. The main machining-induced defects in terms of machining CFRPs are delamination and burrs which bring about inaccuracies and also damage the structure of the workpiece [?].

Although the formation of burrs in quasi-homogeneous materials like metals has been studied for decades, research into burr formation in fibrous composites is not that extensive. In fibre reinforced polymer composites, the burr formation mechanism strongly depends on the following five key factors: the material to be machined, the fibre cutting angle ( $\theta$ ), the machining direction, the supporting plate in use and the cutting edge radius ( $r_\beta$ ). Four types of chip-removal mechanisms are associated with machining unidirectional CFRPs when the rake angle ( $\gamma$ ) is positive and the cutting edge radius

( $r_\beta$ ) is small: type I:  $\theta = 0^\circ/180^\circ$ , type II:  $\theta = 45^\circ$ , type III:  $\theta = 90^\circ$ , and type IV:  $\theta = 135^\circ$ . The fibre cutting angle has a significant effect on the texture of the machined surface as well as on the burr formation mechanism [?]. Jia et al. [?] examined the effect of the machining direction at the working point. They observed that in the absence of an external supporting plate, the machining is bending-dominated and the probability of uncut fibres and burrs forming increased. However, if the fibre is supported by either a plate or a material, the machining is fracture-dominated and the possibility of surface damage is minimal.

Fuji et al. [?] investigated the effect of the cutting edge radius and fibre cutting angle on surface defects after machining and found that if  $r_\beta$  is relatively small, machining will occur with fracture-dominated fibre cutting. However, should  $r_\beta$  be too large, bending-dominated thread cutting takes place, where there is no guarantee that cutting will be successful. They also studied burr formation during drilling and observed that the area around the hole can be divided into four separate regions, where the boundaries of the regions were chosen based on the fibre cutting angles. These four regions are symmetrical in pairs and the same processes take place in them, as can be seen in Fig. ?? . If the fibre cutting angle is within the

\*Correspondence: [geier.norbert@gpk.bme.hu](mailto:geier.norbert@gpk.bme.hu)

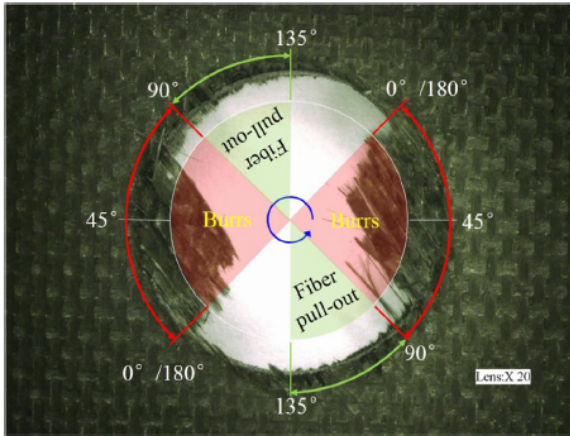


Figure 1: Surface damage as a result of drilling CFRP laminates using a worn tool [?]

range of  $90^\circ < \theta < 180^\circ$ , the material is machined under favourable conditions. This range is not characterized by burr formation but fibre pull-out occurs more frequently (depicted by the green range in the figure). If the fibre cutting angle is within  $0^\circ < \theta < 90^\circ$  (illustrated by the red range in Fig. ??), the tool will machine the material under adverse conditions. Within this interval, if the tool edge radius is large, burrs will always form here.

Xu et al. [?] examined burr formation, tearing and delamination with a digital microscope and an ultrasonic C-scan technique using three tools with different geometries. They observed that the feed has a significant effect on the extent of drilling defects. They also noted that while the cutting performance of brad and spur drills is the best during drilling, the dagger drill was the least satisfactory.

The primary purpose of machining is to produce clear as well as burr- and damage-free geometrical features. Several suggestions have been made for the parameter set and the use of special cutting tools to ensure damage-free machining. Yu et al. [?] investigated a new tool geometry for CFRP drilling. The double-pointed tool had an extra-grooved helical cutting edge, which was significant due to the removal of burrs formed during drilling. The experiment was also performed with a conventional drill as a reference and later compared to the two results which showed that no burrs occurred at the exit point of the holes, even after more than 100 drilling operations had been performed.

In the case of the improper selection of a machining technology and parameters, the remaining burrs can

be reduced by deburring methods. Islam et al. [?, ?] investigated the effectiveness of deburring strategies using electrical discharge machining (EDM) and observed that the material removal rate increased for the negatively charged tool and as the capacity increased, the voltage and gas pressure also rose during both solid-state dielectric EDM processes. In addition, compared to conventional oily EDM, oxygen caused the material removal rate to almost triple and that of air to nearly double. Based on these results, it was stated that dry EDM is much more effective than oily EDM with regard to the deburring of CFRP. Park et al. [?] investigated a hybrid cryogenic method for deburring. They compared four setups and established that the final setup was the most effective with a burr removal rate of 100%.

Even though the aforementioned deburring technologies are suitable to remove CFRP burrs, their material removal rate is not as good as the mechanical equivalent. A relatively wide range of cutting tools can be used for mechanical deburring [?], e.g., compact tools that can remove both the entrance and exit burrs (like spiral slot drills) as well as those that can only remove burrs on one side of the composite (like tapered countersink drills). However, since the number of studies examining their effectiveness is relatively low in the field of CFRP deburring, the main aim of the present study is to analyse the mechanical deburring of drilling-induced burrs in unidirectional CFRP composites.

## 2. Experimental setups

The deburring experiments were examined on a pre-drilled vinyl ester-based unidirectional carbon fibre reinforced polymer (UD-CFRP) plate. The main mechanical properties of the UD-CFRP plate at different fibre orientation angles ( $\Phi$ : angle between the fibre direction and load directions of the mechanical tests) are listed in Table ?. The pre-drilled composite can be seen in Fig. ?. The diameter of the pre-drilled holes was  $d = 10$  mm. Given that the performance of the mechanical deburring was tested on the exit burrs, the entrance burrs were removed by a sheet of sandpaper to prevent them from influencing the evaluation.

The deburring experiments were conducted on a Konidia B640 3-axis machining centre. A Nilfisk GB733 industrial vacuum cleaner was used to remove the carbon fibres from the machining zone. A FRAISA 20340.450 uncoated, solid carbide compression end mill with coarse teeth was used with a diameter of  $D = 10$  mm and a point angle of  $\sigma = 135^\circ$ . The schematic diagram of the

Table 1: Main mechanical properties of the applied UD-CFRP

Mechanical properties	$\Phi = 0^\circ$	$\Phi = 30^\circ$	$\Phi = 60^\circ$	$\Phi = 90^\circ$
Tensile strength (MPa)	$547.85 \pm 45.78$	$61.22 \pm 5.15$	$17.36 \pm 1.31$	$19.01 \pm 1.83$
Charpy impact strength (kJ/m <sup>2</sup> )	$263.17 \pm 24.76$	$26.83 \pm 2.24$	$9.35 \pm 1.16$	$5.28 \pm 0.20$
Average Shore D hardness (-)		$88.2 \pm 0.4$		
Average interlayer shear strength (MPa)		$21.77 \pm 0.70$		

Table 2: The values of the parameters at different levels

Parameters	Levels		
	1	2	3
Cutting speed ( $v_c$ m/min)	20	60	100
Feed ( $f$ mm/rev)	0.05	0.075	0.1

deburring cycle is illustrated in Fig. ???. The applied deburring cycle was a rolling circular interpolation motion, where the cutting point of the tool was at the middle of the main cutting edge at the point denoted by  $T$  in the absence of a cooling fluid. The experiments were designed by the full factorial method. The parameter set was chosen based on previous works [?, ?] and suggestions from tool producers. The parameter sets can be seen in Table

???. The set values of the parameters are interpreted at the  $T$  position of the cutting tool. Each experimental setting was repeated five times and their order was randomized to eliminate hidden errors during the experiment. A Dino-Lite Premier AD7013MZT digital handheld microscope was applied for image capturing before and after deburring. The drilled and deburred holes were captured by the microscope from the top side while they were illuminated from the bottom side by an LED source to improve the contrast of the images. The digital images taken before and after deburring were processed to determine the burr area ( $A_b$ ). The main steps of the digital image processing are illustrated in Fig. ???. Firstly, the original image was taken, before being filtered and segmented in the second step. Finally, the image was cut to form a particular shape

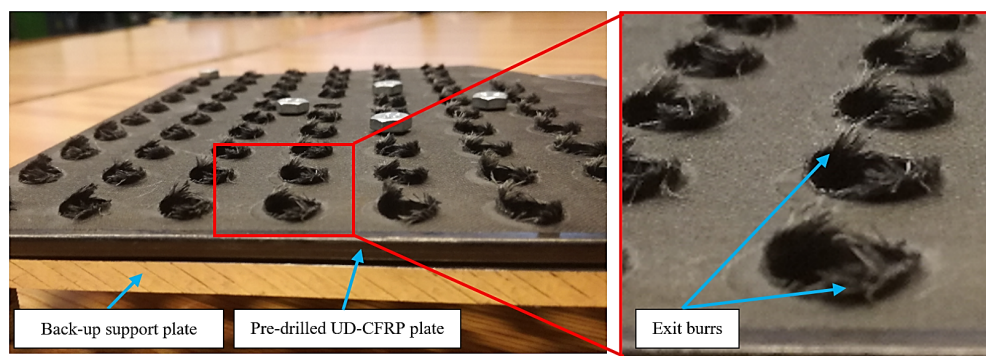


Figure 2: Drilling-induced exit burrs at the edges of the pre-drilled holes in the CFRP composite

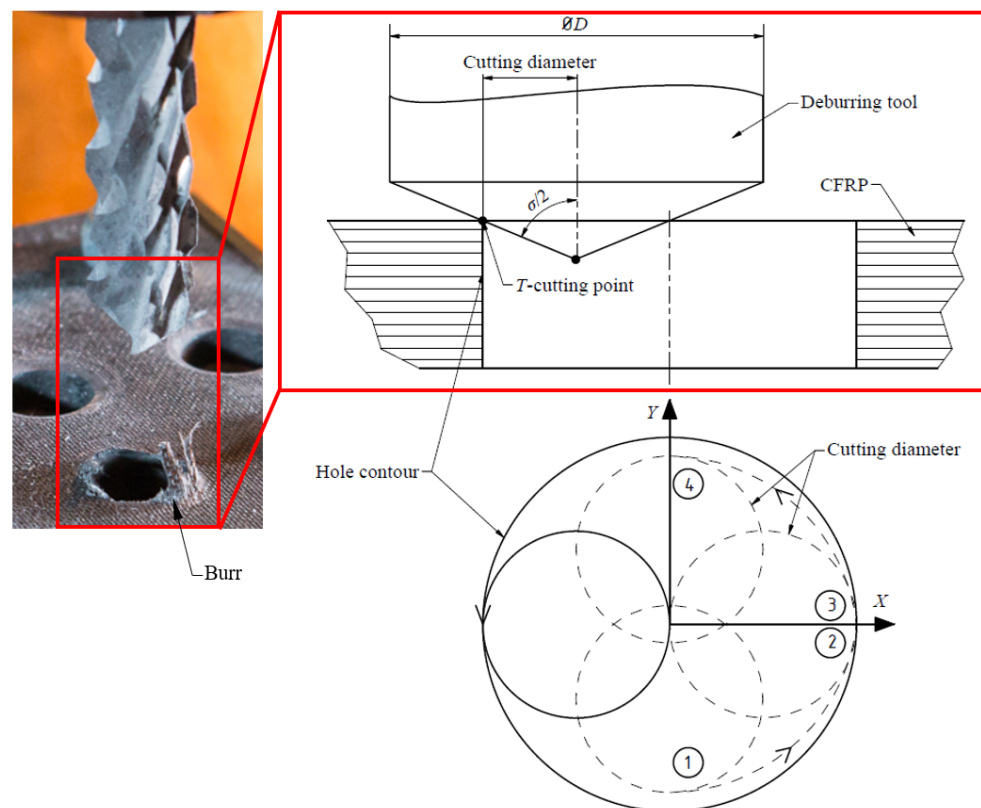


Figure 3: The rolling circular interpolation motion and the  $T$  cutting point of the tool

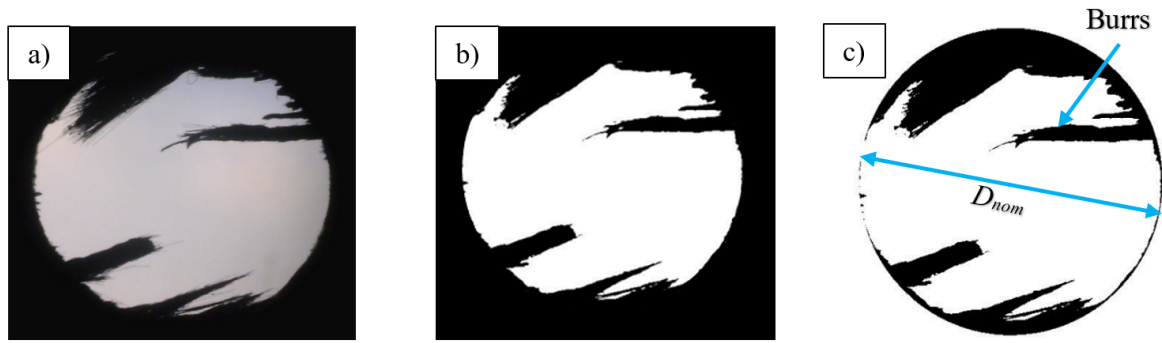


Figure 4: Main steps of the digital image processing method: (a) original image, (b) filtered and segmented image, (c) cut around hole

in order to determine the burred area parameter by pixel counting and transformation. The  $A_{b0}$  parameters, which are listed in Table ??, were determined before the deburring experiments.

### 3. Results and discussion

The efficiency of mechanical deburring was examined in this study on drilling-induced exit burrs by comparing the parameters  $A_{b0}$  and  $A_b$ . Each parameter was determined by a digital image processing method of images taken before and after deburring. The digital image processed holes – before and after deburring – are summarised in Fig. ?. As can be seen, the holes contained a significant amount of burr before deburring, which was radically reduced by the applied deburring cycle. It can be stated that the deburring experiment was successfully completed. In addition, based on the images, the examined parameters seem to have no significant effect on the results because the exit burrs were totally removed under all experimental conditions. Furthermore, some remaining burrs can be seen on the post-deburring photos. These errors could be the result of the following three main issues: (i) an error in terms of the digital image processing method could distort the filtered and segmented photos, (ii) the inner surface of the holes can reflect light or contain some uncut fibre which can also distort the photos, and (iii) if the entrance side of the hole contour contains burrs or uncut fibres, these will be visible on images as well as disfigure

the filtered and segmented photos.

The  $A_b$  parameters were also determined by the digital image processing method. In Fig. ??, the parameters  $A_{b0}$  and  $A_b$  were both depicted so they can be easily compared. These  $A_b$  values were consistent with the photos. It can be seen on the diagram that the deburring cycle minimized the average amount of burr ( $A_b = 2.496 \text{ mm}^2$ ), where the standard deviation was relatively low ( $s(A_b) = 0.422 \text{ mm}^2$ ).

In addition to the analysis of the burred area, the deburred workpiece was quantitatively evaluated by taking a high-resolution photo of each hole which were then visually evaluated by searching for machining-induced surface defects, e.g., uncut fibres, fragmentation, delamination, burr formation and burnout. These enlarged images of the holes present all the macro-type errors which could be observed and identified (Fig. ??a-h). The properties of the critical holes can be seen in Table ?. It was observed that the macro-type errors were characteristically uncut fibres. It can also be noticed that the defects mostly appeared symmetrically on the chamfers as a result of the directional dependence of the unidirectional CFRP plate, as was also observed by Fuji et al. [?].

It can be seen that 4 out of the 5 repetitions with the parameters  $v_c = 20 \text{ m/min}$  and  $f = 0.1 \text{ mm/rev}$  contained macro-type errors, so this parameter set can be identified as the most unfavourable setup and the set  $v_c = 60 \text{ m/min}$  and  $f = 0.1 \text{ mm/rev}$  with 3 out of the 5 repetitions containing such areas as the second least

Table 3: Burr areas before deburring ( $A_{b0}$ )

No.	$A_{b0} \text{ (mm}^2\text{)}$								
1	22.0168	10	15.9655	19	17.1038	28	12.7630	37	15.5607
2	16.3193	11	12.5244	20	11.7950	29	13.7123	38	17.7133
3	17.6914	12	12.1362	21	11.8991	30	27.4602	39	14.9731
4	15.9935	13	10.3192	22	22.1512	31	18.0514	40	25.4493
5	14.1156	14	23.8615	23	16.8891	32	19.2630	41	17.4130
6	16.0116	15	14.4638	24	13.9843	33	12.6162	42	14.4501
7	13.0983	16	11.1045	25	11.8457	34	14.7083	43	22.6858
8	16.6144	17	13.7582	26	12.8019	35	33.3027	44	14.4981
9	20.3942	18	12.2648	27	15.2845	36	14.7146	45	12.4184

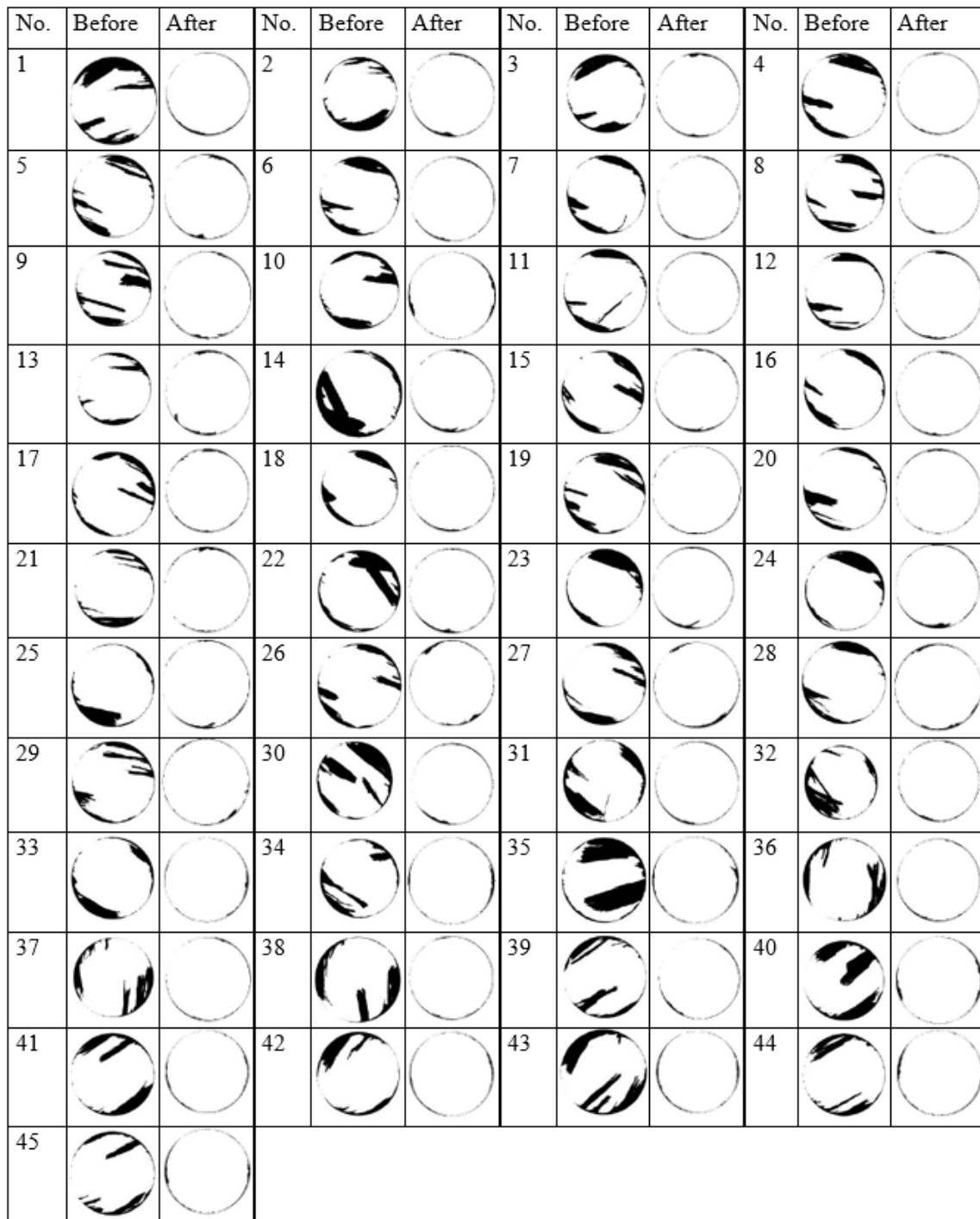


Figure 5: The digital image processed holes – before and after deburring

favourable. Only 1 out of the 5 repetitions for the parameter set  $v_c = 20$  m/min and  $f = 0.01$  mm/rev consisted of macro-type errors, possibly as a result of a random influential effect. No macro-type errors were visible by the naked eye in the other holes.

By taking into account that each experimental setup analysed resulted in efficient deburring, the maximum  $v_c = 100$  m/min and  $f = 0.1$  mm/rev is recommended to achieve the maximum material removal rate (MRR).

Although the present experimental results show that

the developed mechanical deburring technology is efficient over the whole analysed parameter range of  $v_c = 20 - 100$  m/min and  $f = 0.05 - 1$  mm/rev, a significant degree of chamfer formation was observed. Since the size of these chamfers probably depends on the size of delamination-induced material deformations and process control, this should be compensated for or monitored in the future.

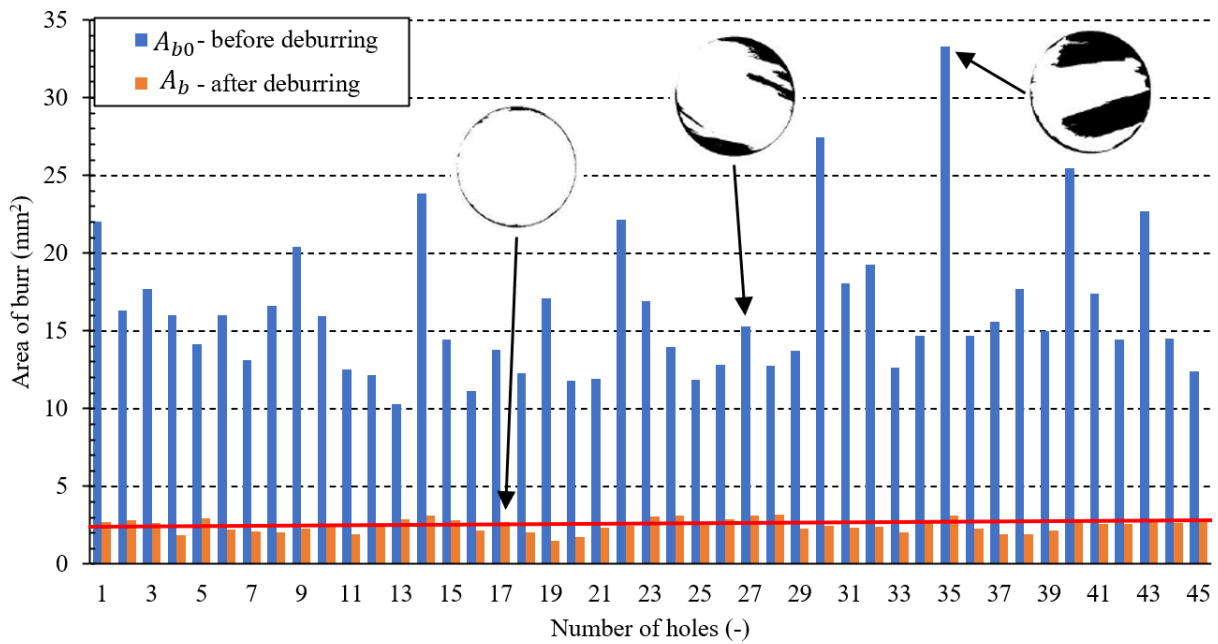


Figure 6: Comparison of burr areas before ( $A_{b0}$ ) and after ( $A_b$ ) the applied deburring cycle 8

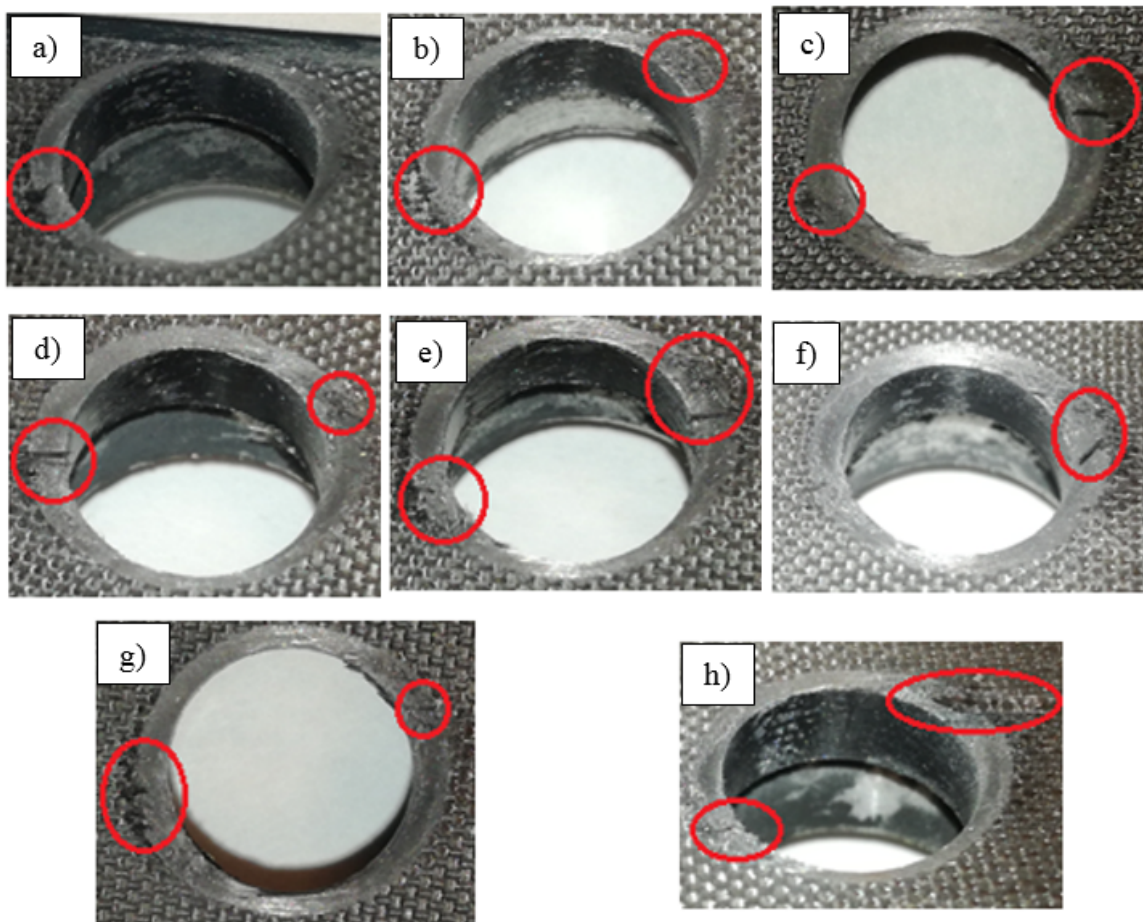


Figure 7: The holes with observed macro-type errors: a) burrs, b) uncut fibres and rough surface roughness, c) burrs and uncut fibres, d) uncut fibres and rough surface roughness, e) rough surface roughness, f) uncut fibres, g) burrs and uncut fibres, h) rough surface roughness and delamination

Table 4: Properties of the holes containing macro-type errors

Presented picture	No. of hole	Applied parameters during deburring	
		$v_c$ (m/min)	$f$ (mm/rev)
a)	4	20	0.1
b)	5	20	0.1
c)	13	20	0.01
d)	15	60	0.1
e)	17	60	0.1
f)	20	20	0.1
g)	39	20	0.1
h)	45	60	0.1

#### 4. Conclusions

In the present study, the influence of the cutting speed ( $v_c$ ) and feed ( $f$ ) on the efficiency of mechanical deburring was experimentally analysed. The efficiency of mechanical deburring was examined by digital image processing. According to the present study, the following conclusions can be drawn:

- The applied mechanical deburring technology successfully removed all CFRP burrs in each experimental setup.
- The experimental results show that neither the feed nor the cutting speed have a significant influence on deburring over the analysed parameter range.
- According to the quantitative evaluation, the observed holes with macro-type errors show that the parameters  $v_c = 20$  m/min and  $f = 0.1$  mm/rev can be identified as the most unfavourable setup, followed by the parameter set  $v_c = 60$  m/min and  $f = 0.1$  mm/rev.
- As the mechanical deburring was successful when implementing each parameter set, it is recommended that the maximum parameters  $v_c = 100$  m/min and  $f = 0.1$  mm/rev be applied in order to maximise the material removal rate (MRR).
- During the deburring process, a significant degree of chamfer formation was observed. Since the size of these chamfers depends on the size of the delamination-induced material deformations and process control, this should be compensated for or monitored in the future.

#### Acknowledgements

This research reported in this paper and carried out at BME was partly supported by the National Research, Development and Innovation Office (NKFIH) No. OTKA-PD20-134430, the NRD Fund (TKP2020 NC, Grant No. BME-NC) based on the charter of bolster issued by the NRD Office under the auspices of the Ministry for Innovation and Technology, and the project “Centre of Excellence in Production Informatics and Control”

(EPIC) No. EU H2020-WIDESPREAD-01-2016-2017-TeamingPhase2-739592. The authors acknowledge the support of Csongor Pereszlai and Dániel István Poór in their experimental work.

#### REFERENCES

- [1] Poór, D. I.; Geier, N.; Pereszlai, C.; Xu, J.: A Critical Review of the Drilling of CFRP Composites: Burr Formation, Characterisation and Challenges. *Compos. B Eng.* 2021, **223**, 109155 DOI: [10.1016/j.compositesb.2021.109155](https://doi.org/10.1016/j.compositesb.2021.109155)
- [2] Geier, N.; Davim, J. P.; Szalay, T.: Advanced Cutting Tools and Technologies for Drilling Carbon Fibre Reinforced Polymer (CFRP) Composites: A Review. *Compos. A Appl. Sci.* 2019, **125**, 105552 DOI: [10.1016/j.compositesa.2019.105552](https://doi.org/10.1016/j.compositesa.2019.105552)
- [3] Jia, Z.; Fu, R.; Niu, B.; Qian, B.; Bai, Y.; Wang, F.: Novel Drill Structure for Damage Reduction in Drilling CFRP Composites. *Int. J. Mach. Tools Manuf.* 2016, **110**, 55–65 DOI: [10.1016/j.ijmactools.2016.08.006](https://doi.org/10.1016/j.ijmactools.2016.08.006)
- [4] Wang, F.-j., Yin, J.-w.; Ma, J.-w.; Jia, Z.-y.; Yang, F.; Niu, B.: Effects of Cutting Edge Radius and Fiber Cutting Angle on the Cutting-Induced Surface Damage in Machining of Unidirectional CFRP Composite Laminates. *Int. J. Adv. Manuf. Technol.* 2017, **91**, 3107–3120 DOI: [10.1007/s00170-017-0023-9](https://doi.org/10.1007/s00170-017-0023-9)
- [5] Xu, J.; Li, C.; Mi, S.; An, Q.; Chen, M.: Study of Drilling-Induced Defects for CFRP Composites Using New Criteria. *Compos. Struct.* 2018, **201**, 1076–1087 DOI: [10.1016/j.compstruct.2018.06.051](https://doi.org/10.1016/j.compstruct.2018.06.051)
- [6] Yu, Z.; Li, C.; Kurniawan, R.; Park, K. M.; Ko, T. J.: Drill Bit with a Helical Groove Edge for Clean Drilling of Carbon Fiber-Reinforced Plastic. *J. Mater. Process. Technol.*, 2019, **274**, 116291 DOI: [10.1016/j.jmatprotec.2019.116291](https://doi.org/10.1016/j.jmatprotec.2019.116291)
- [7] Islam, M. M.; Li, C. P.; Won, S. J.; Ko, T. J.: A Deburring Strategy in Drilled Hole of CFRP Composites Using EDM Process. *J. Alloys Compd.* 2017, **703**, 477–485 DOI: [10.1016/j.jallcom.2017.02.001](https://doi.org/10.1016/j.jallcom.2017.02.001)
- [8] Islam, M. M.; Li, C. P.; Ko, T. J.: Dry Electrical Discharge Machining for Deburring Drilled Holes in CFRP Composite. *Int. J. Precis. Eng. and Manuf. Green Tech.* 2017, **4**(2), 149–154 DOI: [10.1007/s40684-017-0018-x](https://doi.org/10.1007/s40684-017-0018-x)
- [9] Park, K. M.; Kurniawan, R.; Yu, Z.; Ko, T. J.: Evaluation of a Hybrid Cryogenic Deburring Method to Remove Uncut Fibers on Carbon Fiber-Reinforced Plastic Composites. *Int. J. Adv. Manuf. Technol.* 2019, **101**(5), 1509–1523 DOI: [10.1007/s00170-018-3045-z](https://doi.org/10.1007/s00170-018-3045-z)
- [10] Sorrentino, L.; Turchetta, S.; Bellini, C.: A New Method to Reduce Delaminations during Drilling of FRP Laminates by Feed Rate Control. *Compos. Struct.* 2018, **186**, 154–164 DOI: [10.1016/j.compstruct.2017.12.005](https://doi.org/10.1016/j.compstruct.2017.12.005)



## COMPARATIVE ANALYSIS OF BURRS IN UD-CFRP COMPOSITES USING ADVANCED HOLE MACHINING TECHNOLOGIES

ANNA NIKOLETTA HELLE<sup>1</sup>, CSONGOR PERESZLAI<sup>1</sup>, ANDRÁS GÖDRI<sup>1</sup>, AND NORBERT GEIER\*<sup>1</sup>

<sup>1</sup>Department of Manufacturing Science and Engineering, Budapest University of Technology and Economics, Műgyetem rkp. 3, Budapest, 1111, HUNGARY

Machining of carbon fibre reinforced polymer (CFRP) composites is challenging due to their inhomogeneous and anisotropic structure as well as the strong effect of the carbon fibres on wear. Burrs are critical machining-induced macro-geometrical defects in the case of the machining of CFRP composites, which may lead to assembly difficulties. Nowadays, although novel hole-machining technologies reduce the likelihood of burrs occurring, these technologies are often more costly and require longer machining times. The current experimental study focuses on the analysis of burrs induced by advanced hole machining technologies (helical milling, tilted helical milling and wobble milling) and comparison with a conventional one (conventional drilling). A total of 32 experiments were carried out in a VHTC 5-axis machining centre using uncoated solid carbide end mills. Furthermore, these technologies are compared and discussed based on the burrs experienced and average material removal rate (AMRR). Experimental results show that conventional drilling caused the lowest amount of burrs, followed by wobble milling, tilted helical milling and helical milling. Even though wobble milling is one of the most advantageous technologies in terms of burrs, the AMRR of conventional drilling is twenty times larger than that of wobble milling, therefore, the further development of wobble milling is recommended.

**Keywords:** carbon fibre reinforced polymer, exit burr, drilling, digital image processing

### 1. Introduction

Nowadays, the demand for fibre reinforced polymer composites is increasing and their key role in industry is undeniable. Carbon fibre reinforced polymer (CFRP) composites are no exception. According to a market report made in 2018 by M. Sauer and M. Kühnel [1], their demand by 2017 has more than doubled (114k tons) compared to that of 2010 (51k tons). The reason for this increasing trend lies behind the outstanding material and specific mechanical properties of these composites. CFRPs possess larger strength-to-weight ratios compared to metals, making them exceptionally suitable for parts built into assemblies connected to the aviation, aerospace and automotive industries, reducing fuel consumption [2, 3]. They also exhibit good levels of corrosion resistance and are very strong as well as stiff. However, to be a part of an assembly, these composites must be machinable, that is, can be drilled or milled. CFRPs are difficult to machine, since the carbon fibres significantly contribute to tool wear as well as make the material anisotropic and inhomogeneous. These aspects lead to several difficulties such as delamination, burrs, matrix degradation, micro-cracks or fibre pullouts [3, 4]. Since the present of burrs renders post-machining almost inevitable, in order to reduce the resources necessary for further manufacturing

and achieve the quality that the aviation and automotive industries require, novel technologies have been introduced. In the current study, the most frequently used and promising novel UD-CFRP machining technologies are compared, namely conventional drilling, helical milling, tilted helical milling and wobble milling. The kinematics of these technologies are illustrated in Fig. 1.

The kinematics of conventional drilling (Fig. 1a) is the simplest of the four technologies investigated: the axis of the tool is coincident to the axis of the hole along which the tool is moving downwards while rotating around this axis. Therefore, the diameter of the hole is determined by the diameter of the tool [2, 5]. This simplicity renders machining the least time-consuming and results in a large material removal rate (MRR), however, in the case of drilling, it is highly likely that the surface will be damaged when the tool enters and exits the composite, leading to separation of the laminated layers. This phenomenon is referred to as delamination, which can render parts unsuitable for further assemblies.

To prevent such outcomes, a novel technology, namely helical milling (Fig. 1b) has been introduced. This technology is also known as orbital drilling [6], since the tool is moving on a helical path while rotating around its own axis, which is shifted from the axis of the hole. The kinematics can be carried out by circular inter-

\*Correspondence: [geier.norbert@gpk.bme.hu](mailto:geier.norbert@gpk.bme.hu)

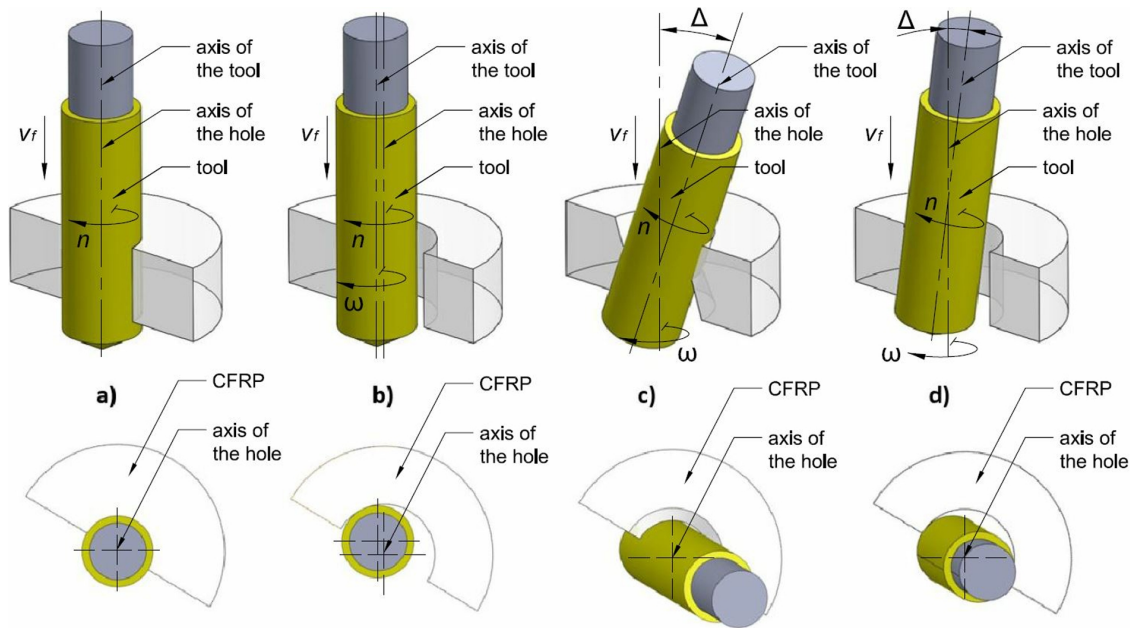


Figure 1: The examined technologies: a) conventional drilling, b) helical milling, c) wobble milling, d) tilted helical milling [3]

polation even with a tool with a smaller diameter to the hole being machined. According to Denkena et al. [5], although smaller forces and tool wear occur during machining, the drawback of this technology is that the effective cutting speed can reduce to zero [7].

To avoid an effective cutting speed of zero, further novel technologies have been introduced, which require a 5-axis machining centre or an industrial robot to be executed. One of them is tilted helical milling (Fig. 1d), during which the tool moves along a helical path while being tilted to the axis of the hole with an angle of  $\Delta$  [7]. The surface of the hole becomes threaded, which leads to a high incremental increase of surface roughness compared to the other technologies.

The novel technology, wobble milling (Fig. 1c), is also based on the principle of tilted axes. The tool chamfers the top and bottom sides of the composite while the axes of both the hole and the tool enclose an angle of  $\Delta$ . This tilted motion compresses the layers of the composite, before the material is eliminated between the chamfers. The advantage of this process is that the surface is less likely to delaminate.

In the case of technologies that can only be executed on the 5-axis machining centres or using industrial robots, since the time required for machining is higher than needed for drilling, a novel characteristic factor shall be introduced for their comparison, namely the average material removal rate (AMRR), which gives the average amount of material that is removed over a unit of time [3].

## 2. Experimental and theoretical methods

This chapter is comprised of three subchapters. The first summarizes the information about the workpieces, tools

and machines required for the experiments. In the second, details regarding the methods applied during the experiment and analysis are provided such as the experimental design, measurements of burrs, AMRR and analysis of variance (ANOVA).

### 2.1 Experimental setup

The workpieces of the present study were composed of UD-CFRP composite plates containing a vinyl ester matrix and long carbon fibres to provide reinforcement. The plates were cut by a water-jet cutting machine into cylindrical parts with a diameter of  $d = 40$  mm and thickness of  $h = 5$  mm.

The experiments were executed on a VHTC-130M-5HT 5-axis CNC machining centre with a tilting head. Two cutting tools were used for the machining: both tools were uncoated solid carbide end mills with only one cutting edge and a helix angle of  $\lambda = 25^\circ$ . For conventional drilling and milling technologies, a tool with a diameter of  $D_1 = 6$  mm (TIVOLY 82329710600) and of  $D_2 = 4$  mm (TIVOLY 82329710400) were used, respectively.

A Nilfisk GB733 industrial vacuum cleaner was used to eliminate chips from the working environment. No coolant was applied during the experiment.

### 2.2 Methods

#### Full factorial experimental design

By focusing on the impact of the technologies (category factor) and feed rate (continuous factor) on the burrs and AMRR, an experimental design was needed that can be applied in the case of category factors as well. In this study, a full factorial experimental design [8] was applied,

Table 1: Parameters and their levels

Levels	Feed rate (mm/min)			Technologies (-)			
	50	100	150	T1	T2	T3	T4

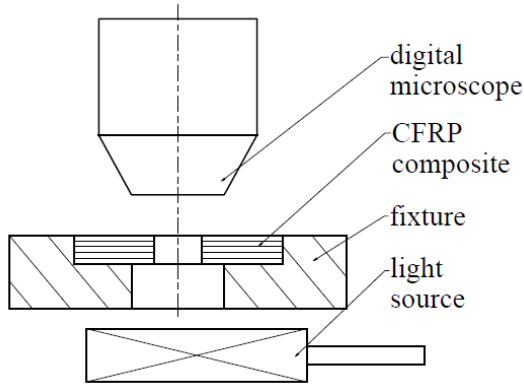


Figure 2: Digital photo capturing

moreover, the impact of the feed rate on the burrs and AMRR was examined in the case of the following technologies: conventional drilling ( $T1$ ), helical milling ( $T2$ ), tilted helical milling ( $T3$ ) and wobble milling ( $T4$ ). During the experiment, a constant cutting speed of  $v_c = 120$  m/min was set, thus the spindle speeds of the tools with diameters of  $D_1 = 6$  mm and  $D_2 = 4$  mm were  $n_1 = 6,366$  RPM and  $n_2 = 9,549$  RPM, respectively. The feed rate was set at the following three levels:  $v_{f,1} = 50$  mm/min,  $v_{f,2} = 100$  mm/min and  $v_{f,3} = 150$  mm/min. At least one of the settings was repeated five times for each technology to ensure the experiment was reproducible. In order to eliminate the hidden errors, the 32 experimental settings were randomized. The parameters and their levels are summarized in Table 1.

### Evaluating burrs

A Dino-Lite AM0413MT digital microscope was used with a 50x magnification and DinoCapture 2.0 software installed to examine the burrs. The photos were taken from the top and bottom sides of the composites which, being denoted by their individual numbers written on top, were identified with ease. A light source was placed beneath the composites to illuminate them, thereby enhancing the view of the uncut fibres as presented in Fig. 2.

In order to create as clear photos as possible, the distance between the composites and the microscope varied at each setting. As a result, since the holes in the photos were of different sizes, a universal evaluation method was needed to eliminate any errors when compared. This was achieved by creating an image of an ideal hole (not containing any black pixels where the white circle and black square meet) before segmenting it and calculating the number of black and white pixels found.

The photos of the machined holes, after being seg-

mented, were cropped given the absence of any black pixels at each side of the square and circular meeting point, as is shown in Fig. 3. Then the number of pixels was determined using the program Wolfram Mathematica, before being listed in Microsoft Excel and used for further calculations in Minitab. The burrs resulting from different technologies were compared based on a burr ratio factor ( $F_{br}$ ) and the length of the longest burr of the holes ( $L_B$ ).

The burr ratio factor

$$F_{br} = 100 \left( 1 - \frac{\frac{W_i}{T_i}}{\frac{W_{id}}{T_{id}}} \right) \quad (1)$$

is based on the quotient of the ratio  $W_i$  (the number of white pixels of the given hole) to  $T_i$  (total number of pixels of the given hole) and the ratio of  $W_{id}$  (the number of white pixels of the ideal hole) to  $T_{id}$  (total number of pixels of the ideal hole). The larger  $F_{br}$  is, the more burrs found in the hole. By following this method, since the difference in the size of the photos does not affect the results, the comparison of holes does not depend on the distance set between the microscope and the composites.

The length of the longest burr in the case of each setting examined was determined using AutoCAD 2022 by measuring their lengths based on the photos created by DinoCapture 2.0 (Fig. 3a). On the one hand, measurements were made by connecting the endpoint of the longest uncut fibre to the edge of the hole with a straight line and determining the distance between them three times before calculating their mean according to

$$L_B = \frac{1}{3} \sum_{j=1}^3 l_j \quad (2)$$

where  $l_j$  ( $\mu\text{m}$ ) denotes the measured length of the longest burr and  $L_B$  ( $\mu\text{m}$ ) represents the average length of a given burr used for comparison.

On the other hand, a corrected burr length ( $L_{B,corr}$ ) was calculated by measuring the length of the burr via the creation of a polyline: the five break points of these polylines were nearly equidistant from each other and each hole was measured three times. The lengths of the polylines were calculated by

$$L_{B,corr} = \frac{1}{3} \frac{1}{5} \sum_{j=1}^3 \sum_{i=1}^5 l_{ij} \quad (3)$$

where  $l_{ij}$  ( $\mu\text{m}$ ) denotes a segment of the polyline of the longest burr and  $L_{B,corr}$  ( $\mu\text{m}$ ) represents the length of the burr used for comparison.

### Average material removal rate

The AMRR ( $\text{mm}^3/\text{min}$ ), which gives the average amount of material removed, was calculated using

$$\text{AMRR} = \frac{hd^2\pi}{\Delta t} \quad (4)$$

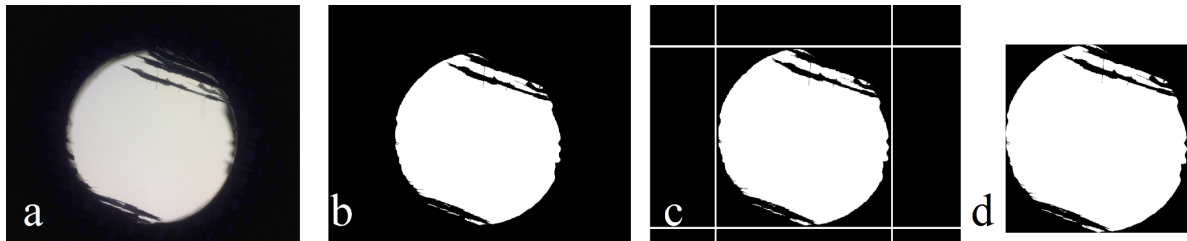


Figure 3: Digital image processing: a) photo captured by the digital microscope, b) segmented image, c) cropping the image, d) image used for the analysis

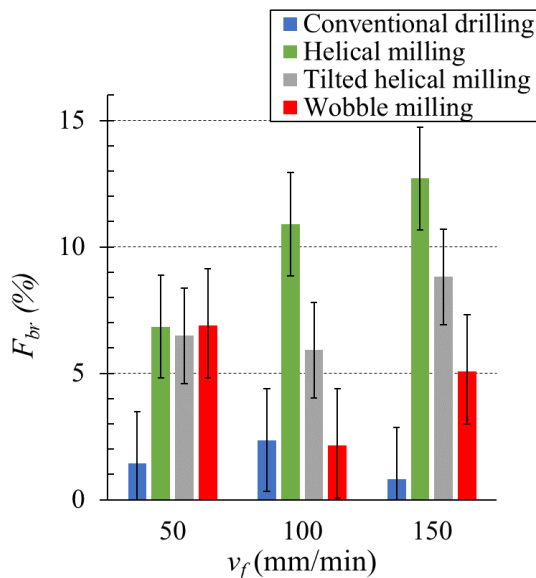


Figure 4: Burr ratio factor – feed rate diagram

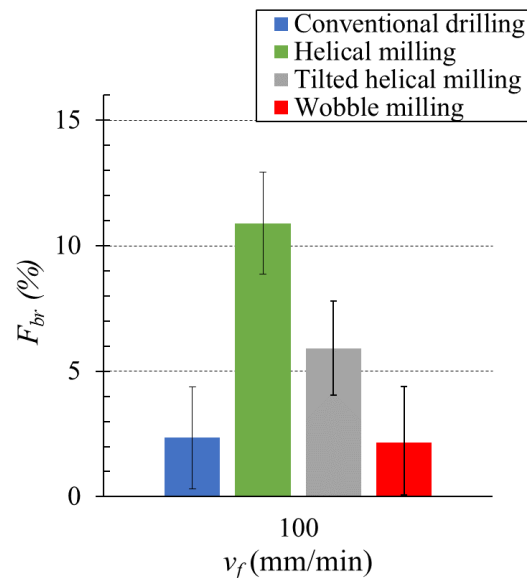


Figure 5: Main effect of the technologies on the burr ratio factor at  $v_f = 100$  mm/min.

by measuring the required time for machining. In Eq. 4,  $h = 5$  mm is the height of the composite,  $d = 6$  mm is the diameter of the holes, and  $\Delta t$  (min) denotes the time required for machining. Furthermore, assuming the holes have the same geometry at each setting, the average material removal rate could be determined.

Since the tool follows a longer path without machining in the case of 5D technologies, material is removed over a longer period of time. Therefore, the average material removal rate is needed to precisely compare these technologies.

### Analysis of variance

In this study, the impact of technologies on burrs was investigated by ANOVA. The null hypothesis states that the technologies have no significant effect on the burrs at a significance level of  $\alpha = 0.05$ .

## 3. Results and discussion

### 3.1 Analysis of burrs

The results show that the holes machined by conventional drilling and wobble milling are the most burr-free compared to the ideal hole, whereas the holes machined by

tilted helical milling and helical milling contain a larger number of burrs as is shown in Fig. 4. Helical milling resulted in the greatest amount of burrs, contradictory to the statements made by Denkena et al. [5] as well as Eguti and Trabasso [7] that helical milling can yield less burrs compared to conventional drilling. Given the main effect of technologies shown in Fig. 5, the null hypothesis was rejected, that is, these technologies have a significant impact on the burr ratio factor.

There is a significant difference between the length of burrs achieved by different technologies as can be seen in Fig. 6. The length of burrs was less than 1 mm for holes machined by conventional drilling and wobble milling, while the length of burrs in holes machined by tilted helical milling exceeded 2 mm at all settings. The longest burrs were produced by tilted helical milling and conventional helical milling, the latter resulted in burrs that were more than four times as long compared to conventional drilling and wobble milling at the greatest examined feed rate. Wobble milling, causing short burrs and a low burr ratio factor, yielded outstanding results compared to technologies based on helical milling.

Analysis of variance showed that with a significance level of  $\alpha = 0.05$  the null hypothesis was rejected, thus

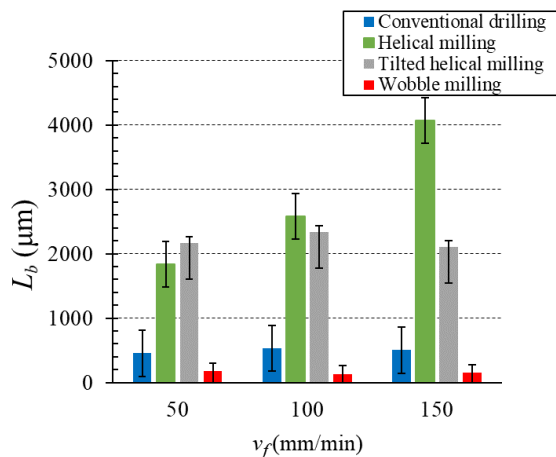


Figure 6: Length of burrs – feed rate

the technologies have a significant effect on the length of burrs.

### 3.2 Analysis of AMRR

AMRR was greatest in the case of conventional drilling. The AMRRs resulting from milling technologies were lower but similar. As is illustrated with the second axis of the diagram in Fig. 7, the AMRRs of the milling technologies are far greater than that of the drilling technology (4–5% of the AMRR). The AMRR values are shown in Fig. 7 with a feed rate of  $v_f = 50$  mm/min.

## 4. Conclusions

In this study, 32 holes were machined by conventional drilling, helical milling, tilted helical milling and wobble milling technologies using solid carbide end mills. The conclusions are summarized as follows.

- The experimental results show that the hole machining technology has a significant effect on the burr ratio factor defined at the exit of the holes.
- It was observed that holes machined by conventional drilling and wobble milling are characterized by the smallest amount of burrs compared to the other examined technologies. Since the burr ratio factors of holes machined by tilted helical milling and helical milling were larger, these holes contain a larger amount of burrs. Holes machined by helical milling are the least ideal of the four technologies examined concerning burrs.
- ANOVA results show that the technologies have a significant effect on the length of burrs in the holes.
- The length of burrs was the longest in the case of holes machined by helical milling, followed by tilted helical milling. However, with a feed rate of  $v_f = 50$  mm/min, holes machined by tilted helical milling contained the longest burrs. Holes machined

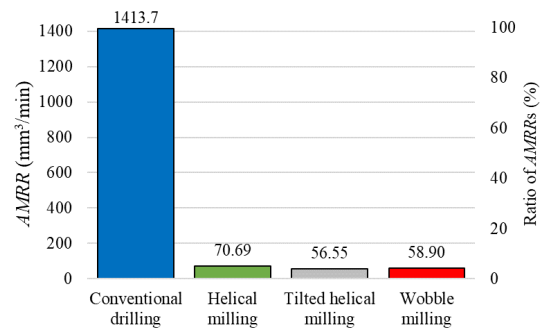


Figure 7: AMRR of the technologies compared to conventional drilling

by conventional drilling and wobble milling contained shorter burrs compared to the other milling technologies. Burrs of holes machined by wobble milling were the shortest, independent of the feed rate.

- The AMRR of conventional drilling is the largest due to the simplicity of its kinematics and the AMRR of the milling technologies is around 4–5% of that of drilling for the parameter set applied during the experiment.
- Although wobble milling is a promising novel hole machining technology, further development is required to increase its material removal rate.

## Acknowledgement

The research reported in this paper and carried out at BME was partly supported by the National Research, Development and Innovation Office (NKFIH) No. OTKA-PD20-134430, the NRDI Fund (TKP2020 NC, Grant No. BME-NC) based on the charter of bolster issued by the NRDI Office under the auspices of the Ministry for Innovation and Technology and the project “Centre of Excellence in Production Informatics and Control” (EPIC) No. EU H2020-WIDESPREAD-01-2016-2017-TeamingPhase2-739592. The authors acknowledge the assistance of Dániel István Poór in their experimental work.

## REFERENCES

- [1] *Composites Market Report 2018*. <https://www.avk-tv.de> download date: 2021
- [2] Boccarusso, L.; Fazio, D.D.; Durante, M.; Langella, A.; Capece Minutolo, F.M.: CFRPs drilling: comparison among holes produced by different drilling strategies. *Procedia CIRP*, 2019, **79**, 325–330 DOI: 10.1016/j.procir.2019.02.075
- [3] Geier, N.; Davim, J. P.; Szalay, T.: Advanced Cutting Tools and Technologies for Drilling Carbon Fibre Reinforced Polymer (CFRP) Composites: A Review. *Compos. A Appl. Sci.* 2019, **125**, 105552 DOI: 10.1016/j.compositesa.2019.105552

- [4] Poór, D. I.; Geier, N.; Pereszlai, C.; Xu, J.: A Critical Review of the Drilling of CFRP Composites: Burr Formation, Characterisation and Challenges. *Compos. B Eng.* 2021, **223**, 109155 DOI: [10.1016/j.compositesb.2021.109155](https://doi.org/10.1016/j.compositesb.2021.109155)
- [5] Denkena, B.; Boehnke, D.; Dege, J. H.: Helical milling of CFRP–titanium layer compounds. *CIRP J. Manuf. Sci. Technol.*, 2008, **1**(2), 64–69 DOI: [10.1016/j.cirpj.2008.09.009](https://doi.org/10.1016/j.cirpj.2008.09.009)
- [6] Pereira, R. B. D.; Brandão, L. C.; de Paiva, A. P.; Ferreira, J. R.; Davim, J. P.: A review of helical milling process. *Int. J. Mach. Tools Manuf.* 2017, **120**, 27–48 DOI: [10.1016/j.ijmactools.2017.05.002](https://doi.org/10.1016/j.ijmactools.2017.05.002)
- [7] Wang, Q.; Wu, Y.; Bitou, T.; Nomura, M.; Fujii, T.: Proposal of a tilted helical milling technique for high quality hole drilling of CFRP: kinetic analysis of hole formation and material removal. *Int. J. Adv. Manuf. Technol.* 2018, **94**(9–12), 4221–4235 DOI: [10.1007/s00170-017-1106-3](https://doi.org/10.1007/s00170-017-1106-3)
- [8] *Full Factorial Design - an overview. ScienceDirect Topics.* 2018 <https://www.sciencedirect.com>

## EXPERIMENTAL IMPLEMENTATION OF A RESOURCE-CONSTRAINED MULTI-PROJECT SCHEDULING PROBLEM SOLVER

KRISZTIÁN MIHÁLY\*<sup>1</sup>, MÓNika KULCSÁRNÉ FORRAI<sup>1</sup>, AND GYULA KULCSÁR<sup>1</sup>

<sup>1</sup>Department of Information Engineering, University of Miskolc, Egyetemváros, Miskolc, 3515, HUNGARY

Nowadays, project-based planning and execution are becoming more and more important in product life cycles; from the conceptual idea and its design to manufacturing and maintenance. Companies execute several projects simultaneously and these projects usually share the same resources resulting in conflicting situations. Since all projects have different requirements, constraints and goals that need to be achieved, the creation of a company-wide optimal schedule is difficult if all the aspects of each project are to be taken into consideration. Our paper presents an extended model and a scheduling problem-solving approach for resource-constrained, multi-project scheduling problems. In addition to defining the theoretical solution, its experimental implementation and results are presented.

**Keywords:** resource-constrained, multi-project, advanced project scheduling, ABAP

### 1. Introduction

Research into project scheduling has a solid and extensive background, moreover, it is still an active research area because – by not taking special cases into consideration – it belongs to the NP-hard (non-polynomial) problems [1]. Detailed reviews of project scheduling can be found in Refs. [2] and [3]. Scheduling problems concerning manufacturing optimization is an active research area [4]. NP-hardness renders any brute force-based calculation for practical problem sizes unrealistic and heuristic or search-based approaches are required to identify a quasi-optimal solution. In our work, an extended model for a resource-constrained multi-project scheduling problem has been developed with an advanced solver concept. The solver is based on a deterministic, rule-based, constructive schedule generation and is combined with search as well as simulation-based methods.

### 2. Resource-constrained project scheduling problem

Our extended model is based on the well-known resource-constrained project scheduling problem (RCPSP). First of all, the RCPSP is presented. In this paper, the following formulation is used to describe the RCPSP.

A given set of tasks (*activities, operations*) must be executed. The full set of tasks is denoted by  $T = \{1, 2, 3, \dots, n\}$ . There is a given set of resource types  $K = \{1, 2, 3, \dots, m\}$ . Practically speaking, a resource

type can represent machines, people or executors. The capacity of any resource type is known, limited and constant in the time horizon. The capacity of a resource type is denoted by  $R_k$ ,  $k \in K$ . Resource types are renewable, that is, after the execution of a given task, all blocked capacity becomes available again and can be used to execute a different task. There is no decreasing or increasing effect on the capacity of the task execution process (*amortization*). A deterministic method can be used to calculate the capacity of the resource type at any future time based on the initial state and actual scheduling.

Tasks are executed on the required resources. Task execution on the assigned resource types cannot be stopped or broken; once the execution has been started, the task must be completed. Pre-emption is not allowed. The processing time of each task is given. A virtual task can be defined, which does not require any resources.

The definition of the scheduling problem is subjected to two constraints: precedence constraints, that is, the prerequisite relation between tasks, and resource constraints. If the task  $j$  ( $j \in T$ ) has immediate predecessor tasks defined by set  $P_j$ , then all tasks  $i$  ( $i \in P_j$ ) must be completed before task  $j$  executed. It is forbidden for any circle to be located in the precedence graph.

If task  $j$  ( $j \in T$ ) requires one or more resources, they are defined by a set of pairs  $(r_{j,k})$ . It is forbidden to exceed the maximum available capacity of the resource type for any given resource need  $(r_{j,k}) \leq R_k$ ,  $\forall k \in K$ ,  $j \in T$ .

Let  $F_j$  denote the completion time of task  $j$  ( $j \in T$ ). A feasible solution can be described as a vector, in which the completion time of each task is given by the corre-

\*Correspondence: [altmihaly@uni-miskolc.hu](mailto:altmihaly@uni-miskolc.hu)

sponding  $F_j$ . Let  $A(t) = \{j \in T | F_j - p_j \leq t \leq F_j\}$  denote the set of tasks that are being processed at time  $t$ .

The objective of the RCPSP is to assign a feasible completion time for each task such that the makespan of the project is minimized, while the precedence and resource constraints are met.

### 3. Multi-project scheduling problems

The allocation of resources and scheduling tasks for multiple projects are NP hard problems that are more difficult than scheduling a single project [1].

In the literature, different classical optimization methods have been used to solve multi-project scheduling problems. A zero-one programming approach has been proposed [2] and an integer programming problem for generating the schedule as well as a simulation method for testing heuristic rules to choose the best schedule introduced [3]. Deckro et al. formulated the multi-project scheduling problem as a general integer programming model and presented a decomposition approach to solve large problems [5]. Jolayemi proposed an integer programming approach for multi-project scheduling problems and considered a special penalty function [6]. These outlined studies provide good solutions to small problems by using traditional optimization approaches. If the size of a problem is medium or large, then the classical methods cannot solve the problems within a reasonable execution time.

In the literature, several heuristic and metaheuristic methods can be found to solve multi-project scheduling problems. Researchers have developed many effective algorithms to generate feasible solutions to multi-project scheduling problems [7]. The goals of these developments were to increase the efficiency of the heuristic methods, extend the scope of the problems with new methods and reduce the computation time.

Many researchers have applied artificial intelligence methods to solve multi-project resource-constrained scheduling problems. For example, Kim et al. proposed a combined genetic algorithm to create a schedule [8] in order to minimize the project completion time. Kumanan et al. applied a genetic algorithm-based approach for generating the schedule of multi-project scheduling problems [9]. The objective function of the optimization was also to minimize the project completion time. Furthermore, Damak et al. proposed a variant of a genetic algorithm using a local search strategy to solve the problem by regarding the minimization of any project delays as the optimization goal [10].

After reviewing the related literature, it can be concluded that efficient and flexible methods need to be developed to improve the quality and robustness of the solutions of resource-constrained multi-project scheduling problems.

### 4. An extended model

The RCPSP describes a project along with its tasks and boundary conditions. As an extension of this problem, a case when different shared resources need to be assigned not only to individual projects but also to a set of projects executed in parallel has to be modelled. In our model, tasks that belong to many projects simultaneously are permitted. The projects can be differentiated from each other. On the one hand, the composition and constraints of each project can be unique, but on the other hand, projects can also have individually defined goals (objective functions).

In our model, a model transformation technique can be used. The essence of this possible transformation is that two new virtual tasks can be added to the set of tasks in the following way:

1. A new virtual task can be created as the starting task of the global project  $GS \in T$ . The GS task is defined as a predecessor task to all the tasks which did not have a predecessor task in the original problem.
2. Another new virtual task can also be added to the model. This task becomes the finalizing task of the global project  $GT \in T$ . All the tasks, which have no successor tasks in the original problem, become predecessor tasks for GT.

By applying this model transformation, the problem of projects executed in parallel is reduced to a single project scheduling problem. However, due to the different objective functions of individual projects, a new structure of objective functions has to be defined. This modelling approach is usually hard to construct in practice.

Instead of reducing the problem to a single RCPSP, the basic entities were reused in the extended problem and additional defining parameters as well as constraints introduced.

The resource types can be defined independently from the projects. One resource type can be described by its identifier and available capacity function. In the current implementation, each resource type can only have a constant basic capacity function, but the designed architecture is capable of defining capacity constraints that change over time.

The tasks, the required capacity with regard to the execution of tasks for each resource type and the precedence relations of tasks can be defined at the task level.

When creating a project, the project identification data and the task assignments can be defined. Furthermore, the weight of assigned project goals (objective functions) can also be specified. Although the list of possible objective functions in the current implementation is fixed, the applied software architecture is capable of extending and implementing further objective functions.

### 5. Problem-solving approach

The applied scheduling algorithm has two main components: the first is the project scheduler based on schedule

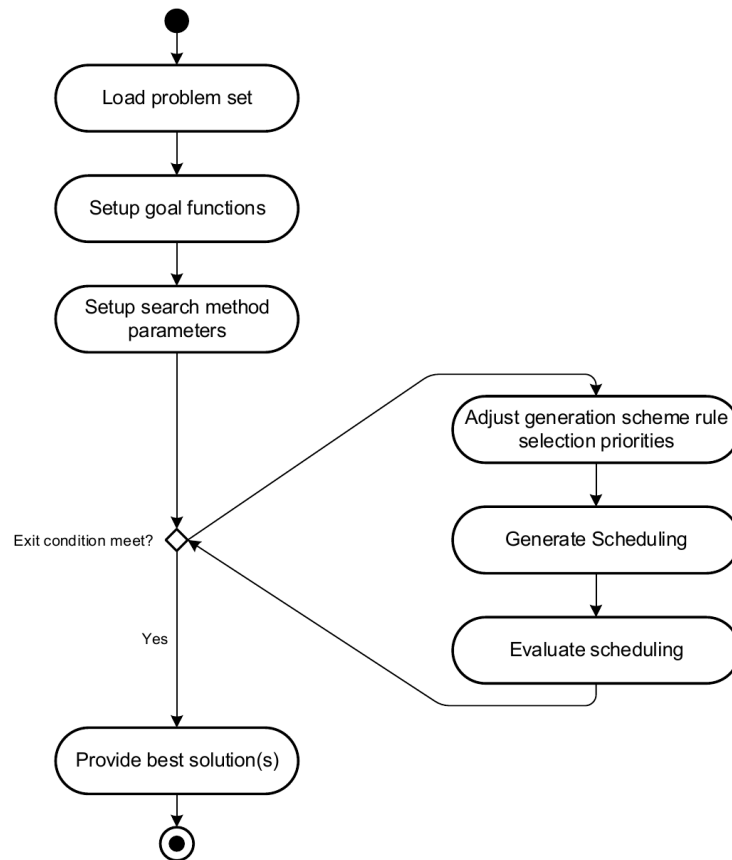


Figure 1: Problem-solving approach

generation schemes and the second is the search engine based on heuristics.

The main principle of the schedule generation scheme-based project scheduler starts with an empty schedule and during each iteration a suitable task can be selected from the set of non-scheduled tasks before being added to the schedule. In the iteration, when the next task is selected, all the given constraints are taken into consideration, which means that all prerequisite tasks are scheduled and all resource requests can be completed simultaneously. A differentiation is made between serial and parallel schedule generation schemes based on the method used to select the next executable task. The serial schedule generation scheme predominantly checks that the prerequisite tasks have been completed. The decision set contains tasks whose prerequisite tasks have all been completed. From this set of tasks, the task with the highest priority value, namely the best candidate, is selected. This task is scheduled in a way that it is added to the schedule as soon as possible, that is, when the required resource capacity can be fulfilled at the same time.

The parallel schedule generation scheme focuses mainly on the earliest starting time. In an intermediate state, the decision set contains the earliest executable tasks. In comparison with the serial schedule generation scheme, not all executable tasks form the basis for selecting tasks. From the decision set, the same priority-based

technique is used to select a candidate like in the serial schedule generation scheme. If more than one task meets the selection criteria, that is, they have the same priority, the schedule generation scheme randomly selects one of them.

In our approach, instead of making a random selection, a deterministic selection was applied, e.g. minimal slack, latest finish time, etc. Instead of only using one heuristic method, many task-selection heuristics are combined where the importance weighting of a heuristic component can be defined by the user. The schedule generation scheme can be influenced by parameters defined by a user or any consumer.

Using the schedule generation scheme as a simulation module, a heuristic search was implemented where the search engine alters the task-selection behavior using heuristic weights. The main flow of this problem-solving approach is depicted in Fig. 1.

In the first step, the problem set is loaded into the internal data model. The user can alter the project goal (objective functions) if the problem set needs to be changed. The user can alter the parameters of the default search module before the scheduler is started. Based on the given parameters, the search module executes simulations using the selected schedule generation scheme. The generated schedule is evaluated based on the defined goal (objective functions) and the search module can decide to reit-

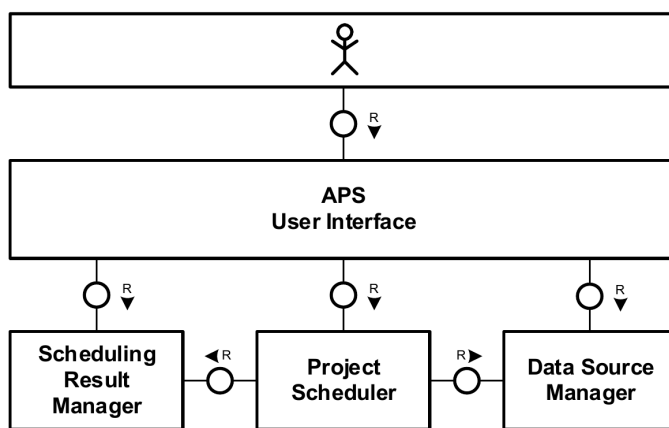


Figure 2: APS system agents

erate or exit. Among the simulations, the behavior of the schedule generation scheme is altered via selection rules.

## 6. Implementation

Enterprise Resource Planning (ERP) systems are predominantly used to manage all resources in an enterprise. An ERP system consists of a set of different modules responsible for coupled, separated and integrated application areas, e.g., manufacturing, finance, project management, etc. Although our study focused on a Systems Applications and Products (SAP) ERP system, our conceptual model can be used by other ERP vendors as well, after adjusting the implemented artefacts to suit the vendor-specific platform.

As with all standard project management (PM) systems, the SAP ERP PM supports the management of project-related entities such as the creation of projects, definition of tasks and dependencies, as well as definition of resources and their task assignments. In the execution phase of the project, execution reporting and collaboration with external parties are covered. In SAP ERP, this module is referred to as PM or project portfolio management (PPM) [11, 12].

A standalone advanced project scheduling (APS) component on the SAP NetWeaver platform was implemented. This high-level concept is presented in Fig. 2. The user accesses the APS user interface via the SAP GUI (graphical user interface). In this graphical user interface, the user can select the data set, decide where the projects can be selected and calibrate the scheduling parameters. When the project scheduler is started, the actual data is read from the data source, the detected scheduling algorithms are executed, and the scheduling results are stored via the scheduling result manager. The scheduling result is displayed in the APS user interface.

The main component of the system is the project scheduling agent. The internal structure of this component is depicted in Fig. 3. The scheduler consists of two disjoint sets of entities; one is visible to APS consumers, while the other is not. The aim of separating the disjoint

sets is to provide a stable interface to code against it and allow the implementation used to be changed. The external interface consists of the defining interfaces of the supported project scheduling problem (CPM, RCPSP), the reading interface of the resource manager and a solver factory.

RCPSPs in the absence of resource constraints can be solved using the critical path method (CPM) algorithm. The CPM result may be an import parameter to calculate a dynamic priority rule, therefore, the RCPSP may require a CPM solver and the CPM is modelled as an individual solver entity. The RCPSP solver has different implementation alternatives which can be changed at any time. The reason for this flexibility is that the implementation alternatives can be analyzed without consuming system artefacts.

The implemented solution realizes the schedule generation-based solvers (serial SGS and parallel SGS) and extended schedule generation-based solvers such as the RCPSP heuristic solver and the multi-objective search-based solver. The resource manager is responsible for checking the feasibility of the schedules provided by the scheduling algorithms.

## 7. Results

The extended model and the designed scheduler have been implemented in our own SAP NetWeaver 7.5 developmental test environment. Since the model and algorithm do not contain SAP-specific elements, both can be mapped to suit any object-oriented programming language. The main reason for this decision is to enhance integration later using the SAP PM module directly on the SAP platform.

The implemented solution was tested on known basic problems and our numerical results compared with the known results of the test problems by applying two methodologies.

In the first case, problems were mapped using special boundary conditions onto the extended model, for which optimal scheduling algorithms are provided. It is

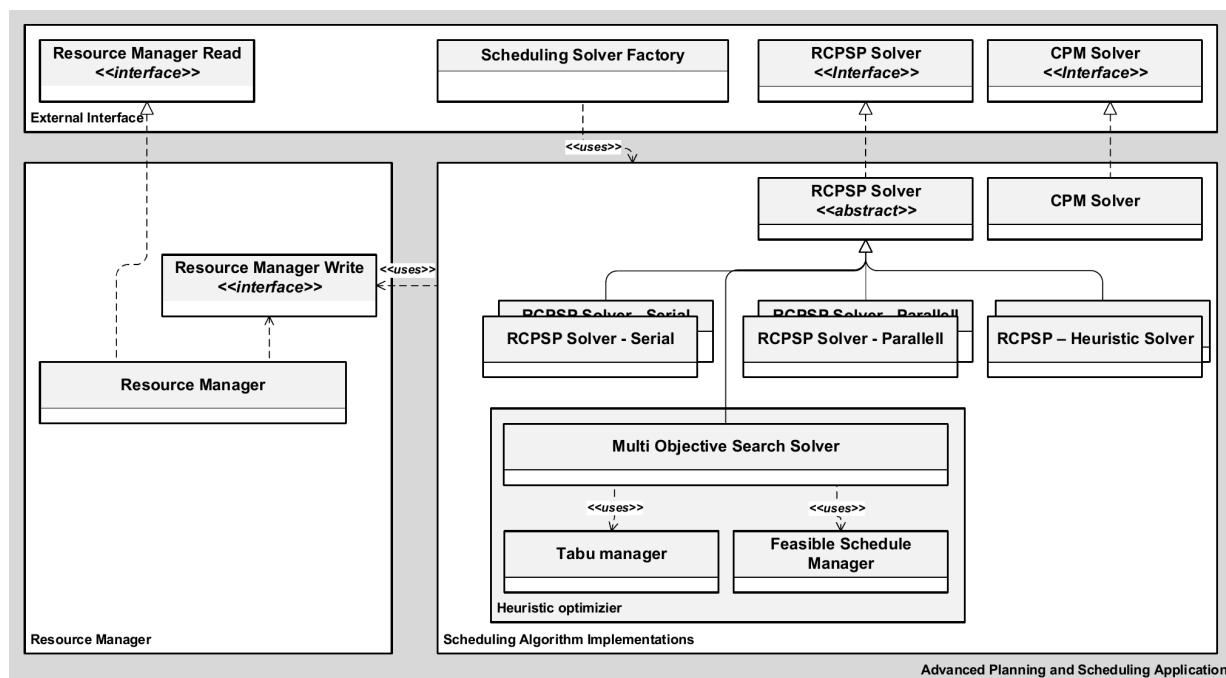


Figure 3: Project scheduler entities

known that Johnson's algorithm yields the optimal solution for permutation flow-shop scheduling problems with a makespan objective function [13]. In most cases (> 95%), our heuristic-based solver identified the optimal solution to small problems (consisting of up to 20 jobs).

In the second case, the basic RCPSP was mapped onto the extended model and the results with regard to the objective function concerning the completion time of the project (Cmax) were compared with the best published results [4, 14]. Our results were compared with the best results from benchmark problems. It was observed that for small problems (consisting of up to 30 jobs), in most cases (> 70%), the best known solution was identified by the scheduler.

## 8. Conclusions

Our research focused on modelling and solving an extended variant of resource-constrained, multi-objective, multi-project scheduling problems. The execution environment of the modelled project includes different resource types and their capacities, many projects with individual objective functions and precedence constraints, task-dependent individual processing times and resource requirements, tasks belonging to many projects, as well as project-dependent due dates.

During the research, new scheduling algorithms were developed that can flexibly solve problems while meeting all constraints. To generate detailed schedules, a predictive search algorithm was developed that includes an advanced simulation concerning the execution of the project. Multi-priority rule-based constructive algorithms were also developed by using schedule generation

schemes embedded in the scheduling engine. To solve the extended problem, a new approach based on the combined usage of search and constructive methods was proposed.

In this paper, the proposed model of the investigated problem, the solution method and the key features of its implementation were described. The effectiveness of the proposed algorithms is demonstrated by presenting two validation methods.

The results show that the proposed approach is efficient and flexible. The developed model of the extended problem was formulated in such a way that the individual requirements of tasks and projects can also be taken into account. By considering several aspects simultaneously, vital practical requirements can be incorporated into the model. The management strategy as well as tactical and operational control policies can be implemented, moreover, logical decisions made by modifying the weights of aspects concerning decision-making, namely objective functions and rules.

## Acknowledgements

This research was supported by the European Union and the Hungarian State, cofinanced by the European Regional Development Fund within the framework of the GINOP-2.3.4-15-2016-00004 project to promote cooperation between higher education and the industry.

## REFERENCES

- [1] Garey, M. R.; Johnson, D. S.: *Computers and intractability: A guide to the theory of NP-completeness*. (W. H. Freeman and Company, 1979) DOI: [10.1137/1024022](https://doi.org/10.1137/1024022)

- [2] Pritsker, A.; Allan, B.; Watters, L. J.; Wolfe, P. M.: Multiproject scheduling with limited resources: A zero-one programming approach. *Manage. Sci.*, 1969, **16**, 93–108 DOI: [10.1287/mnsc.16.1.93](https://doi.org/10.1287/mnsc.16.1.93)
- [3] Mohanthy, R. P.; Siddiq, M. K.: Multiple projects multiple resources-constrained scheduling: Some studies. *Int. J. Prod. Res.* 1989, **27**, 261–280 DOI: [10.1080/00207548908942546](https://doi.org/10.1080/00207548908942546)
- [4] Bálint, R.; Magyar, A.: Refrigerator Optimal Scheduling to Minimize the Cost of Operation. *Hung. J. Ind. Chem.* 2016, **44**(2), 99–104 DOI: [10.1515/hjic-2016-0012](https://doi.org/10.1515/hjic-2016-0012)
- [5] Deckro, R. F.; Winkofsky, E. P.; Hebert, J. E.; Gagnon, R.: A decomposition approach to multi-project scheduling. *Eur. J. Oper. Res.* 1991, **51**, 110–118 DOI: [10.1016/0377-2217\(91\)90150-T](https://doi.org/10.1016/0377-2217(91)90150-T)
- [6] Jolayemi, J. K.: Scheduling of projects under penalty and reward arrangements: A mixed integer programming model and its variants. *Acad. Inf. Manag. Sci. J.* 2012, **15**, 29–52 ISSN: 1524-7252
- [7] Gawiejnowicz, S.; Lin, B. M. T.: Scheduling time-dependent jobs under mixed deterioration. *Appl. Math. Comp.* 2010, **216**, 438–447 DOI: [10.1016/j.amc.2010.01.037](https://doi.org/10.1016/j.amc.2010.01.037)
- [8] Kim, K. W.; Yun, Y. S.; Yoon, J. M.; Gend, M.; Yamazaki, G.: Hybrid genetic algorithm with adaptive abilities for resource-constrained multiple project scheduling. *Comp. Ind. Eng.* 2005, **56**, 143–160 DOI: [10.1016/j.compind.2004.06.006](https://doi.org/10.1016/j.compind.2004.06.006)
- [9] Kumanan, S.; Jegan, J. G.; Raja, K.: Multi-project scheduling using a heuristic and a genetic algorithm. *Int. J. Adv. Manuf. Techn.* 2006, **31**, 360–366 DOI: [10.1007/s00170-005-0199-2](https://doi.org/10.1007/s00170-005-0199-2)
- [10] Damak, N. J. B.; Siarry, P.; Loukil, T.: Differential evolution for solving multi-mode resource constraint scheduling problems. *Comp. Oper. Res.* 2009, **36**, 2653–2659 DOI: [10.1016/j.cor.2008.11.010](https://doi.org/10.1016/j.cor.2008.11.010)
- [11] SAP SE, SAP Project and Portfolio Management 2015 <https://help.sap.com>
- [12] SAP SE, SAP S/4HANA 1709 FPS01, Project System (PS) documentation 2018 <https://help.sap.com>
- [13] Johnson, D. B.: Efficient algorithms for shortest paths in sparse networks. *J. ACM*, 1977, **24**(1), 1–13 DOI: [10.1145/321992.321993](https://doi.org/10.1145/321992.321993)
- [14] Kolisch, R.; Sprecher, A.: PSPLIB - A project scheduling problem library: OR Software - ORSEP Operations Research Software Exchange Program. *Eur. J. Oper. Res.* 1996, **96**(1), 205–216 DOI: [10.1016/S0377-2217\(96\)00170-1](https://doi.org/10.1016/S0377-2217(96)00170-1)

## RESEARCH ON AND PRACTICE OF ADDITIVE MANUFACTURING TECHNOLOGIES

PÉTER FICZERE\*<sup>1</sup>

<sup>1</sup>Department of Railway Vehicles and Vehicle System Analysis, Budapest University of Technology and Economics, Műegyetem rkp. 3, Budapest, 1111, HUNGARY

Today, additive manufacturing technologies are becoming increasingly popular. In order to take advantage of the opportunities offered by these new technologies, a different way of thinking at the design stage needs to be adopted. This new design thinking must be introduced into engineering education. In order to achieve this at the right level, practical experience is needed in parallel with a theoretical background on the technologies. This paper provides a brief overview of my research and results in the field of additive manufacturing.

**Keywords:** additive manufacturing, 3D printing, generative design, fused deposition modeling, material properties

### 1. Introduction

The spread of additive manufacturing technologies continues unabated. More and more applications are becoming commonplace. However, in certain areas, they must be applied cautiously. In many areas, questions are raised about which materials and technology to use from health, mechanical and strength points of view. Similarly, whether it is economically worthwhile to use this manufacturing process if other methods can be implemented to produce the part is a matter of debate.

Since the process is becoming more and more prevalent in industry, its inclusion in higher technical education is necessary. However, practical experience is also needed to ensure an adequate level of education. Another benefit of introducing additive manufacturing technologies into education is that it is a novel, interesting and exciting field that attracts the interest of students, which in turn boosts research in this area.

My research on additive manufacturing technologies began at the Department of Railway Vehicles and Vehicle System Analysis - formerly known as the Department of Vehicle Elements and Vehicle System Analysis (DRVVSA) at the Budapest University of Technology and Economics (BUTE) in 2007 through my PhD research. At that time, my research was supported by VARINEX Zrt. who produced test specimens for the investigations.

In 2015, the department also acquired two Fused Deposition Modeling (FDM) 3D printers, increasing the number of opportunities and expanding the spectrum of

my research. By this time, my investigations mainly focused on handmade pieces.

A significant proportion of the required measurements was carried out at the Department of Polymer Engineering and in the research laboratories at the Biomechanical Cooperative Research Centre both at the BUTE.

The results of my research are presented in this paper.

### 2. Method

A significant amount of experimentation is necessary to properly understand production technologies. During these experiments, questions often arise as to whether this or that can be achieved with this or that technology. Therefore, the fields of application were extended and the printers made available to students, which led to even more interesting and often questionable outcomes.

As the printers purchased (Prusa i3 and Zortrax M200) are open-source, the production parameters could be set as desired and the effects of each setting tested.

Another important and continuously explored as well as developed area is the investigation into the applicability of the technology.

### 3. Results

#### 3.1 Accuracy tests

Specimens of different shapes and geometries were produced to determine the accuracy of the machine and the surface quality of the printed parts.

Unfortunately, the studies did not provide precise and clear figures [1] since their accuracy is affected by

\*Correspondence: [ficzere.peter@kjk.bme.hu](mailto:ficzere.peter@kjk.bme.hu)

- the geometry of the part to be printed (flat or curved surfaces, curvature rate, position of the planes (horizontal, vertical or inclined));
- tolerances of conversion from the original CAD geometry to the STL file (input for the printer)
- the layer thickness
- the printing speed
- the printing temperature
- heating the table
- the orientation
- different levels of accuracy in the  $x$ - $y$  (layer) plane and perpendicular ( $z$ -direction) to it

Of course, these variables refer to printing using the same machine and different values may be obtained should another machine of an alternative type be applied.

It is important to note that some errors due to the manufacturing principle can be eliminated by preliminary modifications of the CAD model (toolpath correction), but some more advanced CAM software (code generators) are already capable of doing this.

The size correction needed to connect parts in operating assemblies was also investigated.

### 3.2 Fields of application

Due to a lack of space, only some of the completed projects are presented here, but many other smaller objects were printed, e.g., parts for robotic cars for the Bosch Future Mobility Challenge, miniature copies of traffic signs for sign-recognition simulations (for the Department of Automotive Technologies at the BUTE), various sprockets, battery holders, unique pieces of “jewellery”, ornaments, parts, representation and marketing materials, utility items, educational aids, etc.

#### Supply of spare parts

In many cases, given that it is not possible to obtain spare parts for a component that has failed in an older device, a copy of the component in question must be manufactured, otherwise the device becomes inoperable and therefore worthless. Although this technology is particularly important for veteran vehicles, in this case special attention must be paid to the stresses and strains on the components produced by the new method, moreover, should the part produced be non-compliant, it could even damage other irreplaceable parts [2].

Several individual parts that seemed to be irreplaceable have also been redesigned and manufactured (Fig. 1).

Nowadays, it is also important to note that more and more people are considering this solution to the lack of spare parts, purely for economic reasons. In the case of a major automotive unit or structure, the supply of spare

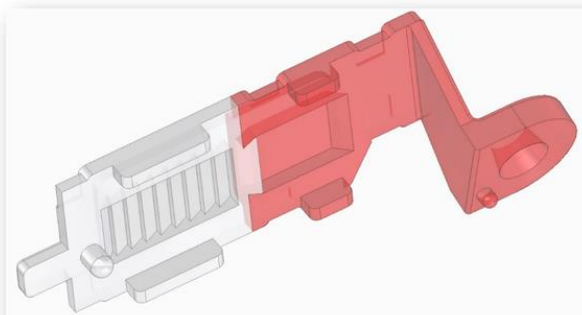


Figure 1: Replacement of individual parts [2]

parts has to be ensured even decades after its production has stopped. It is of course impossible to determine in advance exactly how many parts will need to be replaced. For this reason, manufacturers often accumulate unreasonably large stocks of specific parts, which are extremely costly to store or the machines and tools that produce them are costly to maintain.

#### Prototype development

Several prototypes have been developed at our department. One of the most interesting of which was the development of a medicine capsule. As is well known, the action of so-called retard capsules (composed of soft gelatine that is dissolved by acidic conditions found in the human stomach) is delayed. This delay and the extent of its effect also depend on the individual, making it difficult for the optimal dose of the active ingredient to be

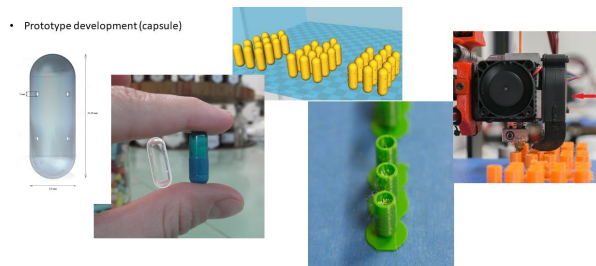


Figure 2: Prototype development (capsule) [3]

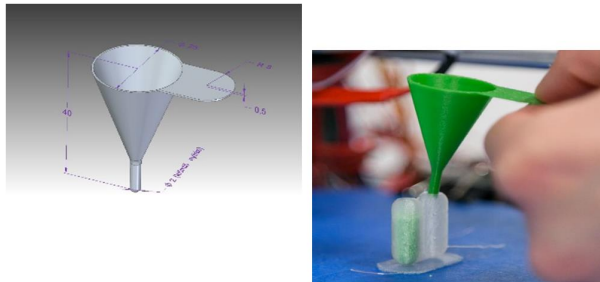


Figure 3: The manufacture of assistive devices [3]

determined correctly. The basic idea was to produce capsules of the same size as the original capsules, with various numbers of holes of different dimensions and shapes. The effect of such modifications on the rate and extent of release was then investigated. For the purposes of the studies, the individually designed capsules were printed and filled with a given quantity of caffeine pellets (Figs. 2 and 3) [3,4].

It can easily be seen that designing a modified mould for a part produced in large quantities by injection moulding before stopping production and changing the mould for a few parts needed for testing is not a cost-effective solution, which can lead to a serious loss of revenue [5].

In the same case, in order to fill the miniscule and lightweight caffeine pellets (it was particularly difficult to fill the capsules with the amount measured out into small sachets to the nearest microgram), a small funnel was designed and printed within a few minutes.

### Making tools and moulds

In many cases, high demands for the material the parts are composed of may be infeasible by applying some additive manufacturing technologies. In a case study when individual castings have to be produced, a casting mould for the remanufacture of a cylinder from the engine of a veteran vehicle can be seen in the middle photo of Fig. 4. On the left-hand side of the figure, a 3D CAD model is shown, which was used to print the mould from acrylonitrile butadiene styrene (ABS) using an FDM printer to produce (and later functionally assemble) the casting (right-hand side of Fig. 4) [6].



Figure 4: CAD model, 3D-printed casting mould and casted cylinder [6]



Figure 5: CAD model of a human metacarpal remodeled from CT scans and the printed pieces [8]

### The manufacture of medical implants and devices

One of the areas where additive manufacturing is expected to make the greatest amount of progress is the rapid and customizable production of medical implants and devices. Since the geometry of a given implant has to perfectly match the intact body parts of the person, very stringent requirements must be met with regard to the formal design (shape) of the model [7, 8].

However, these pieces also need to match the stiffness of a person's individual bone in terms of mechanical strength. The department has carried out several research projects along these lines.

In the case of the human metacarpal shown in Fig. 5 and 6, the geometry had to be modelled from CT scans. The stiffness of the real bone was measured, then the geometry of the 3D CAD assigned to the model with the 3D-printed material properties and the internal geometry changed by shape optimization until the stiffness of the printed piece perfectly matched the stiffness of the original bone.

### Optical photostress investigations

Since it is also possible to print from transparent (translucent) materials, the coating required for optical photostress investigations (which is difficult and time-consuming for complex geometries) can be easily printed given the right thickness and quality, thereby saving much time and reducing the amount of effort required (Fig. 7) [9, 10].

An additional advantage of this method is that it allows us to detect and determine the residual stresses that develop during production (Fig. 8) [11].

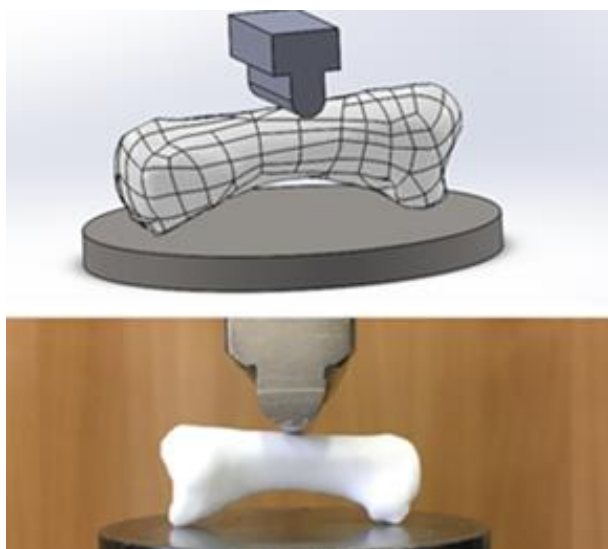


Figure 6: Validation of the material model used by the numerical simulation of a human metacarpal with measurements on a real printed part [7]

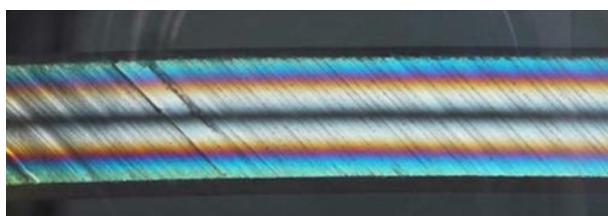


Figure 7: Fringe pattern on a 3D printed test specimen as a result of bending [9]

### 3.3 Economic analysis

When printing individual parts, how manufacturing costs are affected by the production of the workpiece quickly becomes apparent.

- chosen procedure
- production time, the 3D printing speed
- placement on the workspace
- position, orientation
- the quantitative requirement for support materials
- type of support materials
- percentage of filling
- type of filling
- layer thickness
- choice of materials
- number of units to be produced

Several economic calculations have been made to identify areas where the technology offers real advantages over other manufacturing processes [12].

How the aforementioned parameters affect production costs either directly or indirectly has also been investigated [5, 13].



Figure 8: Residual stresses in specimens subjected to tensile testing [11]

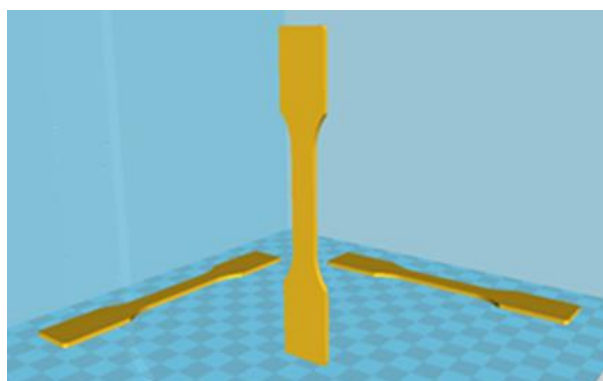


Figure 9: Test specimens produced in different directions and positions [14]

### 3.4 Material investigations

Additive manufacturing technologies are characterized by the fact that they compose arbitrarily complex parts, even with hollow geometries inside, layer by layer [14]. This implies that the bonding of layers to each other is assumed to be different from the bond strength within the layers [15], which has been proven in several cases.

In several manufacturing processes of different materials, how the material properties (of lying and standing specimens) in different directions relate to each other has been investigated (Fig. 9). The tensile curves in the highlighted directions were measured:

- FullCure 720 produced by the PolyJet process [1]
- FDM process and polylactic acid (PLA) [16]
- FDM process and Acrylonitrile Butadiene Styrene (ABS) [17]
- Selective Laser Sintering (SLS) process and polyamide 12 (PA12) [18]
- FDM process and Soft PLA (flexible plastic) [19]
- FDM process and High Temperature (HT) PLA (thermosetting plastic) [20]

Apart from the SLS process, the results show that the behavior of additively manufactured parts can be described by the model of an orthotropic material under all circumstances. Therefore, the determination of the corresponding material properties is a more complex task [21], where it is insufficient to only use Young's modulus  $E$  and Poisson's ratio  $\nu$  to describe the behavior of a material. In addition, the shear modulus of elasticity  $G$  must be measured [22].

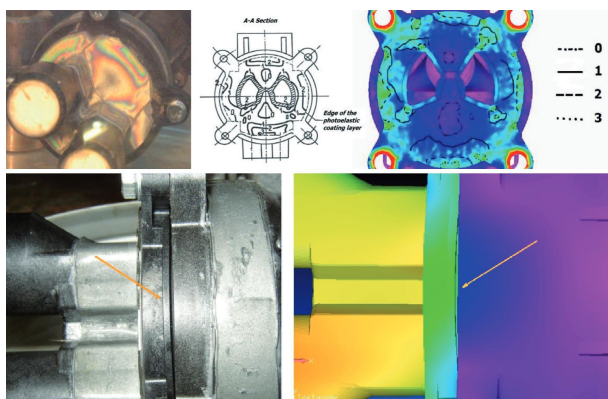


Figure 10: Validation of a material model by the optical photostress method [25]

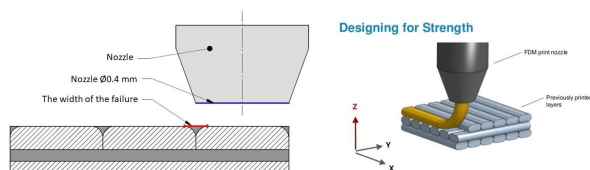


Figure 11: Identifying the causes of errors [25]

Of course, after determining the material models and material properties using a tensile testing machine, the results need to be validated. For this purpose, a method has been developed [23].

The effects of certain manufacturing parameters on strength have also been determined [24] and the reasons for these explored (Figs. 10 and 11) [25].

**Dynamic materials testing**

As certain components are also subject to dynamic loads, it is necessary to examine the parts manufactured by these processes for dynamic stresses. This test method has also been developed and performed on parts composed of PLA manufactured by FDM (Fig. 12) [26].

**Modification options affecting material properties**

Several options have been investigated that influence the mechanical strength parameters, including active cooling [27], the effect of heat treatment (publication in progress) and ironing (publication in progress).

**3.5 Examination of the impact of infill**

The possibilities of producing parts subjected to quasi-uniform stresses in a way that reduces the cumbersome and lengthy post-processing operations were also investigated. Such a method is the modification of the internal filling according to the stresses [28].

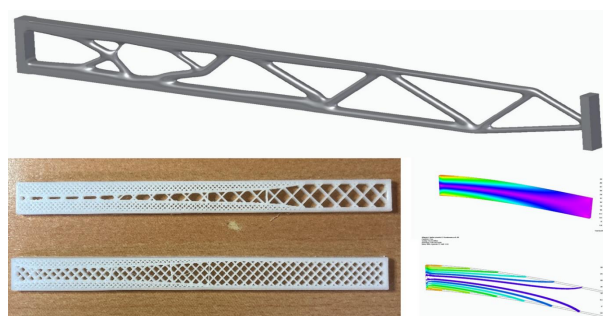


Figure 12: Difficult and easy to manufacture uniform strength supports [28]

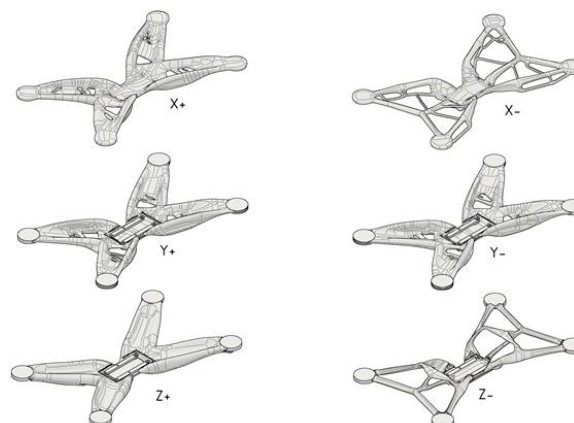


Figure 13: Drone to be manufactured by 3D printing using generative design

**3.6 Generative design in terms of additive manufacturing technologies**

Artificial intelligence-based design methods that can be used to design geometries according to different criteria, which by and large can only be produced by additive manufacturing, are currently being investigated (Fig. 13).

**Acknowledgments**

The author would like to express their gratitude to György Falk (VARINEX Zrt.) who greatly helped with the research in terms of both printing and giving professional advice.

The author is grateful to Dr. László Lovas who, as the head of the department, recognized the research potential of 3D printing and purchased the printers for the department as well as the necessary materials.

Last but not least, the author would like to thank Dr. Gábor Szabó who provided the material investigations.

**REFERENCES**

[1] Ficzer, P.; Borbás, L.; Török, Á.: Theoretical and practical investigation of rapid prototyping, in: Borkowski, S.; Selejdak, J.; Jelacič, D.; Hadzima, B. (Eds.) Toyotarity. Standarizations' Kinds,

- pp. 139–150 (Yurii V. Makovetsky, Dnipropetrovsk, Ukraine) 2011 ISBN: 978-966-1507-77-6
- [2] Janoch, Á.; Ficzer, P.: Additív gyártástechnológiák szerepe a veterán gépjárművek alkatrészellátásában, *GÉP*, 2019, **70**(3), 38–41 <http://epa.niif.hu>
- [3] Horváth, Á.M.; Ficzer, P.: Rapid prototyping in medical sciences. *Prod. Eng. Arch.* 2015, **8**(3), 28–31 DOI: 10.30657/pea.2015.08.07
- [4] Ficzer, P.; Horváth, Á. M.; Sipos, T.: Elalvásos balesetek csökkentési lehetősége additív gyártási eljárással fejlesztett kapszulák segítségével. *Közlekedéstudományi Szemle*, 2020, **70**(1), 77–85 DOI: 10.24228/KTSZ.2020.1.3
- [5] Ficzer, P.; Borbás, L.; Török, Á.: Economic investigation of rapid prototyping. *Int. J. Traffic Transp. Eng.*, 2013, **3**(3), 344–350 DOI: 10.7708/ijtte.2013.3(3).09
- [6] Lovas, L.: Öntőforma készítés 3D nyomtatással. *GÉP*, 2016, **67**(7-8), 13–16
- [7] Ficzer, P.: Design questions of the individual medical implants, in: Haber, I.; Bogdan, Cs.; Szoke, A. (Eds.) Proceedings of 4th international interdisciplinary 3D conference: Engineering section, pp. 57–67 (University of Pécs, Pécs, Hungary), 2018 ISBN: 978-963-429-267-8
- [8] Ficzer, P.; Bogy, P.; Horváth, E.; Lovas, L.: Simplified cad model of human metacarpal for implantation. *Des. Mach. Struct.*, 2018, **8**(2), 5–12 <https://www.uni-miskolc.hu>
- [9] Ficzer, P.: Usage of 3D printing in photostress investigation. *Prod. Eng. Arch.* 2015, **7**(2), 16–19 DOI: 10.30657/pea.2015.07.04
- [10] Ficzer, P.; Borbás, L.: New application of 3D printing method for photostress investigation. *Mater. Today: Proc.* 2016, **3**(4), 969–972 DOI: 10.1016/j.matpr.2016.03.030
- [11] Ficzer, P.; Borbás, L.; Szebenyi, G.: Reduction possibility of residual stresses from additive manufacturing by photostress method. *Mater. Today: Proc.* 2017, **4**(5), 5797–5802 DOI: 10.1016/j.matpr.2017.06.048
- [12] Seregi, B.L.; Ficzer, P.; Borbás, L.: Fémmalkatrészek additív és szubtraktív módon történő gyártásának összehasonlítása. *Acta Periodica*, 2021, **22**, 18–32 DOI: 10.47273/AP.2021.22.18-32
- [13] Ficzer, P.: Effect of 3D printing direction on manufacturing costs of automotive parts. *Int. J. Traffic Transp. Eng.* 2021, **11**(1), 94–101 DOI: 10.7708/ijtte.2021.11(1).05
- [14] Győri, M.; Ficzer, P.: Use of sections in the engineering practice. *Period. Polytech. Transp. Eng.* 2017, **45**(1), 21–24 DOI: 10.3311/PPtr.9144
- [15] Ficzer, P.; Borbás, L.: Material law for numerical analysis of rapid prototype products, in: Cosmi, F.; Iacoviello, F.; (Eds.) Proceedings of the 9th Youth Symposium on Experimental Solid Mechanics, Trieste, Italy, July 7-9, 2010, pp. 120-122 (Gruppo Italiano Frattura, Italy) ISBN: 978-88-95940-30-4
- [16] Ficzer, P.; Borbás, L.; Falk, Gy.: Additív gyártástechnológiák alkalmazhatósági vizsgálata testreszabott orvosi implantátumok méretezéséhez. *Biomech. Hung.* 2018, **11**(2), 69–75 DOI: 10.17489/2018/2/10
- [17] Markiz, N.; Horváth, E.; Ficzer, P.: Influence of printing direction on 3D printed ABS specimens. *Prod. Eng. Arch.* 2020, **26**(3), 127–130 DOI: 10.30657/pea.2020.26.24
- [18] Ficzer, P.; Borbás, L.; Falk, Gy.; Szebenyi, G.: Experimental determination of material model of machine parts produced by Selective laser sintering (SLS) technology. *Mater. Today: Proc.* 2018, **5**(13), 26489–26494 DOI: 10.1016/j.matpr.2018.08.104
- [19] Kis, K.; Ficzer, P.; Kovács, N.K.; Szebenyi, G.: Additív gyártástechnológiával előállítható rugalmas műanyagok vizsgálata. *GÉP*, 2018, LXIX: 4, 49-53 <http://epa.niif.hu>
- [20] Lukács, N.; Ficzer, P.; Szebenyi, G.: The impact of active cooling on heat resistant PLA. *Műszaki Tudományos Közlemények (EN)*, 2020, **13**(1), 118–121 DOI: 10.33894/mtk-2020.13.21
- [21] Ficzer, P.; Borbás, L.: Method to reduce the independent constants of orthotropic materials in rapid prototyping, in: Proceedings of the 11th Youth Symposium on Experimental Solid Mechanics, Braşov, Romania, May 30-June 2, 2012 pp. 129–135 (Curran Associates, Inc., Red Hook, NY, USA) ISBN: 978-1-63439-432-1
- [22] Ficzer, P.; Borbás, L.: Experimental investigation of the shear modulus in the case of pure tensile test. *Trans. Famena*, 2018, **42**(1), 27–36 DOI: 10.21278/TOF.42103
- [23] Ficzer, P.; Borbás, L.; Török, Á.: Validation of numerically simulated rapid-prototype model by photoelastic coating. *Acta Mech. Slovaca*, 2014, **18**(1), 14–24 DOI: 10.21496/ams.2014.002
- [24] Ficzer, P.; Lukács, N.L.: Influence of 3D printing parameters. *IOP Conf. Ser.: Mater. Sci. Eng.* 2020, **903**, 012008 DOI: 10.1088/1757-899X/903/1/012008
- [25] Ficzer, P.; Lukács, N.L.; Borbás, L.: The investigation of interlaminar failures caused by production parameters in case of additive manufactured polymers. *Polymers*, 2021, **13**(4), 556 DOI: 10.3390/polym13040556
- [26] Ficzer, P.: Experimental dynamical analysis and numerical simulation of the material properties of parts made by fused deposition modelling technologies. *Period. Polytech. Transp. Eng.* 2020, **48**(3), 221–225 DOI: 10.3311/PPtr.13947
- [27] Ficzer, P.; Lukács, N.L.: The influence of active cooling on heat resistant PLA in FDM technologies. *Mach. Des.* 2020, **12**(2), 37–40 <http://www.mdesign.ftn.uns.ac.rs>
- [28] Ficzer, P.; Lukács, N.L.: Examination of possibilities of the strength modification in the case of FDM/FFF manufacturing technology. *Des. Mach. Struct.* 2020, **10**(2), 27–34 <https://www.uni-miskolc.hu>

## USING FINITE ELEMENT ANALYSIS IN THE 3D PRINTING OF METALS

HUSSEIN ALZYOD\*<sup>1</sup> AND PÉTER FICZERE<sup>1</sup>

<sup>1</sup>Department of Railway Vehicles and Vehicle System Analysis, Budapest University of Technology and Economics, Műgyetem rkp. 3, Budapest, 1111, HUNGARY

Over the last few years, Additive Manufacturing, or as it is sometimes known, 3D printing, has become a significant research field for researchers worldwide. The necessity to increase the strength of materials and minimize their weight in the automotive and aviation industries has urged engineers and scientists to conduct more investigations and identify manufacturing methods to replace the classical ones. Additive manufacturing involves building a geometry layer by layer from a wide range of materials, which helps to utilize materials efficiently while minimizing the amount of waste produced as well as build complex, large geometries and light-weight components. Furthermore, it minimizes fabrication and processing times. In this paper, three different alloys were printed (TiAl6V4, AlSi10Mg and 316L) using MSC Simufact software to investigate the effect of changing machines on the effective stress and surface deviation. Furthermore, thermal analysis as well as mechanical, thermal and thermomechanical calibrations were carried out to determine a parameter set consisting of the laser power, inherent strains, fraction of exposure energy and volumetric expansion factor.

**Keywords:** additive manufacturing, 3D printing, simufact additive.

### 1. Introduction

Over the last three decades, research into printing technology/additive manufacturing (AM) has progressed from fast prototyping to Industry 4.0 [1, 2]. The Third Industrial Revolution took place in 1987 with the commercial exploitation of the first stereolithography (SLA) machine, which was developed by 3D systems and named SLA-1. After many editions of SLA machines in the early 90s, new AM principle technologies were launched, namely solid ground curing, fused deposition modeling and laminated object manufacturing [3, 4].

This development was followed by many years of continuous improvement in AM technology, from resin to metal powders and from non-functional molding applications to the fabrication of medical implants [5]. AM methods have been characterized in the literature based on a variety of parameters, including direct or indirect process technology, the state of the raw materials, and the materials used. The state of the raw materials is the most commonly used as illustrated in Fig. 1.

AM is a revolutionary manufacturing technique proliferating as major industries transition from conventional to advanced production methods. Three-dimensional printing is used in AM to convert engineering design files into fully functional and durable structures. After the components in the first layer have been bonded together using glue or heat, the second layer

is constructed and the bonding procedure repeated, enabling the construction of previously unimaginable geometries. AM creates samples of products quickly, which is crucial since it reduces the traditional trial-and-error process, allowing novel ideas to enter the market more quickly. It may also be used to rapidly create bespoke metal items to replace old or broken industrial parts.

#### 1.1 Part-building technology

Metal AM can be classified into four main categories as shown in Fig. 2: directed energy deposition, powder bed fusion, sheet lamination and binder jetting. Table 1 shows the thickness of layers in each process [6].

#### 1.2 Fields of application

Metal 3D printing is the fastest-growing sector. Metal AM is increasingly being utilized to create final products

Table 1: The thickness of layers in the metal AM process [6].

Processing	The thickness of layers (mm)
Directed energy deposition	0.089 – 0.203
Powder bed fusion	0.08 – 0.15
Sheet lamination	0.1 – 0.19
Binder jetting	0.089 – 0.203

\*Correspondence: [husein.alzyod@edu.bme.hu](mailto:husein.alzyod@edu.bme.hu)

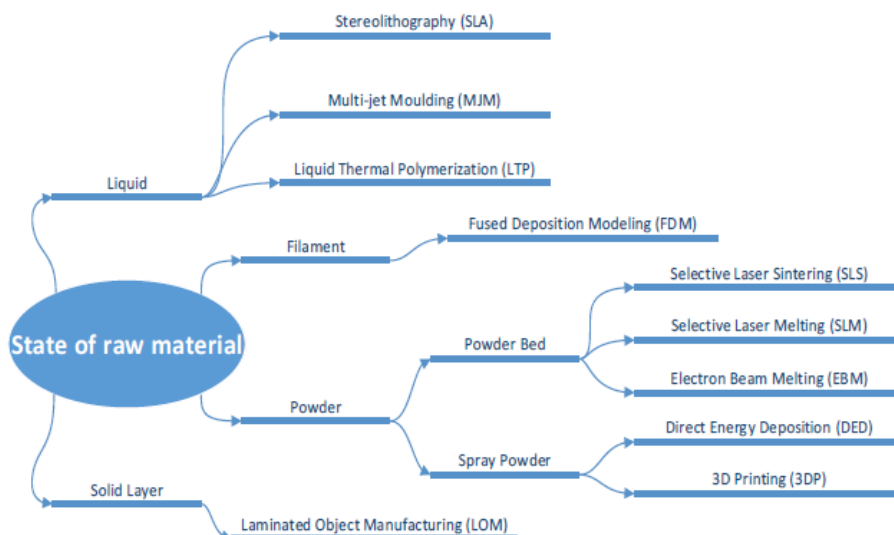


Figure 1: Types of Additive Manufacturing processes based on the state of raw materials [1].

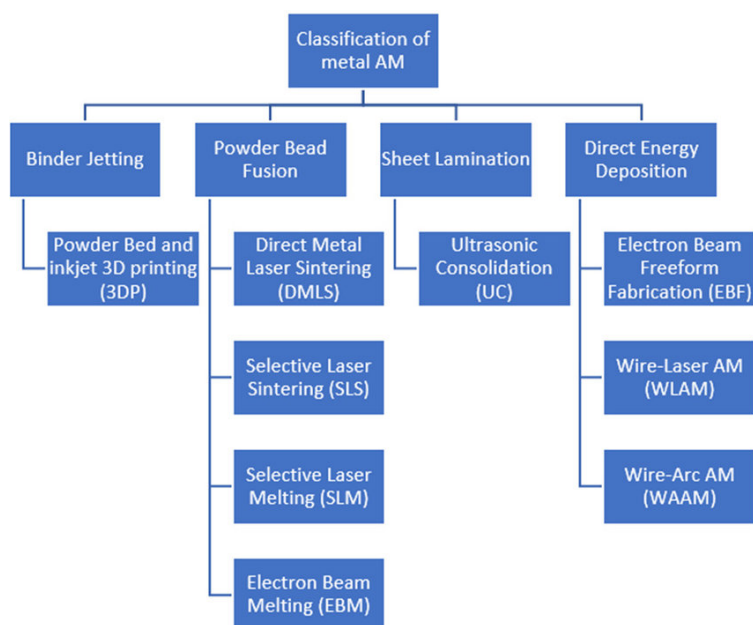


Figure 2: Classification of metal additive manufacturing technologies [5].

in many sectors like in the aviation, automotive, medical implants, material handling robotics as well as lifestyle and sport industries.

**The aviation industry** Companies in this sector are among the most well-known early investors of AM technology since they were among the first to upgrade from modest research projects to large-scale production runs. Norsk Titanium, Airbus, Alcoa and GE amongst others have begun serial production or are planning to invest in significant manufacturing operations within AM [7].

**The automotive industry** For many years, the automotive industry has utilized 3D printing to rapidly prototype single test components or entire visualization models.

Leading companies are experimenting with AM. Small series or customized production may be the first sectors to adopt this technology [7].

### 1.3 Modeling approach in Simufact

Many commercial companies, e.g., Autodesk, General Electric (via Geonx), MSC Software, ANSYS, etc., provide AM simulation, which enables designers to understand where the critical zones in a particular geometry are located and produce approximate first findings within a few hours. With this information, designers can iteratively develop their concept by taking all aspects into consideration using simulation software rather than wasting time and money on the actual manufacture of a possibly unsuitable design. Simufact is a piece of software

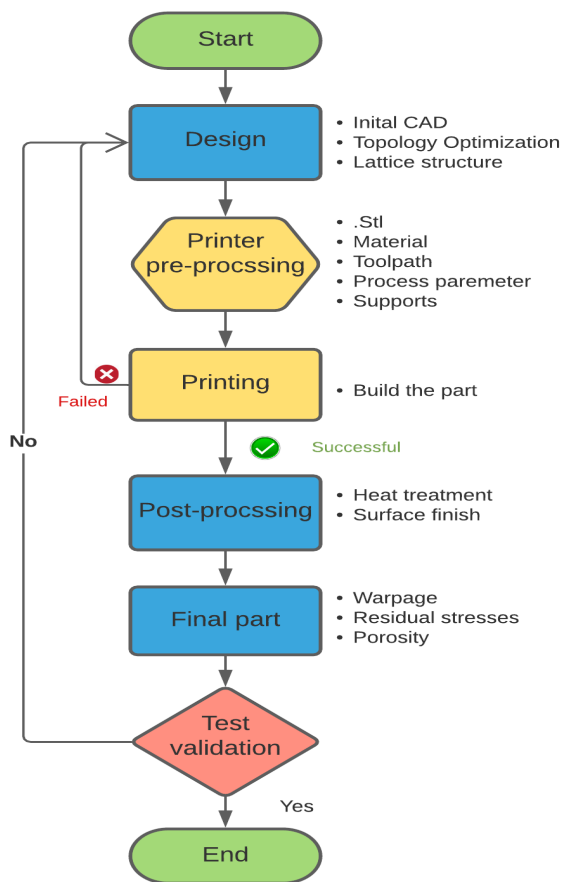


Figure 3: Additive Manufacturing workflow [own edition].

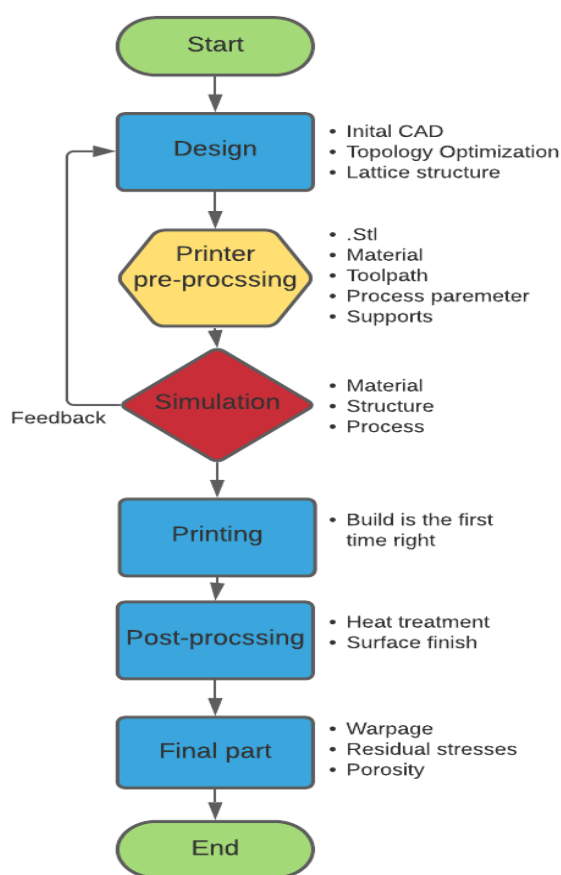


Figure 4: AM simulation workflow [own edition].

that uses finite element analysis to simulate metal AM by focusing on powder bed fusion processes. The difficulties with metal powder bed fusion AM can be addressed and analyzed by simulations [8].

As is shown in Fig. 3, the AM workflow to date has been one of the best traditional manufacturing technologies. The revision of AM goes through those processes to select the best predicted design parameters, build orientation, removal cutting, supporting structure, etc. [9].

Three-dimensional objects are constructed from several thin layers, each of which with a pattern defined by a Computer-aided design (CAD) that is exposed using a scanning laser for stereolithography or a pattern in the absence of a mask. Manufacturing information is obtained from CAD or other design software before being sliced into individual layers using the Standard Tessellation Language [10].

Sometimes, the building fails due to many reasons, e.g. supporting structures or a high degree of distortion. Once the best predicted design parameters have been chosen, construction commences and an inspection is made. If any defects are observed, the component is subjected to a process of trial and error to achieve the desired part. Alternatively, as illustrated in Fig. 4, a virtual model can be built to minimize the number of required physical builds

in the AM simulation workflow. In this virtual model, different approaches can be applied, e.g. various parameters, changing supporting structures, building orientation, and keeping treatment cutting and support removal to achieve the desired product free from any adverse effects of the process the first time it is constructed. Since a feedback loop is included in the simulation, the results of the process simulation can impact topology optimization. The significant benefits of this are that the formation of some of these parts may cost thousands of dollars and the trial-and-error approach is quite undesirable.

## 2. Design methodology and simulation

Given that AM depends on many factors to determine the required parameter set to produce the desired part, e.g., laser power, fraction of exposure energy and volumetric expansion factor, experimental tests should be conducted to measure these parameters.

### 2.1 Sample selection

As is shown in Fig. 5 of the simulation, an aircraft component was chosen because of the complexity of its geometry and the importance of AM in the aerospace industry,

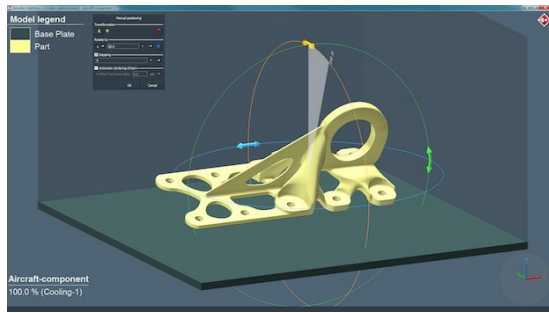


Figure 5: An aircraft component [9].

e.g., in increasing asset uptime, reducing costs, manufacturing lighter parts, enhancing durability and improving customer satisfaction.

## 2.2 Material selection

Three alloys (TiAl6V4, AlSi10Mg and 316L) were chosen with different properties to construct the sample for the purpose of investigating the effect of each material on the surface (shape) deviation with respect to the original sample.

## 2.3 Machine selection

Different types of 3D printing machines are available using this piece of software, e.g. two kinds of Electro Optical Systems (EOS) have been used, namely M280 and M400, the size and power of both differ.

## 2.4 Thermal analysis

The laser power has to be adjusted, moreover, the printing temperature has to be greater than the melting point of each alloy but less than its boiling point.

## 2.5 Mechanical calibration

The purely mechanical, macro-scale analysis approach of Simufact Additive requires the input of the so-called inherent strain values before the simulation. As is shown in Fig. 6, the inherent strain values are produced during the construction process as a result of plastic strain, thermal strain and phase transformations as shown in

$$\epsilon^{\text{inherent}} = \epsilon^{\text{th}} + \epsilon^{\text{pl}} + \epsilon^{\text{ph}}. \quad (1)$$

Moreover, they depend on material properties and process parameters.

These strains can be calibrated from experiments, e.g. by measuring the degree of distortion after cutting a printed cantilever beam and running simulations to match the experimental distortion values that should be less than 3%, or estimated based on the process. This paper used the empirical calibration by printing two cantilevers on the  $X$ - and  $Y$ -axis as is shown in Fig. 7 that are 72 mm

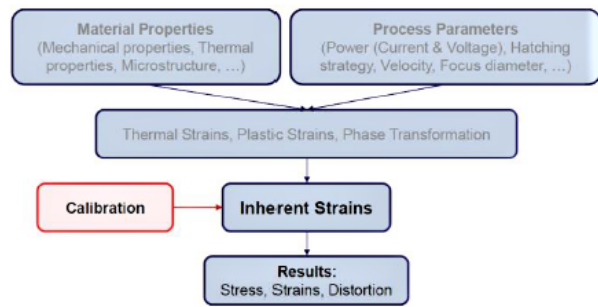


Figure 6: Inherent strain [9].

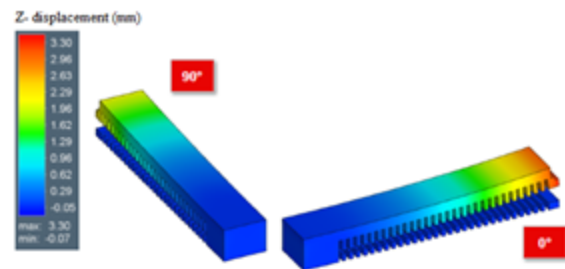


Figure 7: Printing two cantilevers [9].

in length, 12 mm in width, and 9 mm high. Afterwards, the cantilevers are cut in the middle of the teeth, so a particular part of them remains on the base plate. Finally, the maximum observed distortion in the  $Z$ -axis was measured as shown in Fig. 8.

Three values of strains are inputted into the build stage dialogue ( $\epsilon_{xx}$ ,  $\epsilon_{yy}$ ,  $\epsilon_{zz}$ ). These values are dimensionless and defined in three directions,  $X$ ,  $Y$ , and  $Z$ . Default values will be shown in the dialogue [9]:

$$\epsilon_{xx} = -0.008, \quad \epsilon_{yy} = -0.003, \quad \epsilon_{zz} = -0.030. \quad (2)$$

The mechanical calibration was carried out for the three alloys, namely TiAl6V4, AlSi10Mg and 316L, to calculate the inherent strains.

## 2.6 Thermomechanical calibration

The thermomechanical analysis requires that the fraction of the exposure energy and the volumetric expansion factor have been calculated before the simulation is started.

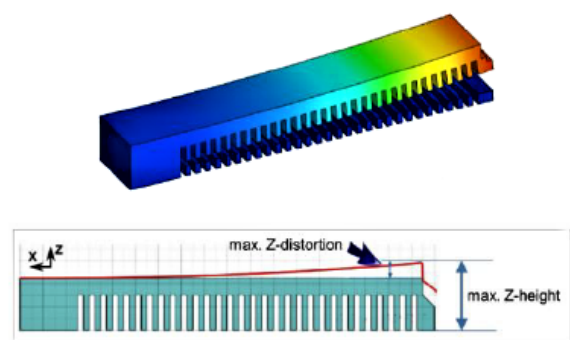


Figure 8: Measuring the distortion in the  $Z$ -axis [9].

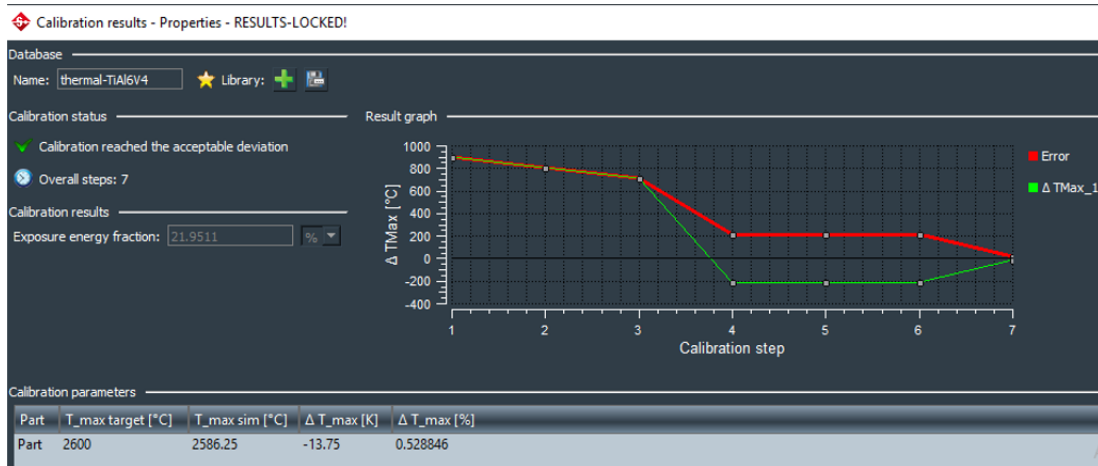


Figure 9: Thermal calibration

Since these values depend on material properties and machine parameters, they need to be carefully calibrated, which should be done experimentally.

## 2.7 Fractions of exposure energy

The fraction of exposure energy is a term that is responsible for the peak temperature of the process. During the exposure time, the energy predominantly (but not only) melts the powder. The rest of the powder reheats the solid material after the exposure time. For the purpose of thermomechanical calibration, it is recommended to carry out the thermal calibration first to determine the optimized exposure energy and then conduct the thermomechanical calibration with the optimized fraction of the exposure energy to calibrate the volumetric expansion factor.

The calibration was carried out using a specimen of a cantilever. The peak temperature has to be measured during the process to determine the maximum degree of distortion in the  $Z$ -axis after cutting, as is shown in Fig. 8. The measured point was chosen on the upper surface because the temperature is the highest there and the average will be recorded between the two surfaces. Thermal calibration of the three alloys, that is, TiAl6V4, AlSi10Mg and 316L, was carried out to determine the fraction of exposure energy. The thermal calibration of TiAl6V4 is shown in Fig. 9.

## 2.8 Volumetric expansion factor

The volumetric expansion factor accounts for the thermal expansion and shrinkage effects caused by the modelling approach, that is, by combining multiple powder layers and repeated heating of the heat source in one element layer. The volumetric expansion factor can either be set to isotropic in all directions or anisotropic for each individual order and scales the thermal expansion factor of the material. Volumetric expansion is the change in the volume of a given mass with temperature. The thermal

expansion factor is a measure of the change in volume in three dimensions as is shown in Eq. ??:

$$V = 3\alpha V_0 \Delta T \quad (3)$$

This equation is usually written as:

$$V = \beta V_0 \Delta T, \quad (4)$$

where  $\beta = 3\alpha$  denotes the volumetric expansion factor,  $V_0$  represents the original volume and  $\Delta T$  stands for the change in temperature.

## 3. Results

Different machines and materials were used to print an aircraft component. As illustrated in Table 2, changing the machine does not have any effect on the design or features of the sample. The effective stress in MSC Simufact was implemented once the printed aircraft component had been compared to calculations regarding residual stresses using Stoney's equation. The effective stress of both the M280 and M400 machines is identical. For the alloys TiAl6V4, AlSi10Mg and 316L, the stresses were 1260 MPa, 370 MPa and 680 MPa, respectively. When the M280 machine was used, the surface deviation, representing the difference between the designed and printed samples, of all three alloys did not change. However, when the M400 machine was used, the surface deviation in each alloy varied.

The laser power of the machine, which is responsible for fusing the powder, is one of the most crucial elements to modify. As a result, the printing temperature of a material, which is roughly twice as high as its melting point, must be higher than its melting point but lower than its boiling point. For each alloy, the changes in laser power as well as the measured temperature are shown in Table 3. For TiAl6V4, 200 W is a suitable power, while the optimal laser power for AlSi10Mg and 316L is 100 W.

The mechanical calibration was carried out to identify the inherent stresses. For measuring the distortion in

Table 2: The effects of the machines and alloys.

Material Used	EOS Machine	Effective Stress [MPa]	Surface Deviation [mm]	
			Max	Min
TiAl6V4	M280	1262.03	0.17	-0.16
	M400	1288.13	0.88	-0.93
AlSi10Mg	M280	370.01	0.13	-0.12
	M400	370.02	0.36	0.26
316L	M280	683.19	0.17	-0.16
	M400	680.65	0.16	-0.15

Table 3: Adjusting the laser power.

Alloy used	Melting point (C°)	Laser power (W)	Printing temperature (C°)
TiAl6V4	1600	200	2650
		150	3098
		100	2084
AlSi10Mg	660	200	4220
		150	3098
		100	2084
316L	1400	200	4454
		150	3500
		100	2463

the beam, two points on the cantilever were chosen at heights of 3.09 and 2.01 mm. The simulation repeatedly printed the specimen until the permissible distortion error became less than 3%. The sample was printed seven times to achieve an acceptable degree of distortion. Table 4 shows the inherent strains of the three alloys.

Since the volumetric expansion factor is a crucial parameter in 3D printing, the simulation carried out the thermomechanical calibration to determine the volumetric expansion factor, as is shown in Table 5.

#### 4. Conclusion

The simulation tool Simufact was used to print a component of an airplane out of different alloys using AM technology to determine the specified parameter and carry out virtual printing. As indicated in Table 3, since the laser power has a massive effect on the printing temperature, it should be regulated carefully. Furthermore, as indicated in Tables 4 and 5, in order to determine the inherent strains and volumetric expansion factor, the component must be printed multiple times.

#### REFERENCES

- [1] Hernandez Korner, M.E.; Lambán, M.P.; Albajez, J.A.; Santolaria, J.; Ng Corrales, L.d.C.; Royo, J.: Systematic literature review: integration of additive manufacturing and industry 4.0. *Metals*, 2020, **10**(8), 1061 DOI: 10.3390/met10081061
- [2] Alex, S.; Árpád, T.: XBRL utilization as an automated industry analysis. *Hung. J. Ind. Chem.*, 2020, **48**(1), 131–138 DOI: 10.33927/hjic-2020-19

Table 4: Inherent strains of TiAl6V4, AlSi10Mg and 316L.

Metal	$\epsilon_{xx}$	$\epsilon_{yy}$	$\epsilon_{zz}$	$N_s$
TiAl6V4	-0.00488099	-0.0022865	-0.3	7
AlSi10Mg	-0.00637062	-0.0016680	-0.3	18
316L	-0.0198353	-0.0025170	-0.3	3

$N_s$ : Number of samples printed

Table 5: Volumetric expansion factors for TiAl6V4, AlSi10Mg and 316L.

Metal	Volumetric expansion factor	Number of steps
TiAl6V4	0.821869	18
AlSi10Mg	0.60999	2
316L	0.307238	24

- [3] Attaran, M.: The rise of 3-D printing: The advantages of additive manufacturing over traditional manufacturing. *Bus. Horiz.*, 2017, **60**(5), 677–688 DOI: 10.1016/j.bushor.2017.05.011
- [4] Gábora, A.; Varga, T. A.; Kozma, I.; Beke, S.; Mankovits, T.: 3D Geometrical Reconstruction of Closed-Cell Aluminum Foam Using CT Images. in *InCell 2019: Book of Abstracts of the International Conference on Multifunctional Cellular Materials* (UA Editora Universidade de Aveiro.), page 74 ISBN: 978-972-789-611-0 <https://ria.ua.pt>
- [5] Li, J.Z.; Alkahari, M.R.; Rosli, N.A.B.; Hasan, R.; Sudin, M.N.; Ramli, F.R.: Review of wire arc additive manufacturing for 3D metal printing, *Int. J. Autom. Technol.*, 2019, **13**(3), 346–353 DOI: 10.20965/ijat.2019.p0346
- [6] Loughborough, U.: the 7 Categories of Additive Manufacturing, 2019, <https://www.lboro.ac.uk>
- [7] Software solutions, S.S.S.A.S.: Additive Manufacturing Technology, 2017, <https://www.simufact.com>
- [8] Mankovits, T.: Numerical analysis of unit cell models for orthopedic applications, *IOP Conf. Ser.: Mater. Sci. Eng.*, **393**, 012019 DOI: 10.1088/1757-899x/393/1/012019
- [9] Software solutions, S.S.S.A.S.: English webinar on the entire portfolio of MSC Software for Additive Manufacturing, 2017, <https://www.simufact.com>
- [10] Rasiya, G.; Shukla, A.; Saran, K.: Additive Manufacturing-A Review, *Mater. Today: Proc.*, 2021, **47**(1), 6896–6901 DOI: 10.1016/j.matpr.2021.05.181
- [11] Schelhorn, L.; Gosch, M.; Debeugny, L.; Schroter, P.; Schwarz, W.; Soller, S.: Optimal Design and Process Simulation for Additive Manufacturing, in 8th European Conference for Aeronautics and Space Sciences, EUCASS2019-FP0354, Madrid, Spain, 1–15 DOI: 10.13009/EUCASS2019-354

## ANALYSIS OF FORMED CHIPS IN THE CASE OF TURNING DIFFERENT POLYMER MATERIALS

ÁDÁM SARANKÓ<sup>\*1</sup>, GÁBOR KALÁCSKA<sup>1</sup>, AND RÓBERT ZSOLT KERESZTES<sup>1</sup>

<sup>1</sup>Institute of Technology, Hungarian University of Agriculture and Life Sciences, Páter Károly u. 1, Gödöllő, 2100, HUNGARY

In this paper, turning input parameters were defined for 12 different polymer materials that can be used in technical practices. Our goal was to determine turning input parameters where chip formation is favourable or continuous chips do not cause any problems. Our tests included the examination of detached chips and the values of the average surface roughness of the machined surfaces.

**Keywords:** chip formation, polymer materials, turning

### 1. Introduction

Nowadays, in addition to the 3D printing of polymers, the machining of polymer and polymer composite materials still plays an important role. Turning is one of the most productive machining technologies used to make cylindrical products. Polymers that exhibit good levels of machinability favour the development of chip formation. However, technical practices often use polymer materials that exhibit favourable properties (hardness, toughness, flexibility) but are difficult to machine. The most common problem is continuously flowing chips. In this case, rather than the chip being moved away from the material, it is pushed in front of the tool. As a result, the heat cannot dissipate from the chips and the detached chips are in constant contact with the tool, which generates additional heat. Since polymers tend to withstand high temperatures less than metals, their machined surfaces melt and their surface roughness becomes unacceptable.

Researchers have already studied the shape of detached chips. The literature is mainly concerned with the study of types of chips generated during the machining of metallic materials such as C45 [1, 2], Al/SiCp [3] and AISI D2 tool steel [4]. Kharlevich and Venuvinod analysed the formation of 3D chips in general as a result of metal cutting [5, 6], while others have researched methods of chip breaking for machining tools [7, 8].

Although chip detachment and formation are very important aspects in machining, in the case of polymers, this area has not yet been investigated.

### 2. Experimental methods

12 different polymer materials were tested, namely PA6 G-H, PA66 GF30, PET TF, PET, POM-C, POM-GF25, POM-H, PP,

PTFE, PVC, textile bakelite and UHMWPE. According to a manufacturer of polymer materials, the aforementioned materials are the most commonly used, excluding the so-called high-performance ones.

In this research, turning tests were performed to determine input parameters that can be used in practice to avoid such problems, e.g. melted surfaces, caused by continuously flowing chips. The turning tests were run on an E 400 conventional lathe machine and an NCT EUROturn-12B CNC lathe machine. Both devices are located in the workshop of the Institute of Technology. In all the experiments, a SCLCR 20.20 K09 tool shank and a CCGT 09T304-AS IC20 polished turning insert were used. After each test, a close-up photo of the surface was taken and the average surface roughness measured. For surface measurements, a Mitutoyo SurfTest SJ-201P surface roughness tester was used. Furthermore, the formed chips were collected before being analysed.

The input parameters of all the tests are shown in [Table 1](#). In the case of roughing, the depth of cut was 3 mm, while a depth of cut of 0.25 mm was used for finishing.

The air-cooled solution was mainly suitable for blowing off the detached chips. At first, all the experiments were tried without implementing any cooling methods. However, in the case of certain materials, flowing chips were formed in all cases, so chip blowing was used for these materials.

\*Correspondence: [saranko.adam@uni-mate.hu](mailto:saranko.adam@uni-mate.hu)

Table 1: Input parameters of all tests

<b>Input parameters for roughing on a CNC lathe machine (NCT EUROturn-12B)</b>						
	PA6 G-H	PA66 GF30	PET TF	PET	POM C	POM GF25
vc (m/min)	250	250	250	250	250	250
f (mm/rot.)	0.2	0.2	0.15	0.15	0.2	0.2
Cooling	-	-	-	-	-	-
	POM H	PP	PTFE	PVC	Textile bakelite	UHMW-PE
vc (m/min)	250	250	250	250	250	250
f (mm/rot.)	0.2	0.2	0.2	0.1	0.2	0.15
Cooling	-	-	-	-	-	-
<b>Input parameters for finishing on a CNC lathe machine (NCT EUROturn-12B)</b>						
	PA-6 G-H	PA-66 GF-30	PET TF	PET	POM C	POM GF-25
vc (m/min)	300	300	300	300	300	300
f (mm/rot.)	0.1	0.1	0.1	0.1	0.1	0.1
Cooling	air	air	air	air	air	air
	POM H	PP	PTFE	PVC	Textile bakelite	UHMW-PE
vc (m/min)	300	300	300	300	300	300
f (mm/rot.)	0.1	0.1	0.1	0.1	0.08	0.1
Cooling	air	air	air	air	-	air
<b>Input parameters for roughing on a conventional lathe machine (E 400)</b>						
	PA-6 G-H	PA-66 GF-30	PET TF	PET	POM C	POM GF-25
vc (m/min)	61	52	59	75	58	52
f (mm/rot.)	0.75	0.75	0.4	0.4	0.6	0.6
Cooling	-	-	-	-	-	-
	POM H	PP	PTFE	PVC	Textile bakelite	UHMW-PE
vc (m/min)	66	76	58	58	59	58
f (mm/rot.)	0.6	0.75	0.6	0.2	0.75	0.4
Cooling	-	-	-	-	-	-
<b>Input parameters for finishing on a conventional lathe machine (E 400)</b>						
	PA-6 G-H	PA-66 GF-30	PET TF	PET	POM C	POM GF-25
vc (m/min)	65	62	63	79	62	62
f (mm/rot.)	0.1	0.1	0.1	0.1	0.1	0.1
Cooling	-	air	air	air	-	air
	POM H	PP	PTFE	PVC	Textile bakelite	UHMW-PE
vc (m/min)	71	80	57	63	63	62
f (mm/rot.)	0.1	0.1	0.1	0.1	0.1	0.1
Cooling	-	air	air	air	-	air

### 3. Results

The input parameters shown in Table 1 can also be considered as results. These parameters were determined experimentally.

In other aspects, however, the main results are the average surface roughness of the machined surfaces and the properties of the detached chips.

Table 2 shows the results of the average surface roughness measurements.

Although other setups can be used, by applying the parameters described above, safe and productive machining can be achieved by avoiding problems caused by con-

tinuously flowing chips.

The detached chips were examined subjectively rather than by making specific measurements. However, the results obtained in this way can be used in practice and provide a suitable point of reference.

Photos of the detached chips in all cases are presented in Fig. 1, while the properties of these chips are shown in Table 3.

### 4. Conclusions

In general, the turning of tough polymeric materials results in the formation of continuous chips. Due to the big

Table 2: Average surface roughness values

Material	Average surface roughness ( $\mu\text{m}$ )			
	NCT EUROturn-12B		E 400	
	Roughing	Finishing	Roughing	Finishing
PA6 G-H	4.06	1.18	12.95	1.58
PA66 GF30	3.12	1.27	12.32	1.55
PET TF	1.73	0.95	5.24	1.47
PET	1.75	0.9	5.18	1.13
POM-C	3.48	0.66	8.62	1.14
POM-GF25	3.75	1.2	8.56	1.43
POM-H	3.44	0.68	8.72	1.14
PP	3.38	0.89	12.72	1.45
PTFE	5.01	1.77	18.44	1.93
PVC	1.01	0.78	2.35	0.87
Textile bakelite	6.81	3.15	10.30	1.59
UHMWPE	2.53	1.81	11.27	1.67

Table 3: Properties of the detached chips

	Properties of the detached chips			
	NCT EUROturn-12B		E 400	
	Roughing	Finishing	Roughing	Finishing
PA6 G-H	5, 6, 7, 8	5, 6, 9	5, 6, 8	3, 4, 7
PA66 GF30	3, 4	4, 5	3, 4	3, 4
PET TF	4, 5	4, 5	3, 10	4, 5
PET	4, 5	4, 5	5, 10	4, 5
POM-C	1, 2	3, 4	1, 2	3, 4
POM-GF25	1, 2	1, 2	1, 2	3, 4
POM-H	1, 2	3, 4	1, 2	3, 4
PP	4, 5, 6	4, 5	3, 8	4, 5
PTFE	3, 4	3, 4	3, 4	3, 4
PVC	4, 5	4, 5	4, 5	3, 4
Textile bakelite	4, 11	11	1, 4, 11	11
UHMWPE	3, 6, 7, 10	3, 6, 9	3, 6, 7, 8	3, 6, 7

1: elemental, 2: rigid, 3: curved, continuously flowing, 4: easy to tear, 5: straight, continuously flowing, 6: tough, 7: stretches, 8: does not tear, 9: tears after being stretched, 10: hard to tear, 11: dust-like

cross-section of chips during the roughing operation, the mass of individual detached chips influences in which direction they start to flow. This is less of a problem because the ventilation effect of the chuck does not adversely affect the cooling of the chips.

In the case of the finishing operation, the cooling of the chips is critical. It is recommended to use air cooling, although not specifically for the purpose of cooling, in order to blow chips away from the workpiece and tool. Even though the quality of the machined surfaces can be improved by tools with bigger radius, chips can still

cause problems. During the experiments, chip blowing was worthwhile in all cases, especially during smoothing operations.

Future research can be conducted by precisely defining the air-cooling method, applying other tools and investigating high-performance polymeric materials. In the case of chip blowing, the distance between the workpiece and the chuck, the weight of the detached chips as well as the ventilation effect of the chuck must be taken into account. The direction and velocity of the air is also significant. It was found that a strong airflow is not always the

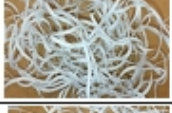
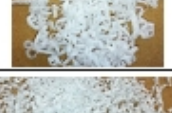
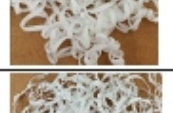
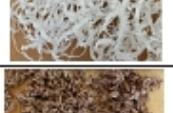
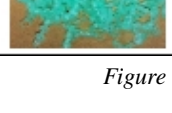
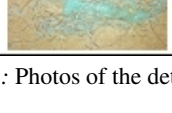
	Photos of the detached chips			
	NCT EUROturn 12-B		E 400	
	Roughing	Finishing	Roughing	Finishing
PA 6 G-H				
PA 66 GF 30				
PET TF				
PET				
POM C				
POM GF 25				
POM H				
PP				
PTFE				
PVC				
Textile bakelite				
UHMW PE				

Figure 1: Photos of the detached chips

most desirable. The distance between the nozzle and the tool is limited by the geometries of the machine as well as the workpiece. By precisely defining these parameters, more practical information can be provided.

### Acknowledgement

The authors would like to thank Quattroplast Kft. for providing the engineering polymeric materials.

### Nomenclature

$v_c$	cutting speed (m/min)
$f$	feed rate (mm/rotation)
$R_a$	average surface roughness ( $\mu\text{m}$ )
PA6 G-H	cast polyamide 6, Hungarian version
PA66 GF30	polyamide 66 with 30 m/m% glass fiber
PET TF	polyethylene terephthalate with the addition of PTFE

PTFE	polytetrafluoroethylene
PET	polyethylene terephthalate
POM-GF25	polyoxymethylene with 25 m/m% glass fiber
POM-C	polyoxymethylene copolymer
POM-H	polyoxymethylene homopolymer
PP	polypropylene
PVC	polyvinyl chloride
UHMWPE	ultra-high molecular weight polyethylene

## REFERENCES

- [1] Segreto, T.; Simeone, A.; Teti, R.: Chip form Classification in Carbon Steel Turning through Cutting Force Measurement and Principal Component Analysis *Procedia CIRP*, 2012, **2**, 49–54 DOI: [10.1016/j.procir.2012.05.038](https://doi.org/10.1016/j.procir.2012.05.038)
- [2] Segreto, T.; Simeone, A.; Teti, R.: Principal component analysis for feature extraction and NN pattern recognition in sensor monitoring of chip form during turning. *CIRP J. Manuf. Sci. Technol.* 2014, **7**(3), 202–209 DOI: [10.1016/j.cirpj.2014.04.005](https://doi.org/10.1016/j.cirpj.2014.04.005)
- [3] Sun, W.; Duan, C.; Yin, W.: Chip formation mechanism in machining of Al/SiCp composites based on analysis of particle damage. *J. Manuf. Proc.* 2021, **64**, 861–877 DOI: [10.1016/j.jmapro.2021.02.032](https://doi.org/10.1016/j.jmapro.2021.02.032)
- [4] Mohan, R.; Harshavardhana, N.; Chaudhari, M.; Jeyanthi, S.; Abimannan, G.: Analysis on surface finish and chip morphology during dry turning process. *Mat. Today: Proc.* 2021, **46**(2), 999–1002 DOI: [10.1016/j.matpr.2021.01.137](https://doi.org/10.1016/j.matpr.2021.01.137)
- [5] Kharkevich, A.; Venuvinod, P. K.: Basic geometric analysis of 3-D chip forms in metal cutting.: Part 2: implications. *Int. J. Mach. Tools Manuf.* 1999, **39**(6), 965–983 DOI: [10.1016/S0890-6955\(98\)00066-2](https://doi.org/10.1016/S0890-6955(98)00066-2)
- [6] Kharkevich, A.; Venuvinod, P. K.: Extension of basic geometric analysis of 3-D chip forms in metal cutting to chips with obstacle-induced deformation. *Int. J. Mach. Tools Manuf.* 2002, **42**(2), 201–213 DOI: [10.1016/S0890-6955\(01\)00115-8](https://doi.org/10.1016/S0890-6955(01)00115-8)
- [7] Wu, M.; Yu, A.; Chen, Q.; Wang, Y.; Yuan, J.; Sun, L.; Chi, J.: Design of adjustable chip breaker for PCD turning tools. *Int. J. Mech. Sci.* 2020, (172), 105411 DOI: [10.1016/j.ijmecsci.2019.105411](https://doi.org/10.1016/j.ijmecsci.2019.105411)
- [8] Yilmaz, B.; Karabulut, S.; Güllü, A.: A review of the chip breaking methods for continuous chips in turning. *J. Manuf. Proc.* 2020, **49**, 50–69 DOI: [10.1016/j.jmapro.2019.10.026](https://doi.org/10.1016/j.jmapro.2019.10.026)



## ANALYSIS OF ROUGHNESS PARAMETERS DETERMINING TRIBOLOGICAL PROPERTIES IN HARD TURNED SURFACES

VIKTOR MOLNÁR\*<sup>1</sup> AND ISTVÁN SZTANKOVICS<sup>1</sup>

<sup>1</sup>Institute of Manufacturing Science, University of Miskolc, Egyetemváros, Miskolc, 3515, HUNGARY

Hard-machined components built into automotive industrial products play an important role because they incorporate working surfaces. The machining of them is crucial; the accuracy, surface quality and lifetime have to be ensured. In this paper the tribological properties of hard-turned surfaces are characterized and analyzed based on 3D and 2D surface roughness parameters. Functional parameters that provide quantitative information about the wear resistance and fluid retention of the machined surfaces were studied. The aim of the study was to summarize the relevant roughness parameters in terms of the functionality of the surfaces and to collect experimental results for their application.

**Keywords:** wear-resistance, hard turning, surface roughness

### 1. Introduction

Many machined surfaces incorporate working surfaces, which move relative to other surfaces. The analysis and development of such surfaces is important because the surface quality [1, 2] and, within this parameter, the topographical characteristics [3, 4] by and large determine the lifetime of parts [5–7]. The characterization of surface topography is highlighted in the automotive industry, that is, predicting the values of roughness parameters [8] and the effect of technological data on the topography are determining factors in the design of machined parts [9]. Due to the development of superhard materials, the machining of hardened surfaces by single-point tools has become more common in recent decades [10].

In this paper, the topography of internal cylindrical surfaces machined by hard turning is analyzed from a tribological point of view. Tribology focuses on the friction, wear and friction-reducing characteristics of surfaces. By analyzing surface topography with the help of several available surface roughness parameters, the wear resistance as well as load-bearing and fluid-retention capacities of surfaces can be characterized [11]. These parameters have been analyzed in numerous studies which only focus on certain parameter groups, e.g. Rk or volume parameters [12–15].

The aim of the present study is to summarize and compare most of the roughness parameters that describe tribological characteristics. These are mainly the areal (3D) roughness parameters because of their exactness [16–18]. If a parameter has a corresponding line parameter (2D), it is also analyzed. While less exact than 3D

results, 2D studies can provide useful practical information and are less time-consuming. Although certain parameters can be considered as more accurate due to their modernity, e.g. volume parameters, most parameters can provide at least directions with regard to the mentioned tribological characteristics.

### 2. Tribology-oriented roughness parameters

The simplest information is provided by the maximum peak height ( $S_p$ ) and maximum valley depth ( $S_v$ ) within the group of height parameters. A higher peak maximum height could be indicative of a relatively long wear-in phase and a higher maximum valley depth of a higher fluid-retention capacity. The skewness ( $S_{sk}$ ) and kurtosis ( $S_{ku}$ ) parameters are also regarded as height parameters. A negative  $S_{sk}$ , e.g., a burnished surface, means a better fluid-retention capacity comparative to the positive values of highly peaky surfaces. In the case of a zero or negative  $S_{sk}$  value, the load-bearing area of the surface is greater, therefore, its wear resistance is also greater [3]. This effect is enhanced by an  $S_{ku}$  of 3 or lower, which is indicative of a relatively filled surface [19]. These characteristics are summarized in Fig. 1 based on 2D profile parameters.

The Abbott-Firestone curve and the related  $S_k$  parameters (Fig. 2) typically help to analyze the functional and tribological properties of a surface [21]. The shape of the curve itself draws attention to some remarkable topographic characteristics. The curve of a random (isotropic) surface, e.g. the ground, is entirely analogous to that of a normal distribution. In the case of periodic, e.g. hard-

\*Correspondence: [viktor.molnar@uni-miskolc.hu](mailto:viktor.molnar@uni-miskolc.hu)

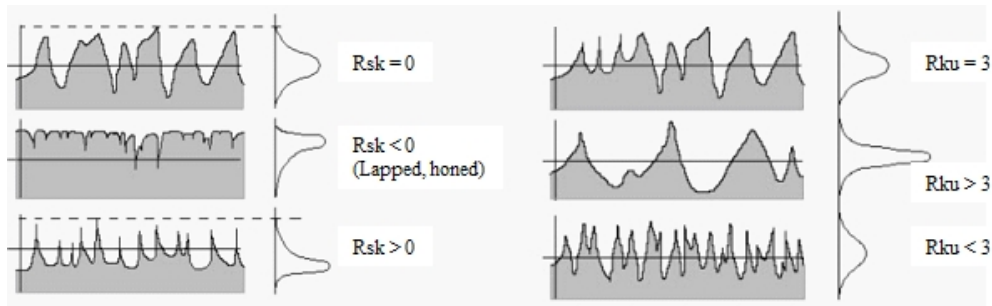


Figure 1: The ranges of the Rsk and Rku parameters for different surface topographies [20]

Table 1: Effects of changes in the parameters determining tribological properties

Change in roughness parameter	Sp: ↓; Ssk: ↓ / ≤ 0; Sku: ↓ / < 3; Spk: ↓; Sa1: ↓; Vmp: ↓; Sbi: ↑	Sv: ↑; Ssk: ↓ / ≤ 0; Svk: ↑; Sa2: ↑; Vvc: ↑; Vvv: ↑; Sci: ↑; Svi: ↑
Change in tribological characteristics	Wear resistance and/or load-bearing capacity increases	Fluid-retention capacity increases

turned, surfaces, the change in the gradient of the curve is uneven and the curve is asymmetrical. The procedures that reduce or eliminate the surface peaks, e.g. diamond or ball burnishing, result in a plateaued topography and a filled surface [4, 22], yielding a relatively straight middle section with a gradual gradient in the curve. In this case, since the material volume of the surface peaks is relatively low, the wear resistance of the surface is higher [11]. Concerning the Sk parameters, the value of the reduced peak height (Spk) is low. The increase in the reduced valley depth (Svk) indicates a higher fluid retention capacity [23]. In the analysis of Sk, volume parameters are also applied to the material volume of peaks (Sa1) and the void volume of valleys (Sa2) [24].

Although similar statements are valid for the volume parameters, this parameter group measures the magnitude of the peak and valley zones in a more exact manner. The lower the peak material volume (Vmp) is, the better its wear resistance capacity, moreover, the higher the core void volume (Vvc) and valley void volume (Vvv),

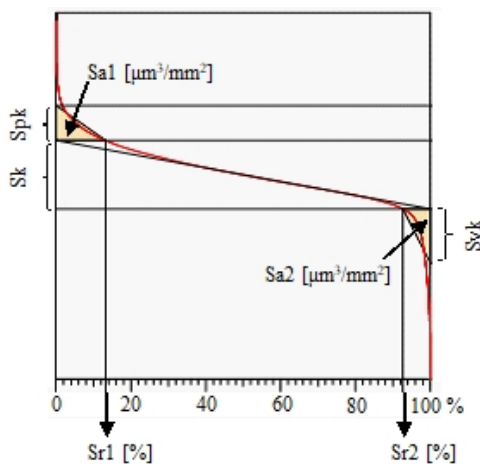


Figure 2: The Abbott-Firestone curve and the determination of the Sk parameters

the better its fluid retention capacity [11]. In the volume analysis the peak zone is defined as the top 10% and the valley zone as the bottom 20% of the topography.

The so-called functional indices are less well-known or at least less frequently applied. Rather than being derived from the Abbott-Firestone curve, they are characterized by the load-bearing and fluid-retention capacities of the surfaces. The higher the surface bearing index (Sbi), the higher its load-bearing capacity, while the higher the core fluid retention (Sci) and the valley fluid retention (Svi) indices, the better its fluid retention capacity. These tribological properties are summarized in Table 1.

### 3. Experimental conditions

Internal cylindrical surfaces ( $S_1$ ,  $S_2$  and  $S_3$ ) of three parts were machined by hard turning. Various feeds resulted in different topographies when the other cutting parameters were fixed. The cutting experiments were carried out by a hard machining tool enter type EMAG VDC 400. The applied insert was of the type CCGW 09T308 NC2 and the tool holder of the type E25T-SCLCR 09-R. The cutting data are summarized in Table 2.

The surfaces were bores of gearwheels built into transmission systems. The parts were composed of the steel 20MnCr5. The physical and mechanical properties as well as the chemical composition of this steel are summarized in Table 3. The diameters of the machined bores were  $d = 88$  mm and their lengths were  $L = 34$  mm.

The surface roughness measurements were carried out on an AltiSurf 520 measuring machine using a CL2-type optical sensor with a nominal measuring range of 0–300  $\mu\text{m}$ . The resolution along the  $z$  axis was 0.012  $\mu\text{m}$  and 5  $\mu\text{m}$  along the  $x$  and  $y$  axes. The scanned area was  $4.8 \times 2.8$   $\text{mm}^2$ . Gaussian filtering was applied to the evaluation and the cut-off wavelength was  $\lambda_c = 0.8$  mm. For the purpose of evaluating the area parameters, a  $2 \times 2$   $\text{mm}^2$  area was taken into account and the evaluation

Table 2: Cutting data of the machined surfaces

Cutting data	Machined surfaces		
	$S_1$	$S_2$	$S_3$
$a_p$ [mm]	0.2		
$n$ [1/min]	615		
$f$ [mm/rev]	0.1	0.2	0.3

Table 3: Physical and mechanical properties as well as the chemical composition of the machined workpieces

Yield Strength $\sigma_s$ (MPa)	Tensile Strength $\sigma_b$ (MPa)	Hardness HRC	Thermal Conductivity $k$ (W/mK)	Density $\rho$ (g/cm <sup>3</sup> )	Elastic Modulus $E$ (GPa)
1034	1158	62 – 64	11.7	7.7 – 8.03	190 – 210

C	Mn	Cr	Si	Cu	S	P	Al
0.17 – 0.22	1.1 – 1.4	1.0 – 1.3	$\leq 0.4$	$\leq 0.4$	$\leq 0.035$	$\leq 0.025$	0.02 – 0.04

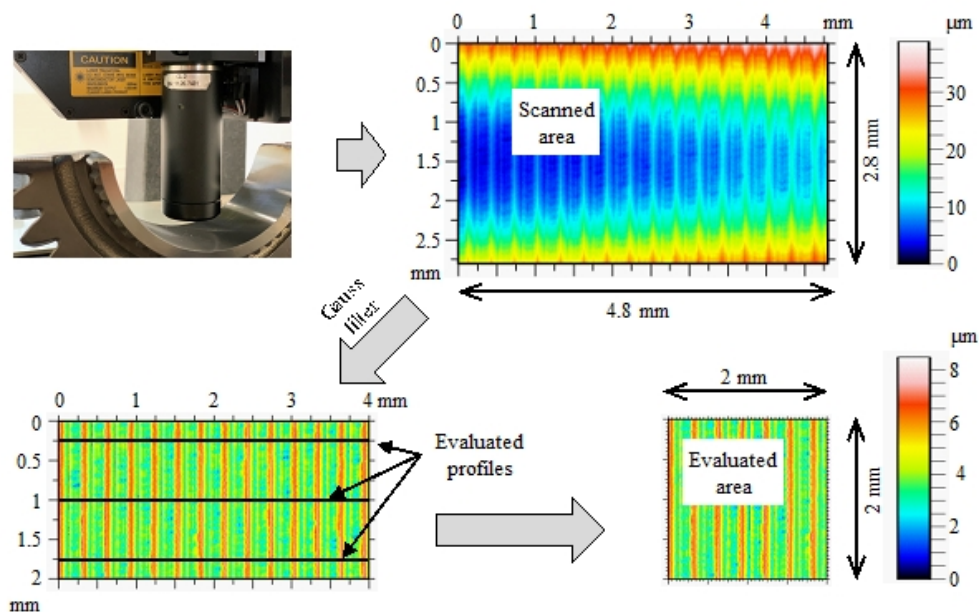


Figure 3: Evaluation area and profiles applied to the surface topography analysis

length for the line parameters was  $l_n = 4$  mm. The analysis of the line parameters was carried out based on the average surface roughness values calculated from three profiles per surface. The line profile was extracted from the 3D area. The measurement setup, evaluation area and location of the 2D profiles are presented in Fig. 3. For the analysis of the 3D parameters, the geometrical product specification (GPS) standard ISO 25178 was used, while the standards ISO 4287 and ISO 13565-2 were used for the 2D parameters. The analyzed functional indices are defined by the standard EUR 15178N.

## 4. Results and discussion

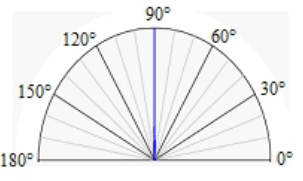
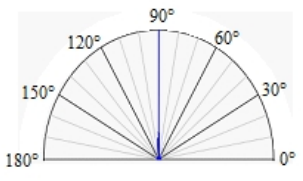
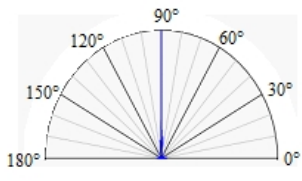
### 4.1 Surface characteristics

Surfaces machined by hard turning exhibit periodic topography in contrast to random surfaces such as ground surfaces. In metrology, this characteristic can be expressed by the degree of isotropy as a percentage or by

using the spatial parameter, Str (ranging from 0 to 1). The analyzed surfaces are definitely anisotropic; their values vary between 1.46 and 4.28%. The degree of isotropy increases as the feed rate increases. The specific direction of measurement ( $X$ ) is identical to the direction of the feed, which is perpendicular to the cutting speed vector. In this direction, the roughness height of the turned surface is at its maximum. This direction of measurement is important because the direction of the extracted 2D profiles is  $X$ . The dominant texture direction (lay) varies between  $90^\circ$  and  $90.05^\circ$ , which demonstrates the accuracy of the measurements. In Table 4, the isotropy of the analyzed surfaces and the texture directions are summarized.

Frequency analysis was performed for additional characterization of the surfaces. In Fig. 4, the Power Spectral Densities (PSD) of the surfaces are presented. It can be observed that the wavelengths are identical to the feed rate values. Additional components appear as periodic noises in the analyses. They might result from fur-

Table 4: Texture direction and isotropy of the analyzed surfaces

Surface		
$S_1$	$S_2$	$S_3$
		
Isotropy: 1.4576%	Isotropy: 1.8917%	Isotropy: 4.2799%
First direction: 89.9956°	First direction: 89.9973°	First direction: 90.0461°

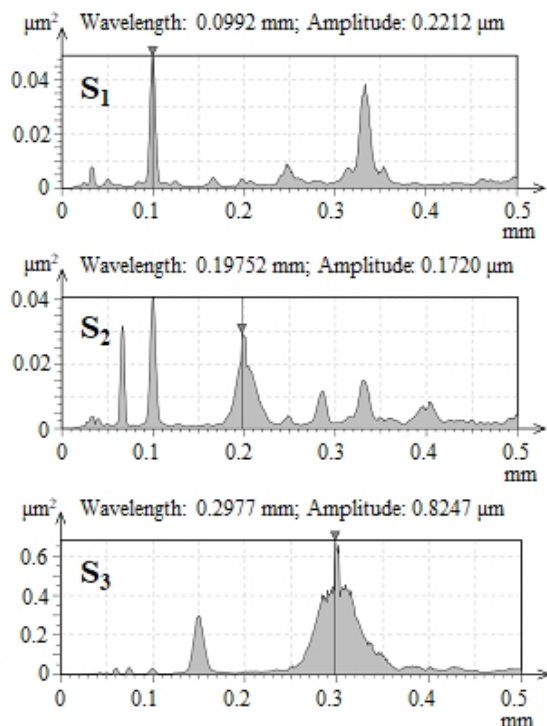


Figure 4: Power Spectral Density (PSD) analysis of the surfaces

ther topographic characteristics of the surfaces or from mechanical circumstances of the machining.

In Figs. 5 and 6, the simple height parameters of the surfaces are demonstrated for 3D and 2D measurements, respectively. The arithmetical mean height ( $S_a$  and  $R_a$ ), the maximum height ( $S_z$  and  $R_z$ ), the maximum peak height ( $S_p$  and  $R_p$ ) and the maximum valley depth ( $S_v$  and  $R_v$ ) have similar values for the different surface topographies, that is,  $S_1$  ( $f = 0.1$  mm/rev) and  $S_2$  ( $f = 0.2$  mm/rev). This phenomenon highlights the necessity of including additional parameters in the topography in order to characterize it in more detail.

By analyzing the deviations in the 2D and 3D height parameters, it can be stated that the maximum peak height ( $S_p$ ) is 1.2–2.2 times higher than the mean of the  $R_p$  values obtained by averaging the three 2D measurements. This multiplier varies between 1.9 and 2.5 in terms of  $S_v$

and  $R_v$  for the surfaces machined using three different feed rates. The maximum height ( $S_z$ ) is 1.5 – 2.3 times higher than the average of the three  $R_z$  values. By comparing the arithmetical mean heights ( $S_a$  and  $R_a$ ), it was found that the 3D values are higher than the 2D ones. The  $S_a$  values are 8 – 15% higher than the  $R_a$  ones and the percentage differences are higher when lower feed rates were applied (Fig. 7).

#### 4.2 Analysis of tribological parameters

The parameters characterizing tribological properties are found in the height,  $S_k$  and volume parameter groups as well as among the functional indices. In Fig. 8, the 3D parameters that provide information about the wear resistance are summarized for the analyzed surfaces. The lower values of  $S_p$ ,  $S_{pk}$ ,  $S_{a1}$  and  $V_{mp}$  indicate better wear resistance. For all four parameters, it can be stated that surface  $S_2$  machined at  $f = 0.2$  mm/rev is the most wear-resistant and surface  $S_3$  machined at  $f = 0.3$  mm/rev is the least. The same is observed according to the  $S_{sk}$  parameter. However, based on the  $S_{ku}$  parameter, the most wear-resistant surface is  $S_3$ , which is machined at  $f = 0.3$  mm/rev. The values of these two parameters indicate that the surfaces that have more filled peak zones and, therefore, whose peaks wear out faster are more wear-resistant. The surface is characterized by the  $S_{bi}$  parameter according to a different method: it is calculated as the ratio of the  $S_q$  parameter to the material volume in the top 5% of the surface. As a consequence, the surface machined at a high feed rate (0.3 mm/rev) is ranked first in terms of wear resistance. It should be noted that among the analyzed parameters, the dimensions of  $S_p$  and  $S_{pk}$  denote length, of  $S_{a1}$  and  $V_{mp}$  represent volume, while  $S_{sk}$ ,  $S_{ku}$  and  $S_{bi}$  are non-dimensional. If the volume parameter  $V_{mp}$  is considered to be the base due to its modernity and accuracy, the order of the surfaces in terms of wear resistance is  $S_2$ ,  $S_1$  and  $S_3$ . This is confirmed by the order of the parameters  $S_p$ ,  $S_{pk}$ ,  $S_{a1}$  and  $S_{sk}$ .

The parameters that provide information about the fluid-retention capacity of the surfaces are summarized in Fig. 9. The parameters  $S_v$ ,  $S_{vk}$ ,  $S_{a2}$ ,  $V_{vv}$  and  $S_{vi}$  characterize the valley zone and the fluid-retention capacity increases as their values increase. The core zone

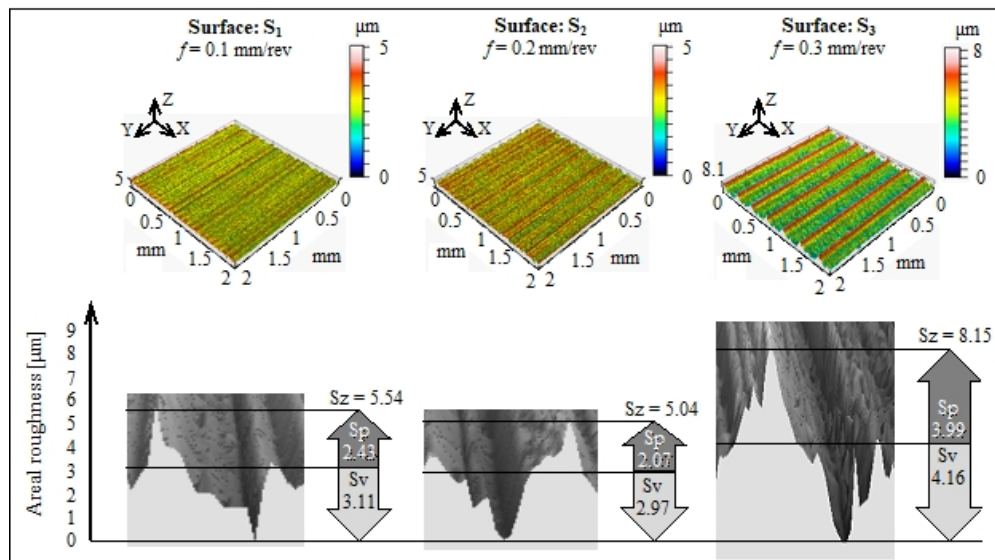


Figure 5: 3D height parameters of the analyzed surfaces

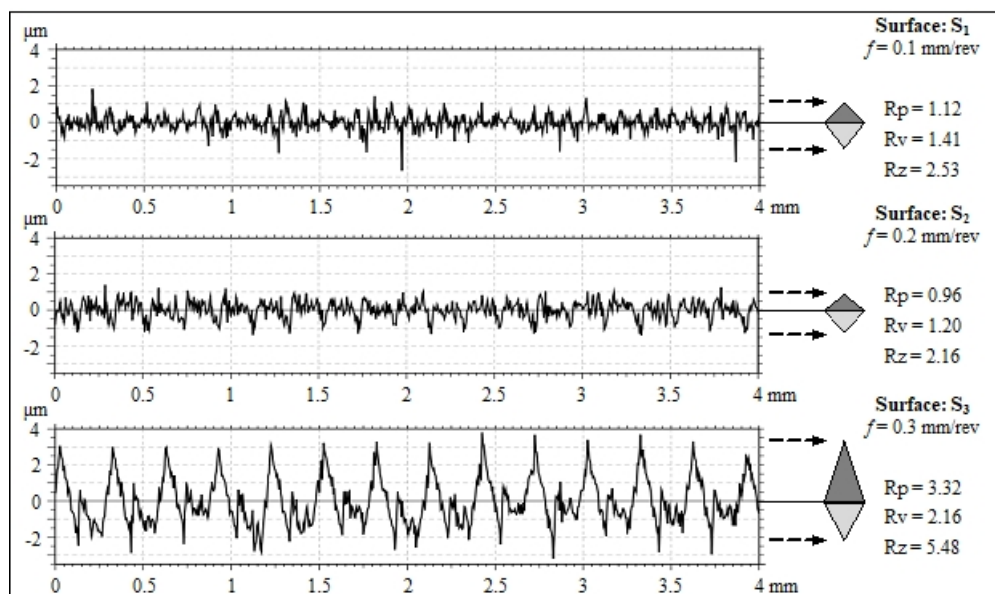


Figure 6: The profiles extracted from the scanned surface (one profile per surface) and their 2D height parameters (average of the data from three profiles)

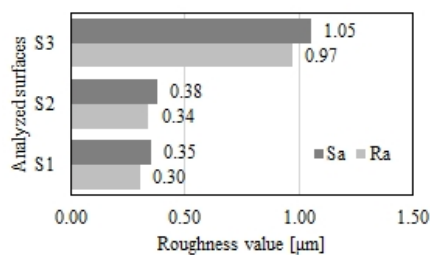


Figure 7: Comparison of the 2D and 3D arithmetical mean heights

ative  $S_{sk}$  values. Concerning the order of the surfaces, deviations can be observed, which may be derived from the different dimensions of the parameters. If the parameter  $V_{vv}$  is considered to be the base, the order of the surfaces is  $S_3, S_2$  then  $S_1$ . This is not confirmed by any other parameters. Regarding the valley zone, the parameters  $S_{sk}, S_{a2}$  then  $S_{vi}$  yield the identical order, that is,  $S_2, S_1$  then  $S_3$ . Based on the fluid-retention capacity of the core zone, that is, parameter  $V_{vc}$ , the order is  $S_3, S_2$  then  $S_1$ . This order is confirmed by the other parameter of the core zone,  $S_{ci}$ .

is characterized by the parameters  $V_{vc}$  and  $S_{ci}$ , moreover, higher values indicate greater fluid-retention capacities. This property is better in the case of low or neg-

By analyzing the 2D profile parameters (Fig. 10), it was found that all of them provide the same order as their 3D counterparts. By considering the 3D values as bases, the following can be stated based on the 2D pa-

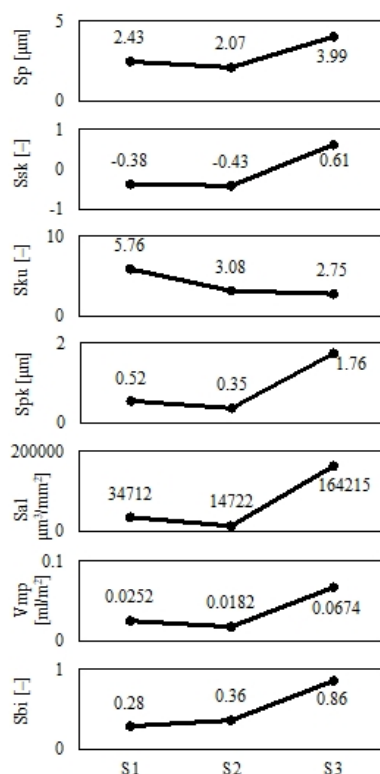


Figure 8: 3D roughness parameters characterizing wear resistance

rameters with regard to the three surfaces. The values of the parameters Rp are 46 to 83% of those of Sp. The rate of the parameter Rv varies between 40 and 52%, while those of Rsk and Rku are 21 – 143% and 71 – 112%, respectively. The differences in terms of Tpk and Rvk are smaller, namely 90 – 112% and 90 – 105%, respectively. In Table 5, the order of the surfaces is summarized based on the findings detailed above concerning wear resistance and fluid-retention capacity.

## 5. Conclusions

From the analysis of the general characteristics of the surfaces, it was found that for the applied cutting data the hard-turned surface is anisotropic and the degree of isotropy varies between 1.5 and 4.3%. The Power Spectral Density analysis clearly determined that the wavelengths are identical to the feed rates. The 3D height parameters (Sv, Sp, Sz, Sa) of the surfaces machined by lower feed rates, namely  $f = 0.1$  and  $0.2$  mm/rev, show absolute differences of between 5 and 17% and this difference in the case of the 2D parameters (Rv, Rp, Rz, Ra) varies between 11 and 17%. By comparing the 3D and 2D parameters, it was found that the Sa value of the 3D measurement is at most 15% higher than the Ra value of the 2D measurement. The Sv, Sp and Sz values can be up to 2.5 times higher than their 2D counterparts. From the analysis of the surface roughness parameters that indicate tribological properties, the following can be stated:

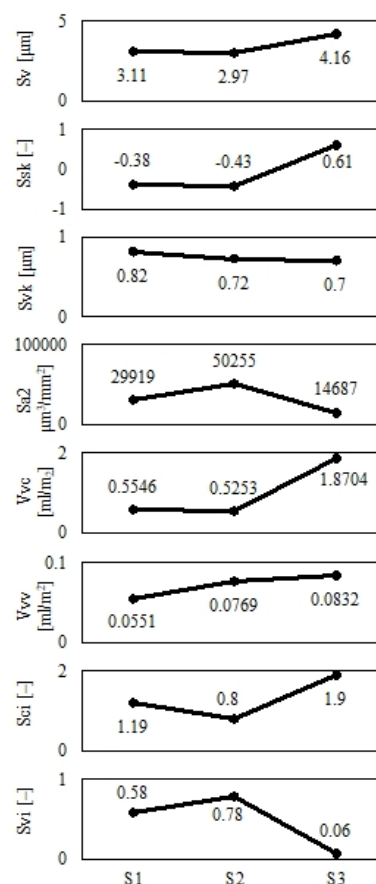


Figure 9: 3D roughness parameters characterizing fluid-retention capacity

1. Based on the parameters that evaluate the roughness peaks and indicate the wear resistance (Sp, Ssk, Spk, Sa1 and Vmp), the most and least wear-resistant are the surfaces hard turned at feed rates of 0.2 and 0.3 mm/rev, respectively. The other parameters yielded different orders, which can be explained by their calculation methods.
2. The order of the surfaces with regard to the parameters of the core zone that indicate the fluid-retention capacity (Vvc, Sci) is identical: the surfaces machined at feed rates of 0.3 and 0.2 mm/rev exhibit the best and worst fluid-retention capacities, respectively.
3. The order of the surfaces with regard to the parameters of the valley zone that indicate the fluid-retention capacity (Ssk, Sa2 and Svi) is identical: the surfaces machined at feed rates of 0.2 and 0.3 mm/rev exhibit the best and worst fluid-retention capacities, respectively. The other parameters yielded different orders, which can be explained by their calculation methods.

Another useful research direction would be the comparison of different workpiece materials. In addition to this, based on systematic experimental design, carrying out

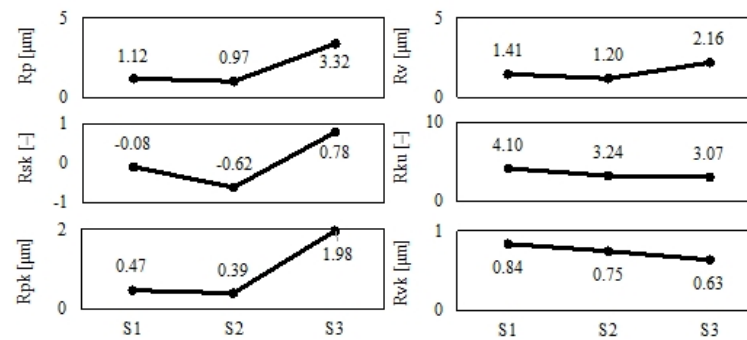


Figure 10: 2D roughness parameters characterizing wear resistance and fluid-retention capacity

Table 5: Order of the surfaces based on the analyzed tribological properties and roughness parameters

Peak parameter	Order	Valley parameter	Order	Core parameter	Order
Sp	$S_2 > S_1 > S_3$	Sv	$S_3 > S_1 > S_2$	Vvc	$S_3 > S_1 > S_2$
Ssk	$S_2 > S_1 > S_3$	Ssk	$S_2 > S_1 > S_3$	Sci	$S_3 > S_1 > S_2$
Sku	$S_3 > S_2 > S_1$	Svk	$S_1 > S_2 > S_3$		
Spk	$S_2 > S_1 > S_3$	Sa2	$S_2 > S_1 > S_3$		
Sa1	$S_2 > S_1 > S_3$	Vvv	$S_3 > S_2 > S_1$		
Vmp	$S_2 > S_1 > S_3$	Svi	$S_2 > S_1 > S_3$		
Sbi	$S_3 > S_2 > S_1$				

machining experiments using various cutting parameter setups would lead to generalizable statements. Furthermore, why the fluid-retention capacity of the valley zone is characterized by relatively large deviations based on the different roughness parameters could be investigated.

## REFERENCES

- [1] Blawucki, S.; Zaleski, K.: The effect of the aluminium alloy surface roughness on the restitution coefficient. *Adv. Sci. Technol. Res. J.*, 2015, **9**, 66–71 DOI: 10.12913/22998624/59086
- [2] Gogolin, A.; Wasilewski, M.; Ligus, G.; Wojciechowski, S.; Gapinski, B.; Krolczyk, J.; Zajac, D.; Krolczyk, G.: Influence of geometry and surface morphology of the U-tube on the fluid flow in the range of various velocities. *Measurement*, 2020, **164**, 108094 DOI: 10.1016/j.measurement.2020.108094
- [3] Karkalos, N.E.; Karmiris-Obratanski, P.; Kurpiel, S.; Zagorski, K.; Markopoulos, A.P.: Investigation on the surface quality obtained during trochoidal milling of 6082 aluminum alloy. *Machines*, 2021, **9**, 75 DOI: 10.3390/machines9040075
- [4] Sagbas, A.: Analysis and optimization of surface roughness in the ball burnishing process using response surface methodology and desirability function. *Adv. Eng. Softw.*, 2011, **42**, 992–998 DOI: 10.1016/j.advengsoft.2011.05.021
- [5] Linins, O.; Krizbergs, J.; Boiko, I.: Surface texture metrology gives a better understanding of the surface in its functional state. *Key. Eng. Mater.*, 2013, **527**, 167–172 DOI: 10.1016/j.precisioneng.2016.06.001
- [6] Kundrak, J.; Nagy, A.; Markopoulos, A.P.; Karkalos, N.E.: Investigation of surface roughness on face milled parts with round insert in planes parallel to the feed at various cutting speeds. *Cut. Tools Technol. Syst.*, 2019, **91**, 87–96 DOI: 10.20998/2078-7405.2019.91.09
- [7] Grzesik, W.; Rech, J.; Zak, K.: High-precision Finishing Hard Steel Surfaces Using Cutting, Abrasive and Burnishing Operations. *Procedia Manuf.*, 2015, **1**, 619–627 DOI: 10.1016/j.promfg.2015.09.048
- [8] Felho, C.; Kundrak, J.: Characterization of topography of cut surface based on theoretical roughness indexes. *Key Eng. Mater.*, 2012, **496**, 194–199 DOI: 10.4028/www.scientific.net/KEM.496.194
- [9] Kundrak, J.; Gyani, K.; Felho, C.; Deszpoth, I.: The effect of the shape of chip cross section on cutting force and roughness when increasing feed in face milling. *Manuf. Techn.*, 2017, **17**(3), 335–342 DOI: 10.21062/ujep/x.2017/a/1213-2489/MT/17/3/335
- [10] Mamalis, A.G.; Kundrak, J.; Horvath, M.: On a novel tool life relation for precision cutting tools. *J. Manuf. Sci. Eng.*, 2005, **127**, 328–332 DOI: 10.1115/1.1794158
- [11] Grzesik, W.; Zak, K.; Kiszka, P.: Comparison of Surface Textures Generated in Hard Turning and Grinding Operations. *Procedia CIRP*, 2014, **13**, 84–89 DOI: 10.1016/j.procir.2014.04.015
- [12] Charles, A.; Elkaseer, A.; Thijs, L.; Hagenmeyer, V.; Scholz, S.: Effect of process parameters on the generated surface roughness of down-facing surfaces in selective laser melting. *Appl. Sci.*, 2019, **9**, 1256 DOI: 10.3390/app9061256
- [13] Zawada-Tomkiewicz, A.: Analysis of surface roughness parameters achieved by hard turning with

- the use of PCBN tools. *Estonian J. Eng.*, 2011, **17**, 88 DOI: [10.3176/eng.2011.1.09](https://doi.org/10.3176/eng.2011.1.09)
- [14] Pytlak, B.: The roughness parameters 2D and 3D and some characteristics of the machined surface topography after hard turning and grinding of hardened 18CrMo4 steel. *Kom. Budowy Masz. PAN Oddz. w Pozn.*, 2011, **31**, 53–62 DOI: [10.2478/amst-2014-0004](https://doi.org/10.2478/amst-2014-0004)
- [15] Shivanna, D.; Kiran, M.; Kavitha, S.: Evaluation of 3D Surface Roughness Parameters of EDM Components Using Vision System. *Procedia Mater. Sci.*, 2014, **5**, 2132–2141 DOI: [10.1016/j.mspro.2014.07.416](https://doi.org/10.1016/j.mspro.2014.07.416)
- [16] Przystacki, D.; Majchrowski, R.; Marciniak-Podsadna, L.: Experimental research of surface roughness and surface texture after laser cladding. *Appl. Surf. Sci.*, 2016, **388**, 420–423 DOI: [10.1016/j.apsusc.2015.12.093](https://doi.org/10.1016/j.apsusc.2015.12.093)
- [17] Kumar, R.; Seetharamu, S.; Kamaraj, M.: Quantitative evaluation of 3D surface roughness parameters during cavitation exposure of 16Cr–5Ni hydro turbine steel. *Wear*, 2014, **320**, 16–24 DOI: [10.1016/j.wear.2014.07.015](https://doi.org/10.1016/j.wear.2014.07.015)
- [18] Aidibe, A.; Nejad, M.K.; Tahan, A.; Jahazi, M.; Cloutier, S.G.: A Proposition for New Quality 3D Indexes to Measure Surface Roughness. *Procedia CIRP*, 2016, **46**, 327–330 DOI: [10.1016/j.procir.2016.03.136](https://doi.org/10.1016/j.procir.2016.03.136)
- [19] Kovacs, Z., Viharos, Z.J., Kodacsy, J.: The effects of machining strategies of magnetic assisted roller burnishing on the resulted surface structure. *Mater. Sci. Eng.*, 2018, **448**, 012002 DOI: [10.1088/1757-899X/448/1/012002](https://doi.org/10.1088/1757-899X/448/1/012002)
- [20] Bitelli, G.; Simone, A.; Girardi, F.; Lantieri, C.: Laser Scanning on Road Pavements: A New Approach for Characterizing Surface Texture. *Sensors*, 2012, **12**, 9110–9128 DOI: [10.3390/s120709110](https://doi.org/10.3390/s120709110)
- [21] Chen, L.; Liu, Z.; Wang, B.; Song, Q.; Wan, Y.; Chen, L.: Surface Characterization and Tribological Performance of Anodizing Micro-Textured Aluminum-Silicon. *Materials*, 2019, **12**, 1862 DOI: [10.3390/ma12111862](https://doi.org/10.3390/ma12111862)
- [22] Zhu, L.; Guan, Y.; Wang, Y.; Xie, Z.; Lin, J.; Zhai, J.: Influence of process parameters of ultrasonic shot peening on surface roughness and hydrophilicity of pure titanium. *Surf. Coatings Technol.*, 2017, **317**, 38–53 DOI: [10.1016/j.surfcoat.2017.03.044](https://doi.org/10.1016/j.surfcoat.2017.03.044)
- [23] Suha, A.I.; Polycarpou, A.A.; Conry, T.F.: Detailed surface roughness characterization of engineering surfaces undergoing tribological testing leading to scuffing. *Wear*, 2003, **255**, 556–568 DOI: [10.1016/S0043-1648\(03\)00224-2](https://doi.org/10.1016/S0043-1648(03)00224-2)
- [24] Wojciechowska, L.; Wiczorowski, M.; Mathia, T.G.: Transition from the boundary lubrication to scuffing—the role of metallic surfaces morphology. *Wear*, 2017, **392–393**, 39–49 DOI: [10.1016/j.wear.2017.09.011](https://doi.org/10.1016/j.wear.2017.09.011)

## COMPLEMENTARY MANIPULATOR TOOL DEVELOPMENT FOR SAFE COBOT-ASSISTED HYDROPONICS

IMRE PANITI<sup>\*1,2</sup>, JÁNOS NACSA<sup>1,2</sup>, DÁVID SZŰR<sup>1</sup>, SÁNDOR RÁCZ<sup>3</sup>, AND JÓZSEF TÓTH<sup>4</sup>

<sup>1</sup>ELKH SZTAKI, Centre of Excellence in Production Informatics and Control, Kende u. 13–17, Budapest, 1111, HUNGARY

<sup>2</sup>Széchenyi István Egyetem, Egyetem tér 1, Győr, 9026, HUNGARY

<sup>3</sup>Green Drops Farm Kft., Hold u. 56, Debrecen, 4034, HUNGARY

<sup>4</sup>Hepenix Kft., Petőfi Sándor u. 39, Diósd, 2049, HUNGARY

Human–robot collaboration is gaining ground in Manufacturing, Healthcare and Logistics but also in Agriculture. Different types of applications in the latter field are becoming more common. However, in all scenarios, safety assessment and verification are crucial to cope with the related standards and specifications. In this paper, the development and safety testing of a complementary manipulator tool (Clip) is presented which can by design limit the physical interaction energy in a hazardous collaborative robot (cobot) scenario, namely when loading the plant of a Hydroponic System.

**Keywords:** hydroponics, human-robot collaboration, safety

### 1. Introduction

Using robots in agriculture is a rather old field of interest with many difficult automation problems. Incorporating automation can help hydroponic systems become more efficient and productive because - according to Ref. [1] - labor is the biggest cost in this domain. In a review [2] about smart hydroponic systems, some robotic applications were mentioned, e.g. harvesting strawberries and cleaning greenhouses. In the real business world, some companies offer completely robot-based hydroponic environments, e.g. a start-up called Iron Ox has just received a big investment [3] for their complete hydroponic farming solution. The safety aspects in indoor farming environments were also investigated [4]. In this paper, the technical criteria of a cobotised Hydroponic System are presented alongside the development of a complementary manipulator tool which is finally tested against a safety protocol.

### 2. Technical criteria

In order to create a safe, cobotised Hydroponic System, the Directive 2006/42/EC of the European Parliament and of the Council of 17 May 2006 on machinery [5], and amending Directive 95/16/EC (recast [6] needs to be applied, together with the Low Voltage Directive 2014/35/EU [7] which is applicable from 20th April 2016, i.e. the Council Directive 2006/95/EC of

12th December 2006 on the electrical equipment designed for use within certain voltage limits, amended by (93/68/EEF) and the EMC directive (2014/30/EU [8] applicable from 20th April 2016), that is, the Council Directive 2004/108/EC of 15th December 2004 on the approximation of the laws of the Member States relating to electromagnetic compatibility.

Furthermore, although a large number of initially considered harmonized standards are present, the main relevant ones are the following:

- ISO 13855:2010 [9] - Safety of machinery. Positioning of safeguards with respect to the approach speeds of parts of the human body.
- EN 547-3:2009 [10] - Safety of machinery. Human body measurements.
- ISO 14123-1:2015 [11] - Safety of machinery - Reduction of risks to health from hazardous substances emitted by machinery - Part 1: Principles and specifications for machinery manufacturers.
- EN 1005-1:2001+A1:2008 [12] - Safety of machinery - Human physical performance - Part 1: Terms and definitions.
- EN 1005-3:2002+A1:2008 [13] - Safety of machinery - Human physical performance - Part 3: Recommended force limits for machinery operation.
- ISO 10218-1:2011 [14] - Robots and robotic devices. Safety requirements for industrial robots.

\*Correspondence: [imre.paniti@sztaki.hu](mailto:imre.paniti@sztaki.hu)

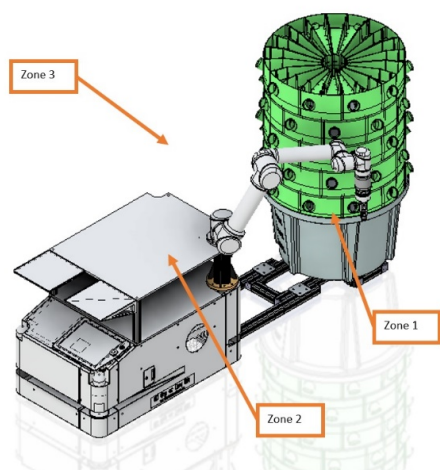


Figure 1: Set-up of the Cobotised Hydroponic System with 3 Zones.



Figure 2: Hydro pot.

- ISO 3691-4:2020 [15] - Industrial trucks. Safety requirements and verification - Part 4: Driverless industrial trucks and their systems.
- IEC 61508-3:2010 [16] - Functional safety of electrical/electronic/programmable electronic safety-related systems - Part 3: Software requirements.
- SIST EN 61508-5:2011 [17] - Functional safety of electrical/electronic/programmable electronic safety-related systems - Part 5: Examples of methods for the determination of safety integrity levels.

The technical specification, ISO/TS 15066:2016 [18] - Robots and robotic devices - Collaborative robots, should also be taken into consideration.

These directives and standards were necessary because the cobotised Hydroponic System consists of an UR5 cobot arm mounted on an Automated Ground Vehicle (AGV) which is docked to the hydroponic growing tower with an electric pump (see Fig. 1).

Based on the set-up, 3 hazard zones were defined:

- Zone 1: Primary process area
- Zone 2: Secondary process area
- Zone 3: Surrounding equipment



Figure 3: Plant roots in the Hydro pot.

### 3. Risk assessment

The risk analysis was carried out for Zone 1 according to a normal methodology, following the steps of the ISO 12100:2010 standard [19]. After recognizing the hazards and the injuries, a risk graph had to be categorized based on ISO 13849-1:2015 [20]. As a result of the categorization, the risk level of each hazard could be calculated. The risk level of each hazard was calculated using the worst result.

As the cobot arm is equipped with a two-finger gripper and is responsible for loading the seedlings, this is one of the crucial elements of the system in terms of safety. Special care needs to be taken when manipulating the plants as on the one hand, damage to the crops, leaves and roots should be avoided, but on the other hand an unintended collision with a plant carrier should not exceed the biomechanical threshold values defined in Ref. [18].

### 4. Clip development

Green Drops Farm Kft. developed its hydroponic system using a commercially available product called a hydro pot (see Fig. 2) with a diameter of 50 mm for creating holes to plant plants by following the same practices adopted by similar pieces of equipment.

During the development of automation and robotization, a problem occurred, namely that as the crops grow their roots overgrow the hydro pot so the plant becomes stuck where it is (see Fig. 3). As a result, the arm of the cobot is unable to handle the pots, which cannot be used again.

In order to be sustainable and recycle, several versions of clips have been designed and commercially available rockwool cubes used.

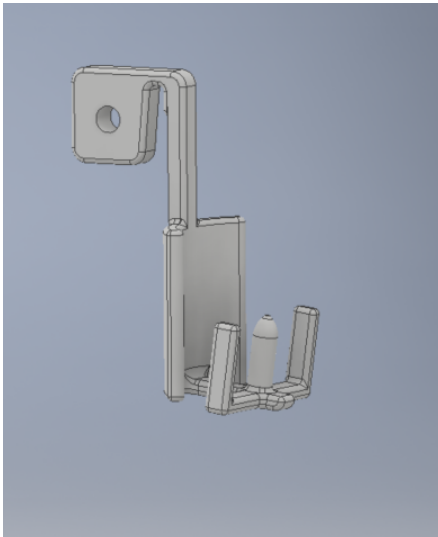


Figure 4: One of the first clip prototypes.



Figure 6: Clip prototypes with horizontal spikes.



Figure 5: Clip prototypes with vertical spikes.

As the cobot arm could not handle the clips because the part (a flag-like handle) it would grab (see Fig. 4) had become overgrown by the plant, that part had to be re-designed.

In the first versions of the design, the spike on the clips was vertical, but during testing it was demonstrated that it could cause serious injuries to people (see Fig. 5), despite the fact that the clips had been created using 3D printing.

The end of the spike needed to be blunted and placed horizontally in order to avoid causing potential injuries (see Fig. 6). Even though horizontal rockwool cubes were produced to facilitate its installation, the plants could still fall off.

In the final version, nooks were placed on the clips on which semicircular plant holder rings can be placed at different heights. This prevents plants from falling off and it is safer moving them using the cobot arm (see Fig. 7).

## 5. Collision tests

Tests were carried out on the clips according to a testing protocol entitled "Test robot arm for collision with movable object (Impact)" from the COVR Toolkit [21], which functions also as a library for protocol testing of cobot applications. These tests are in harmony with the standards within the frame of cobot usage as described in Ref. [22]. Force measurements were recorded with a GTE KMG 500-75 force cell (Spring rate: 75 N/mm with the damping material SH70) while pressure values were measured with Fuji Prescale LLW-type Films (see Fig. 8).

The results of 3 experiments at a cobot speed of 0.1 m/s showed that for a human hand only a transient collision can occur with a maximum force of 47 N (see Fig.

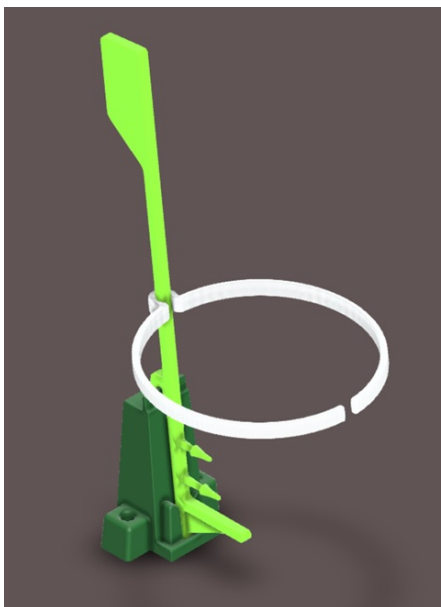


Figure 7: Final clip design with a clip and plant holder.



Figure 8: Clip collision testing set-up with a force cell and pressure-sensitive measurement film.

9) as in all cases the 3D-printed clip breaks at the same position.

The maximum pressure was 300 N/cm<sup>2</sup> (see Fig. 10).

As in some cases the pressure can be close to the threshold, the use of gloves while carrying out clip-assisted plant loading is highly recommended.

## 6. Conclusion

Hydroponics is a subset of hydroculture, which is an environmentally friendly technology for growing plants in the absence of soil by using mineral nutrient solutions dissolved in water. Many tasks in the Hydroponic production process cannot be fully automated and require safe human-robot collaboration, moreover, cobotised tasks like the loading of plants must be tested with a safety protocol similar to the one followed in this paper. The proposed 3D-printed complementary manipulator tool (clip) was tested by following the protocol "Test robot arm for collision with movable object (Impact)." Test results showed that only transient collisions can occur and force as well as pressure values are below the threshold in the case of a collision with a human hand.

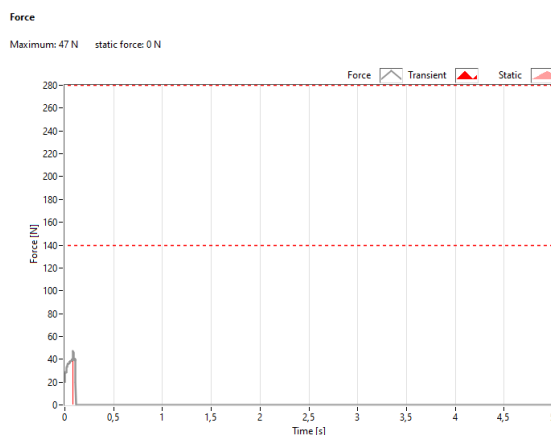


Figure 9: Force measurement results.

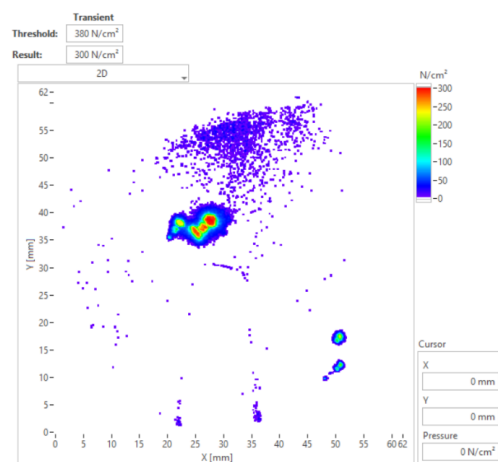


Figure 10: Pressure measurement results.

However, to maximize safety, it is recommended that gloves are worn.

## Acknowledgement

This project was funded by the European Union's Horizon 2020 research and innovation programme under grant agreement No. 779966. Furthermore, this research was supported by the 'Thematic Excellence Programme – National Challenges Subprogramme – Establishment of the Center of Excellence for Autonomous Transport Systems at Széchenyi István University (TKP2020-NKA-14)' project.

## REFERENCES

- [1] Currey, C. J.: Automation for hydroponics, Produce Grower, 2019 <https://www.producegrower.com>
- [2] Modu, F.; Adam, A.; Aliyu, F.; Mabu, A.; Alhaji Musa, M.: A Survey of Smart Hydroponic Systems. *Advances in Science, Technology and Engineering Systems Journal*, 2020, **5**, 233-248 DOI: [10.25046/aj050130](https://doi.org/10.25046/aj050130)

- [3] Leading Ag-Tech Start-up Iron Ox Closes \$53 Million Investment Round Led by Breakthrough Energy Ventures (news); <https://ironox.com>
- [4] Gnauer, C.; Pichler, H.; Tauber, M.; Schmittner, C.; Christl, K.; Knapitsch, J.; Parapatits, M.: Towards a secure and self-adapting smart indoor farming framework. *Elektrotechnik und Informationstechnik* 2019, **136**(7), 341-344 DOI: 10.1007/s00502-019-00745-0
- [5] Directive 2006/42/EC, <https://eur-lex.europa.eu>
- [6] Directive 95/16/EC, <https://eur-lex.europa.eu>
- [7] Directive 2014/35/EU, <https://eur-lex.europa.eu>
- [8] Directive 2014/30/EU, <https://eur-lex.europa.eu>
- [9] ISO 13855:2010, <https://www.iso.org>
- [10] EN 547-3:2009, <https://webstore.ansi.org>
- [11] ISO 14123-1:2015, <https://www.iso.org>
- [12] EN 1005-1:2002+A1:2008, <https://standards.iteh.ai>
- [13] EN 1005-3:2002+A1:2008, <https://standards.iteh.ai>
- [14] ISO 10218-1:2011, <https://www.iso.org>
- [15] ISO 3691-4:2020, <https://standards.iteh.ai>
- [16] EN 61508-3:2010, <https://standards.iteh.ai>
- [17] EN 61508-5:2011, <https://standards.iteh.ai>
- [18] ISO/TS 15066:2016, <https://www.iso.org>
- [19] ISO 12100:2010, <https://www.iso.org>
- [20] ISO 13849-1:2015, <https://www.iso.org>
- [21] COVR Toolkit. <https://www.safearoundrobots.com/home>
- [22] Valori, M.; Scibilia, A.; Fassi, I.; Saenz, J.; Behrens, R.; Herbster, S.; Bidard, C.; Lucet, E.; Magisson, A.; Schaake, L.; Bessler, J.; Prange-Lasonder, G.B.; Kühnrich, M.; Lassen, A.B.; Nielsen, K.: Validating Safety in Human–Robot Collaboration: Standards and New Perspectives. *Robotics*, 2021, **10**, 65. DOI: 10.3390/robotics10020065



## GRIPPER FINGER DESIGN FOR SPECIAL PURPOSE APPLICATIONS

MIKLÓS BOLERACZKI<sup>\*1</sup>, ISTVÁN GÁBOR GYURIKA<sup>1</sup>, AND DÉNES FODOR<sup>1</sup>

<sup>1</sup>Research Centre for Engineering Sciences, University of Pannonia, Egyetem u. 10, Veszprém, 8200, HUNGARY

The trend towards collaborative robots is resulting in these "machine workers" working alongside humans in many workplaces. They can be used for a wide range of tasks and, most importantly, can rapidly switch between tasks. When it is no longer necessary for them to work at one location, they can simply be transferred to support another production process. With their universal gripper they can handle a wide range of tasks, however, custom accessories may need to be produced in specific areas. One such accessory could be sleeves that are mounted on the grippers to extend the use of the universal gripper. This paper aims to provide assistance on how to design these fingers.

**Keywords:** collaborative robot, gripper finger, 3D-printed jaw

### 1. Introduction

Robotization is a common solution in industrial environments. Despite being very expensive, it offers a relatively quick return on investment. In addition to the robot, the cost of robotization includes other service and auxiliary units such as effectors, feeders, fixtures and tooling. How is a robot gripper chosen? [1] For example, on the basis of dexterity, how much it can grip and how much it can open. Gripper fingers are applied less than small jaws which are preferred because of their flexible elements.

One of the significant advantages of collaborative robots, which are currently emerging in industry, is that they can be used to conduct multiple tasks with the need for minimal modifications. In the past, installed and enclosed industrial robots were usually purchased as well as prepared for a single purpose, typically to be operated in a production cell. Currently, collaborative robots often perform a range of tasks in collaboration with humans [2], partly because if a robot is no longer needed at one workstation, it can be used on another line at another workstation. As a result, the amount of reassembly and installation work that maintenance and line engineers are required to do is minimal.

### 2. Gripper selection

It is recommended to choose a solution for the robot effector that is best suited to such a general manufacturing environment. Although grippers are available in a variety of sizes, it is also worth considering their cost. In general, a more expensive gripper can handle multiple tasks,

while a cheaper version may be less capable of adapting to the task at hand.

The gripper is a mechanical interface between the robot and its environment [3]. Without it, the robot cannot perform its task, e.g. packing or assembling. The cited article introduces various designs of grippers. The first group of gripper fingers include several notches in the gripping surfaces, which make it possible to grip workpieces of different shapes. This is usually only suitable for workpieces of a similar size and weight. Even though they are simple to make and low-cost, the number of notches that can be cut is limited. Since the number of notches required for all workpieces must be specified, the design time may be longer. Programming the robot can also be a lengthy process because the gripper must be correctly oriented to the workpieces. Another method is to change the fingers of the gripper so that differently shaped workpieces can be handled by changing the gripper fingers. The fingers are stored on a rack and the robot knows the exact position of each finger. A reliable mechanical device to accurately clamp and unclamp the fingers is essential in this case, moreover, their replacement time should be minimized. Therefore, the gripper and robot will be able to handle a wide range of workpieces and easily adapt to other applications. This method is more flexible than the previous one, which is more application-specific.

The third technique is to replace grippers. For this purpose, complete tool changer grippers can be purchased, which are expensive but precise and allow grippers to be quickly replaced. They are used when a gripper cannot handle the differences in size, geometry and weight between workpieces. Therefore, several grip-

<sup>\*</sup>Correspondence: [boleraczki.miklos@mk.uni-pannon.hu](mailto:boleraczki.miklos@mk.uni-pannon.hu)

pers are needed to cover a range of workpieces. The robot must be provided with precise information about each gripper and its position, which usually also requires a power supply and sensors. In general, this gripper changeover can be used for different types of grippers, e.g. mechanical, vacuum, magnetic, etc. As the changeover time increases the downtime, it should be kept to a minimum. Although modern tool changers are equipped with a number of energy transfers (air and electrical connections), they are expensive.

A fourth solution is to attach several grippers to the robot simultaneously in a revolving or linear arrangement. In the simplest case, two grippers are mounted for loading/unloading operations, which significantly speeds up the service time of the machine. The fifth option presented in this article are active and passive universal grippers. Grippers that can adapt to the workpiece, e.g. in an elastic manner, with a passive (non-actuated) degree of freedom can be considered as passive universal grippers. They are characterized by the fact that they do not provide a precise position of the workpiece in the coordinate system of the robot. They are well-suited for simple pick-and-place tasks where a high degree of precision is not required. Active universal grippers mimic the universal gripping ability of human hands. Even though such experiments have been conducted in the past, nowadays, with the addition of 3D printing, some open source projects include such active universal robotic hands. At the time of writing that article, these robotic hands were expensive and unreliable so inapplicable on an industrial scale, which is still true today. Although they are constantly being improved and better products are being developed, their real applications are in the service robotics market rather than in industrial manufacturing despite research being carried out in this field as well [4].

Zubair et al. have developed [5] an attachable core gripper for a collaborative robot that can be operated without the robot using its own power source, which is an uncommon solution in the market. Detachable robotic grippers not only work as a fully functional gripper when attached to the robot but also once detached. In terms of their physical design, 4 electromagnets are located on the side which is attached to the robot, while on the other side, 4 fingers grasp objects. The whole device is located in a 3D-printed housing. The usability of their gripper has also been tested by 12 participants. The development solution is predominantly intended to be used in a non-industrial environment.

Long et al. designed a multifunctional gripper for grasping general objects [6] because many places, e.g. warehouses, require simple pick-and-place tasks and the level of automation is increasing due to rising costs of manpower. Underactuated grippers consist of two fingers, each of which has three degrees of freedom with a five-bar mechanism actuated by two motors. Experience has shown that the gripper, which combines two types, is versatile and reliable for the purpose of manipulating a wide range of objects.

In terms of workpieces, it is easiest to categorize the many different products into families, thereby simplifying and economizing the process required to select grippers. According to a survey of 1,000 workpieces, the most necessary requirements for a gripper are an inexpensive rugged type of jaw with a stroke of 50 mm and a clamping force of less than 100 N.

### 3. Promising attempts

Current conventional robotic grippers have a number of drawbacks, namely their large volume, high weight as well as energy consumption and significant cost. A promising trend is the exploration of shape memory alloy-actuated grippers. Shape memory alloys (SMAs) can change their shape under stress [7]. The gripper presented in this research is powered by 9 100 mm-long SMA wires with a diameter of 0.4 mm. The wires are tied together sequentially so that their displacement is added and the opening of the stroke gripper is long. Conventional grippers have servo or stepper motors and pneumatic or hydraulic actuators, rendering the gripper heavy and expensive as well as requiring a high power consumption. In contrast, SMAs as actuators are characterized by their high energy density, low energy consumption, quick response and repetitive actuation. Another special feature of the gripper presented in this article is that it has four parallel jaws on one finger. The outer two are rigid, while the inner two are flexible. At the time of writing, the gripper also has some defects, the most critical of which is that since the SMA wire is cooled naturally, the time required for the finger to close is more than 5 seconds.

Horacio Leon et al. are developing a robotic hand that consists of 5 fingers, with an extra thumb instead of a little finger [8]. The thumb is important for two reasons, namely for precision grip and power grip. The thumb is particularly critical because it increases the functionality of the hand by 60 %. In the article, the concept DFAM (design for additive manufacturing) was used to develop the object quickly and cheaply by building it layer by layer using a variety of materials, that is, plastic, ceramic, metal or even concrete and glass. The method is based on reducing the amount of resources, print time, weight and cost. It also brings about quality enhancement like strength and functionality. A common practice is referred to as “remixing,”- that is, a 3-dimensional design refers to other designs that are used. Eight different versions of remixing have been created, the first of which is the open InMoov robotic hand, which consists of 36 parts and 17 degrees of freedom, namely its parameters are identical to those of the human hand. The first remix version, “Parloma Hand,” has 22 degrees of freedom. The article also gives an important account of the methodology, which consists of three main parts: inspiration, ideation and implementation. By its very nature, remixing is an iterative process, which is also reflected in the methodology. Finally, a gripper was developed that has two thumbs, one

on both the right and left side of the hand, with three fingers in between them. The hand called “Kool” is composed of 33 components and has 19 degrees of freedom, moreover, its weight, cost and printing time has been reduced compared to the original hand. Since the thumb can also grip more firmly, it is also more secure and, therefore, more functional.

Based on the aforementioned classification, the types of grippers created in the context of soft robotics can be considered as active universal grippers, which do not essentially have rigid articulated links but can be described by continuous kinematics. Developers expect these to be more effective in everyday life because they better replicate the structure of living beings, i.e. given that most of them are made of soft materials rather than rigid ones, they are more adaptable to changes in the environment. Although some connect rigid members with hinges, other studies have experimented with grippers made of a material that is truly continuously soft. An example of this is the printed soft gripper [9] presented in the article by Slesarenko et al. Their method involved inserting wires and inserts into a polymer gel in various ways to create a more controllable as well as deformable shape and even reduce the actuating force required. The basic principle of a hollow polymeric fuselage thread was used and the shape as well as internal design of the fuselage varied by sectioning it, stiffening it in certain places and weakening it in others. The resulting gripper is suitable for manipulating small objects. The recommended strategy can be applied to other types of soft actuators. Based on the presented gripper, it would be worthwhile to investigate how these grippers can be combined with conventional ones.

Nowadays, the greatest need is for a gripping system that can quickly adapt to the task. Robotic head exchange systems are available that typically consist of two parts, one to be placed on the robot and the other on the gripper, which can then be connected together. More than one gripper can be used to adapt the robot to suit different tasks. This system requires several grippers and the tool changer must be purchased as well as integrated. Another problem is the weight of the head exchanger, which is grooved according to the payload of the robot. Typically, this is undesirable for companies wishing to use collaborative robots for multiple tasks. A better solution might be to attempt to use the gripper for each significantly different task by changing the finger itself. These fingers can be precisely fitted to the gripper, moreover, are relatively simple to manufacture and replace. Additive manufacturing can be used to reduce production time and costs.

#### 4. Methods to design fingers of the gripper

According to the design methodologies, the easiest solution would be to use a given template. By following a series of well-established steps, a finger can be obtained that is suitable for the current gripper and task. By following these steps, the design time is also significantly reduced because it is unnecessary to intuitively guess a

solution, which can take an uncertain amount of time. The easiest way to proceed is to create a spreadsheet or flowchart in which the following questions can be answered to achieve the required outcome:

1. What type of gripper is used?
2. What product is to be gripped?
3. How accurate is our robot?
4. What material are the gripper fingers composed of?

The proposed methodology shown in Fig. 1 builds on the main elements outlined above with a more detailed description as follows. Firstly, which component (or families of components) are to be manipulated needs to be determined. Its size, weight, geometry, surface quality and material need to be taken into consideration. Furthermore, the robot gripper must be analyzed to determine the type and size of its opening as well as how the gripper fingers can be connected to it. The next step is to start the design process, which requires knowledge of the manufacturing technologies available in the factory, namely the 3D printing machines themselves, their characteristics and the type of materials used. The design process should be carried out by bearing in mind the aspects discussed above with a focus on good printability. Finally, based on the design, the 3D printing of the fingers results in physical parts. The solution to the problem is then tested by mounting the gripper fingers on the robot.

Replicating the grip and timing of the fingers is sought. For this purpose, the quickest and most efficient manufacturing solution is 3D printing. Since numerous excellent review articles on 3D printing have been published, researchers are easily provided with an up-to-date overview of the technology [10]. The article presents a comparative analysis of the available technologies and materials. As various additive manufacturing machines are becoming available in more and more factories, it is important to understand the manufacturing requirements that need to be met in the design [11]. By taking into consideration the most common FDM (Fused Deposition Modeling) machines, it is recommended that the printed finger has a flat surface which can be placed on the print bed. By maintaining an angle of 45° when designing upwardly extending gripper fingers, the finger can extend the gripper’s field of application by increasing its maximum opening width. It can also be adapted to suit more precise gripping tasks by designing shaped fingers.

Universal grippers can also meet specific needs. Other design considerations are:

1. The fingers should consist of one or more pieces;
2. The fingers should be composed of at least one material and produced by at least one technology.
3. In 3D printing, composite materials, both continuous and short fiber-reinforced, are also commonly used [12].

The design should take into consideration both sides, one of which is the surface of the workpiece. Between the two

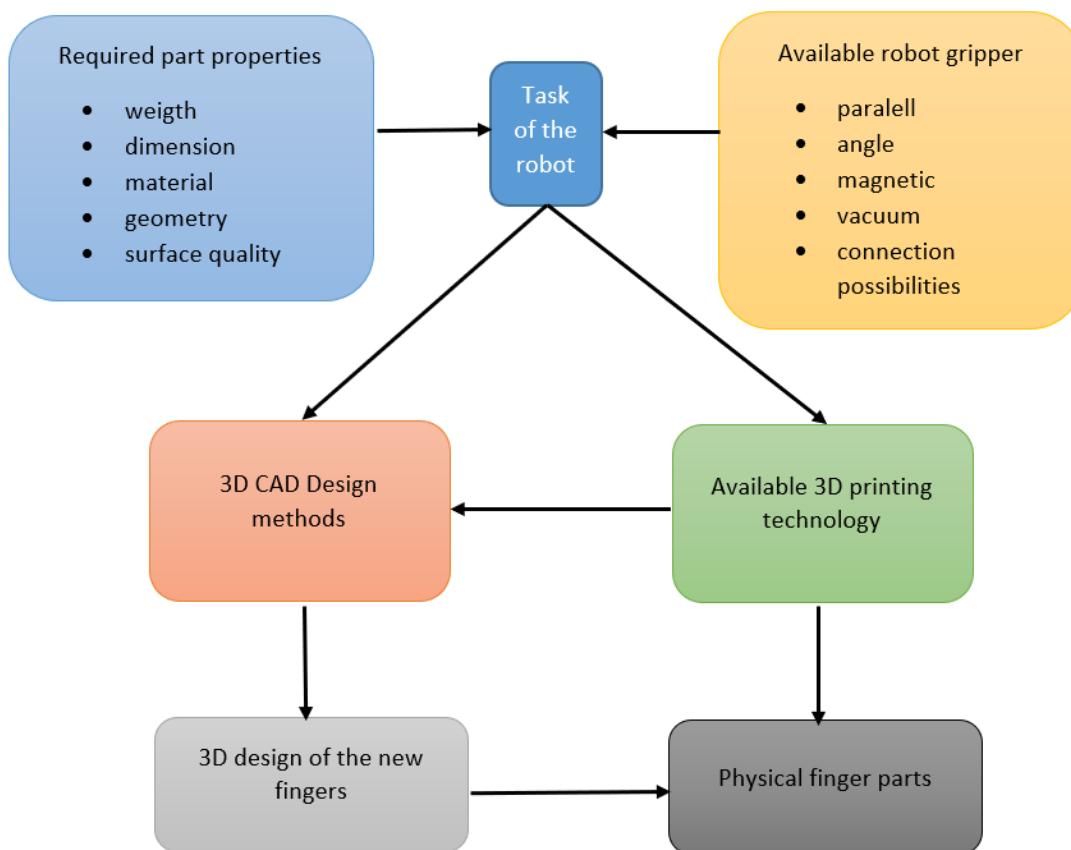


Figure 1: Methods of designing and manufacturing fingers

main components, a form that can be printed easily must be fitted. The available 3D printing processes must be assessed and the one that best suits the task selected. PLA (Polylactide), ABS (Acrylonitrile butadiene styrene) and nylon are the most common materials used by FDM machines.

## 5. Example design of a finger

Based on the aforementioned methodology, two examples are presented in Fig. 2. Firstly, in order to grip a cylindrical workpiece, it is necessary to extend the opening width. Besides, the finger has a prismatic shape, which renders the gripping concentric. In this case, the limitation of this printing technology, namely the  $45^\circ$  overhang, must be taken into consideration. In the second image, a small PCB (printed circuit board) must be moved by fingers, which include notches to guide their orientation against the short gripping surface. In this finger design, the  $45^\circ$  overhang is not important because of its small dimensions. The gripper is an RG2-type universal gripper with an electric motor. 3D printing can be used to produce a rapid prototype for the purpose of experiments, which is advantageous due to its rapid nature and as the fingers can be produced very cheaply.

## 6. Summary and future work

Choosing a suitable gripper is important in terms of its application and once selected, it must be implemented as effectively as possible. The present paper aimed to provide guidance on how this can be achieved by extending its range of uses with custom-designed fingers. In the future, it is expected that composite 3D printers will become more widespread in the industrial environment, fur-

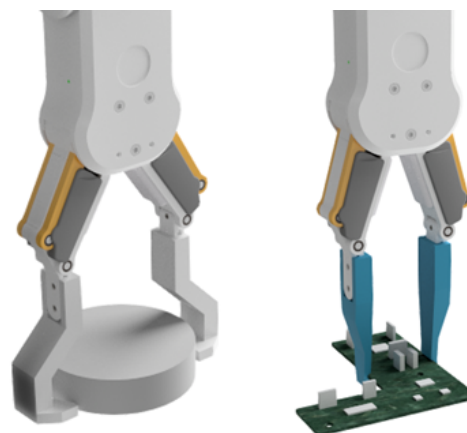


Figure 2: Cylindrically shaped workpiece and PCB-gripping fingers

ther expanding the application areas covered by 3D printing. A similarly exciting topic would be the integration of mobile robots into the manufacturing environment, for which additive manufacturing could also be used.

## 7. Acknowledgment

This work was supported by the TKP2020-NKA-10 project financed under the 2020-4.1.1-TKP2020 Thematic Excellence Programme by the National Research, Development and Innovation Fund of Hungary.

## REFERENCES

- [1] Pham, D. T.; Yeo, S. H.: A knowledge-based system, for robot gripper selection: Criteria for choosing grippers and surfaces for gripping. *Int. J. Mach. Tools Manuf.* 1988, **28**(4), 301–313 DOI: [10.1016/0890-6955\(88\)90045-4](https://doi.org/10.1016/0890-6955(88)90045-4)
- [2] Azima, M.S.; Lobov, A.; Pastukhov, A.: Methodology for implementing universal gripping solution for robot application. *Proc. Eston. Acad. Sci.* 2019, **68**(4), 413–420 DOI: [10.3176/proc.2019.4.11](https://doi.org/10.3176/proc.2019.4.11)
- [3] Pham, D. T.; Yeo, S. H.: Strategies for gripper design and selection in robotic assembly. *Int. J. Prod. Res.* 1991, **29**(2), 303–316 DOI: [10.1080/00207549108930072](https://doi.org/10.1080/00207549108930072)
- [4] Staretu, I.: Robotic Arms with Anthropomorphic Grippers Robotic Technological Processes. *Proceedings*, 2021, **63**(1), 77 DOI: [10.3390/proceedings2020063077](https://doi.org/10.3390/proceedings2020063077)
- [5] Iqbal, Z.; Pozzi, M.; Prattichizzo, D.; Salvietti, G.: Detachable Robotic Grippers for Human-Robot Collaboration. *Front. Robot. AI*, 2021, **8**, 644532 DOI: [10.3389/frobt.2021.644532](https://doi.org/10.3389/frobt.2021.644532)
- [6] Kang, L.; Seo, J.-T.; Kim, S.-H.; Kim, W.-J.; Yi, B.-J.: Design and Implementation of a Multi-Function Gripper for Grasping General Objects. *Appl. Sci.*, 2019, **9**(24), 5266 DOI: [10.3390/app9245266](https://doi.org/10.3390/app9245266)
- [7] Lu, Y.; Xie, Z.; Wang, J.; Yue, H.; Wu, M.; Liu, Y.: A novel design of a parallel gripper actuated by a large-stroke shape memory alloy actuator. *Int. J. Mech. Sci.* 2019, **159**, 74–80 DOI: [10.1016/j.ijmecsci.2019.05.041](https://doi.org/10.1016/j.ijmecsci.2019.05.041)
- [8] León, H.: Design for Additive Manufacturing of a Robotic Hand with Two Thumbs. In: González Díaz C. et al. (eds.) VIII Latin American Conference on Biomedical Engineering and XLII National Conference on Biomedical Engineering. CLAIB 2019. IFMBE Proceedings, vol 75. Springer, Cham. DOI: [10.1007/978-3-030-30648-9\\_133](https://doi.org/10.1007/978-3-030-30648-9_133)
- [9] Slesarenko, V.; Engelkemier, S.; Galich, P.I.; Vladimirsky, D.; Klein, G.; Rudykh, S.: Strategies to Control Performance of 3D-Printed, Cable-Driven Soft Polymer Actuators: From Simple Architectures to Gripper Prototype. *Polymers*, 2018, **10**(8), 846 DOI: [10.3390/polym10080846](https://doi.org/10.3390/polym10080846)
- [10] Krajangsawasdi, N.; Blok, L.G.; Hamerton, I.; Longana, M.L.; Woods, B.K.S.; Ivanov, D.S.: Fused Deposition Modelling of Fibre Reinforced Polymer Composites: A Parametric Review. *J. Compos. Sci.*, 2021, **5**(1), 29 DOI: [10.3390/jcs5010029](https://doi.org/10.3390/jcs5010029)
- [11] Diegel, O.; Nordin, A.; Motte, D.: A Practical Guide to Design for Additive Manufacturing, Springer, 2020 DOI: [10.1007/978-981-13-8281-9](https://doi.org/10.1007/978-981-13-8281-9)
- [12] Wang, K.; Li, S.; Rao, Y.; Wu, Y.; Peng, Y.; Yao, S.; Zhang, H.; Ahzi, S.: Flexure Behaviors of ABS-Based Composites Containing Carbon and Kevlar Fibers by Material Extrusion 3D Printing. *Polymers*, 2019, **11**(11), 1878 DOI: [10.3390/polym11111878](https://doi.org/10.3390/polym11111878)



## BUILDING A REUSABLE DATA MODEL TO SUPPORT SYSTEMATIC LAYOUT PLANNING WITH DISCRETE EVENT SIMULATION OF FLEXIBLE MANUFACTURING SYSTEMS

ZSOLT MOLNÁR\*<sup>1</sup>, PÉTER TAMÁS<sup>1</sup>, AND BÉLA ILLÉS<sup>1</sup>

<sup>1</sup>Institute of Logistics, University of Miskolc, Egyetemváros, Miskolc, 3515, HUNGARY

Manufacturing has undergone a greater change in recent years than it has over almost the entire past century. Due to the variety of products, shortening delivery times and changing customer habits, the COVID-19 pandemic has demanded greater flexibility from manufacturing companies than ever before. One of the fundamental parts of manufacturing flexibility is the design of manufacturing layouts, which has so far not followed automation and methodological developments with regard to technological areas of manufacturing. In this article, a new method for supporting traditional factory design methods with digital manufacturing tools is introduced.

**Keywords:** flexible manufacturing, simulation, layout design, Systematic Layout Planning

### 1. Introduction

Very few complete methodologies cover and support the entire process of designing manufacturing layouts. When the designing of a layout is considered, what are the most important parameters? The space available and the complexity of the manufacturing process of the product, which is directly proportional to the material flow and the costs, immediately come to mind. Our goal was to design an extendable method to be supported by digital manufacturing tools for the purposes of improving as well as speeding up the design and evaluation of future manufacturing layouts.

In terms of project planning, the study by Schenk et al. [1] comprehensively covers the design of factories and production lines but deals relatively little with the specific challenges of implementation. Their 0+5+X method is much more of a project planning and management method.

The study by Wiendahlet al. [2] presents many more concrete design methods. In addition to examining workplace design, including the connection between layout elements, it handles the workplace, work area, building and site design separately, albeit only to a limited extent, for the purpose of integrating these aspects into a complete system.

To the best of our knowledge, the Systematic Layout Planning (SLP) methodology by Muther and Hales [3] is the most comprehensive methodology to date. It addresses the data requirements of layout design and creates

production layouts by following a top-down approach. The design methodology takes into consideration relationships, space and adjustments. As this methodology also contains practical examples, templates and formulae for the steps of layout designs, this method is best suited for use with digital tools. In its current state, this method mainly focuses on traditional manufacturing processes and does not include specific methods for the design of Flexible Manufacturing Systems (FMS) [4] or Reconfigurable Manufacturing Systems (RMS).

Since this method was developed in the 1970s, it was mainly designed for paper-based workflows used to design classic dedicated manufacturing lines. Given the advancement of FMSs, understanding to what extent SLP can be supported by digital manufacturing as well as simulation tools and thus to what degree it can be used to design FMS's is a current research topic.

During the research, the Siemens Plant Simulation was used as a platform for the digital twin. The Siemens Plant Simulation is a discrete event-based piece of simulation software that takes into account a wide range of factory objects, e.g. material flow and logistics, as well as customization possibilities via its built-in programming environment [5, 6]. Another advantage of the system is that since the table component it contains is very versatile, it is also suitable for handling tabular and matrix data [7].

### 2. Digital twin

The digital twin has now become a basic tool for the development of production processes. A digital twin is

\*Correspondence: [zsolt.molnar.zsolt@outlook.com](mailto:zsolt.molnar.zsolt@outlook.com)

Table 1: Products and bill of materials

Product	Component	Qty	Operation number
A	B	3	20
C	B	2	10
A	D	1	10

Table 2: A typical product routing

Product	Operation number	Activity Point
A	10	M1 or M2
	20	M3

the mapping of production in a digital model to develop the production process within the framework of the digital model. The depth of formation of the digital twin is determined in each case by the development goal [8]. Process development in the digital model is typically cheaper, providing more what-if analysis possibilities than an analysis or trial of a real-life production system [9].

During the current research, the first steps to digitalize the SLP method and make it available to use for the design of flexible manufacturing lines were taken.

### 3. Data model

SLP works according to 5 elements: product, quantity, routing, supporting service and timing. The implications of these 5 groups of data on flexible manufacturing systems is outlined below.

In the case of products, the main purpose of flexible manufacturing systems is to facilitate the production of several products as a result of their flexibility. FMS's always try to implement high-mix and low volume production. The product data should include the related bill of materials along with information outlining which operation refers to the related necessary quantity of a part that is assembled or used to build the product. Example product data with information concerning the bill of materials is shown in Table 1

In terms of FMS lines, the most important parameter is routing, which determines the flexibility of the line itself. A typical product route with the order of operations and the machines (activity points) that are capable of executing the process step is shown in Table 2. An activity point is a location where something happens to a product. Details of this definition will be provided and expanded on later. Although the order of operations is usually fixed (or hardly modifiable), most of these lines include a machine to substitute bottleneck resources to make routing more flexible.

The routing data should include the product data and process steps, including the alternative routings which are very common in flexible manufacturing cells.

A typical product routing is presented below.

In the case of flexible manufacturing, the data model should be able to handle the alternative routings. For the

Table 3: First alternative routing of Product A

Product	Operation number	Activity Point
A	10	M1 or M2
	20	M3

Table 4: Second alternative routing of Product A

Product	Operation number	Activity Point
A	10	M3
	20	M1 or M2

sake of clarity, each alternative routing was stored separately along with the full routing data, thereby ensuring that it can be handled faster and more easily with a route search algorithm. Tables 3 and 4 show alternative routings for the same product.

Given the routing tables, the question may arise as to where to store product-dependent parameters during the simulation, e.g., how long should the production time of Product A be on machines M1 and M2? The data model follows the Industry 4.0 philosophy of storing data where data-related decisions are made, that is, on machines. In this case, machine M1 knows how much time Product A spends on it and this information can be made available to other elements of the production system at any time.

The most important areas of the supporting services are maintenance and raw material supply. Both are critical to the operation of the line. Although the supply of raw materials influences the design and layout at a basic level, maintenance is vital to ensure a functional operation. Since operational services are mostly machine-related, they must be handled by the machine (activity point).

Repair and rework are special supporting services. If quality control and repair take place within the machine, the necessary time can be regarded as the duration of a process step. If quality control is carried out elsewhere, it should be treated and mapped as part of the routing.

The time-based parameter of the SLP design process can determine when items will be produced. Usually, the number of pieces and product mix over a given period, e.g. monthly, are available here. Based on this, orders can be generated in the simulation, the distribution of which corresponds to the given data.

The relationship between the SLP layout design process and the simulation is shown in Fig. 1. Apparently, the steps of the design process can be mapped to the steps of building a simulation model.

### 4. Activity points

During a manufacturing process, a part could be subjected to six activities:

1. Can be processed (assembled, disassembled or manufactured in any way)
2. Can be moved or transported

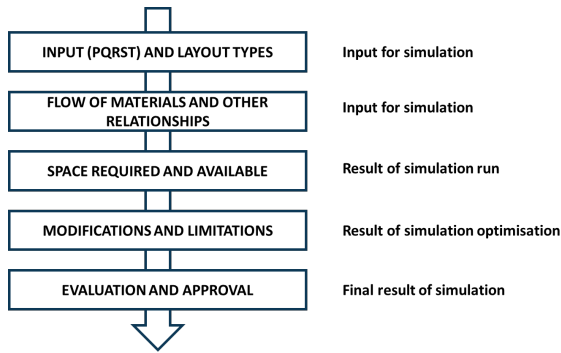


Figure 1: SLP steps in relation to the simulation process [1]

3. Can be handled to support processing (change in orientation, placed in a tool, etc.)
4. Can be handled to enhance quality (inspected, tested, counted, repaired or reworked)
5. Can be forced to wait due to technological reasons (to cool down, etc.) or for the rest of the batch to catch up
6. Can be stored

To manage activities uniformly, the concept of an activity point was introduced, which is a generic object that can handle the aforementioned six activities in one object depending on the settings specified.

A manufacturing object, e.g., an activity point, can be a milling machine, 3D printer or even a buffer as shown in Fig. 2.

The main attributes of an activity point are:

- Object type (processing, handling, transferring, buffering, quality handling, storage)
- Processing type
- Processing time (product-dependent)
- Setup parameters
- Capacity
- 3D block size parameters (x, y, z)
- Logic of supporting services

With the help of activity points, the simulation model can be easily built and modified.

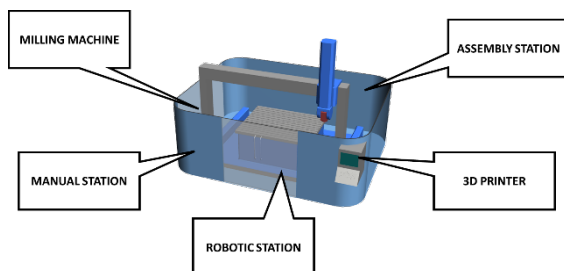


Figure 2: An activity point can represent different types of process objects

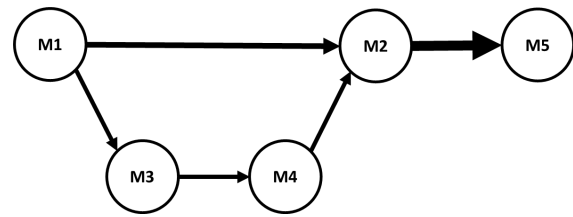


Figure 3: Material flow visualization

Depending on how comprehensive the analysis is, an activity point could be planned by a department or a single processing machine.

### 5. Simulation results

The simulation model is suitable for generating the results required for the further steps of the SLP analysis.

The simulation automatically creates a Sankey (or spaghetti) diagram characterizing the material flow intensity between each activity point (Fig. 3).

The most important result is the so-called Travel Chart that shows how much material has moved between each activity point. The upper diagonal of the table shows the amount of material that has moved forwards, while the quantity that has moved backwards, e.g. a loop in progress or returned for repair, is depicted below the diagonal. On the diagonal, all values are, by definition, zero.

Based on the data table, the material movement (or flow) between two activity points can be calculated, which is defined as:

$$m_{ij} = \text{material flow from activity } i \text{ to activity } j \quad (1)$$

Due to the possible backward material flow, the total material movement between two activity points can be calculated by this formula:

$$M_{ij} = m_{ij} + m_{ji}, \text{ for all } i > j \quad (2)$$

SLP uses an REL (relationship) chart to visualize the importance of how close the different departments are to each other. The REL chart replaces the numbers in the Travel Chart with a closeness category. Six categories are defined to represent the level of importance [3]:

- A – Absolutely necessary
- E – Very important
- I – Important
- O – Fairly important
- U – Unimportant
- X – Undesirable

Table 5: Travel Chart (From-To chart)

	M1	M2	M3
M1	0	$m_{12}$	$m_{13}$
M2	$m_{21}$	0	$m_{21}$
M3	$m_{31}$	$m_{32}$	0

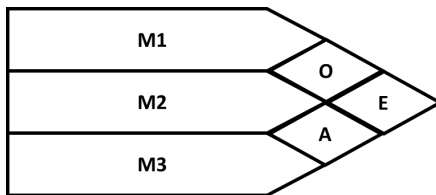


Figure 4: Simple chart depicting the importance of how close each activity is to each other

Table 6: Summarized Travel Chart

	M1	M2	M3
M1	0	$M_{12}$	$M_{13}$
M2	–	0	$M_{21}$
M3	–	–	0

Table 7: Chart depicting the importance of the proximity of the activity points to each other

	M1	M2	M3
M1	0	O	E
M2	-	0	A
M3	-	-	0

In the example (Fig. 4), 3 departments (activity points) are present to evaluate our layout. The intersections denoted by letters depict the importance of how close the departments are to each other.

From the simulation model, the results of the Travel Chart can be transformed into a full Travel Chart (Table 6) which includes the total material flow between the activity points.

By taking the largest and smallest values from the table as well as dividing the range into 6 parts, six categories can be created to determine the importance of the proximity of the activity points to each other. The content of the resulting table is identical to the chart depicting how important the proximity between activity points is which is required to evaluate the SLP methodology (Table 7).

Based on the table, decisions can be made as to which departments and machines should be placed close to each other as well as how the layout elements should be designed.

## 6. Summary and further research

Supporting and further developing traditional factory design methods with digital manufacturing and simulation

tools is a new approach to design better production lines and shorten design processes.

As the aforementioned method is rather generic, that is, applicable to many scenarios, it does not completely fulfill the special requirements of the production lines in FMS's or RMS's. The next phase of this research will strive to include the product mix, namely the variety of processes, in the model. Another important field of this research is how to evaluate an automation level of the production lines and determine which automation level is optimal by taking into consideration the material flow as well as technical and investment parameters.

## REFERENCES

- [1] Schenk, M.; Wirth, S.; Müller, E.: *Factory Planning Manual*, Springer-Verlag Berlin Heidelberg, 2010 ISBN: 978-3-642-03634-7, DOI: 10.1007/978-3-642-03635-4
- [2] Wiendahl, H. P.; Reichardt, J.; Nyhuis, P.: *Handbook of Factory Planning and Design*, Springer Heidelberg New York Dordrecht London, 2015 ISBN: 978-3-662-46390-1, DOI: 10.1007/978-3-662-46391-8
- [3] Muther, R.; Hales, L.: *Systematic Layout Planning*, Marietta, GA: Management & Industrial Research Publications, 2015, ISBN 978-0-933684-06-5
- [4] Košťál, P.; Velíšek, K.: *Flexible Manufacturing System*, Zenodo, 2011 DOI: 10.5281/zenodo.1075605
- [5] Erdélyi, F.; Tóth, T.; Kulcsár, G. Y.; Mileff, P.; Hornyák, O.; Nehéz, K.; Körei, A.: *New Models and Methods for Increasing the Efficiency of Customized Mass Production*, *J. Mach. Manuf.*, 2009, **49**, 11–17
- [6] Tamás, P.; Illés, B.; Tollár, S.: *Simulation of a flexible manufacturing system*, *Adv. Logist. Syst.* 2012, **6**(1), 25–32
- [7] Bratley, P.; Fox, B. L.; Schrage, L. E.: *A Guide to Simulation*, 2nd ed., Springer: New York, NY, USA, 1987 ISBN: 978-1-4612-6457-6.
- [8] Cselényi, J.; Illés, B.: *Planning and Controlling of Material Flow Systems (Textbook)*, Miskolc, Hungary: Miskolci Egyetemi Kiadó, 2006
- [9] Dörgő, G.; Abonyi, J.: *Group Contribution Method-based Multi-objective Evolutionary Molecular Design*. *Hung. J. Ind. Chem.*, 2016, **44**(1), 39–49 DOI: 10.1515/hjic-2016-00056